Spring 2021

# Applications and Mechanisms of Near Infrared Spectroscopy For Age Estimation in Otoliths of Red Snapper *Lutjanus Campechanus*

Michelle S. Passerotti

# APPLICATIONS AND MECHANISMS OF NEAR INFRARED SPECTROSCOPY FOR AGE ESTIMATION IN OTOLITHS OF RED SNAPPER *LUTJANUS CAMPECHANUS*

by

Michelle S. Passerotti

Bachelor of Science
Florida State University, 2003

Master of Science
Louisiana State University, 2007

---

Submitted in Partial Fulfillment of the Requirements

For the Degree of Doctor of Philosophy in

Biological Sciences

College of Arts and Sciences

University of South Carolina

2021

Accepted by:

Joseph M. Quattro, Major Professor

Thomas J. Hilbish, Committee Member

Marcel J. M. Reichert, Committee Member

David Reisman, Committee Member

Ryan R. Rykaczewski, Committee Member

Tracey L. Weldon, Interim Vice Provost and Dean of the Graduate School

# ACKNOWLEDGEMENTS

I would first like to thank Marcel Reichert, Wally Bubley, Bryan Frazier, Joey Ballenger, and a host of others at the SC DNR Marine Resources Research Institute for their incredible support over the course of this project. I would also like to thank Michael Myrick, Elle Belliveu, and Arelis Colon from the U of SC Department of Chemistry, as well as Joshua Brennan and Jason Erickson from Bruker Scientific for their patience and assistance in learning the fundamentals of spectroscopy and chemometrics, and to Nathan Earl, Bailey Robertory, and Justin Weeks, for volunteering time and facilitating data collection for this project. Many thanks to lab mates Kate Levasseur and Keith Fuller for moral and logistical support. I am very grateful to my committee members for their time, support, and helpful expertise over the years. Special thanks go to my advisor Joe Quattro for always having faith in my ideas, providing guidance when it was needed, and giving so generously of his time to facilitate the growth of this work. I thank my other collaborators at NOAA, Florida Fish & Wildlife Conservation Commission, and the Stefik Lab at U of SC, without whom this work would not have been possible. Funding and other specific acknowledgements can be found at the end of each chapter.

Finally, I would like to thank my family and friends for their love and support in this endeavor. Tracy, Tyler, and Brandon: thank you for being my “why”, for keeping me grounded, and for never resenting how badly my samples made the house smell. Thanks to my parents and extended family for believing in me when I said I’d make it here, even at 39 years old. Thanks especially to Dad, for always taking me fishing.

# ABSTRACT

Near infrared spectroscopy (NIRS) is a light spectroscopy method useful for non-invasively discriminating and quantifying chemical composition of a wide variety of substances. Recently-developed applications of NIRS to fish age estimation across a range of taxa have sparked intense interest in exploring the feasibility of its use for rapid age estimation in fisheries population management. In this pursuit, development of species-specific calibration models relating traditionally-derived age estimates (i.e., those estimated from growth band counts) to NIR spectral signatures from ageing structures is required to derive predictive models that can then estimate age from rapid scans of whole ageing structures alone. Otoliths and corresponding traditionally-derived ages of juvenile and adult red snapper *Lutjanus campechanus* were used to generate NIRS models for predicting both daily and annual ages. NIRS-predicted daily ages were accurate to within six days of traditional estimates and were not significantly different than traditionally-derived ages for juveniles aged 39 – 120 days when used to produce length-at-age models. NIRS-predicted annual ages were accurate to within approximately one year in fish aged 0 – 30 years, but prediction error rose substantially for fish aged 31 – 38 years. Across all models, age-related otolith morphometric dynamics changed the physical interaction of NIR light with the structures and impacted the resolution of age prediction models. When size and otolith morphometrics for a subset of otoliths (n=26) were standardized by grinding and subsampling a fixed mass from each for NIRS analysis, NIRS prediction error increased by approximately 30% but ages remained accurate to

within 2 years of traditional ages; hence, otolith structure is of some importance to predictive models but ontogenetic compositional changes underlie most of the correlation of NIRS otolith spectral signatures with age. Protein concentration (% otolith weight) was positively correlated with traditional age, but the impact of this relationship on otolith spectral signatures was not easily discernable. However, comparison of otolith spectral signatures to those of two primary otolith constituents, calcium carbonate and type I collagen, revealed that absorbance features at characteristic wavenumbers for each constituent were correlated to NIRS otolith age prediction, providing the first insights to the NIRS age-prediction mechanism in otoliths.

# TABLE OF CONTENTS

# LIST OF TABLES

# LIST OF FIGURES

# CHAPTER 1

# INTRODUCTION

Age determination of individuals within a population is a key component in assessing demography and population dynamics for managed species, including fish populations. Age-structured population models are currently the most common tool used by fisheries managers to assess exploited populations (Walters and Martell, 2004). Age- (or life stage-) specific survival and fecundity underlie the link between life history and natural mortality (Roff, 2002). Knowledge of the population age structure is used to generate mortality estimates based on catch at age (Walters and Martell, 2004), but an overall knowledge and understanding of other life history traits such as birth and growth rates are also critical to generating reference points for monitoring population size and compensatory capacity (Goodwin *et al.* 2006; Clark, 2011; Thorson *et al.* 2012; Zhou *et al.* 2012; Mangel *et al.* 2013; Kindsvater *et al.* 2016; Hutchings and Kuparinen, 2017). Exploitation can induce changes in size and age at maturity by way of preferential removal of certain phenotypes, e.g., larger individuals, and hence can be a mechanism of selection for individuals that mature at smaller sizes (Stearns and Koella, 1986; Law, 2000, 2007; Stearns, 2000; Conover and Munch, 2002). Differential fishing pressure across age classes can, through selection, alter life history traits such as growth rates, maximum size, and lifespan (Hixon *et al.* 2014). Environmental changes can also alter life history parameters of fish due to the increased susceptibility of poikilotherms to environmental fluctuations (Campana and Thorrold, 2001). Inaccurate age data in age-

structured population assessments can induce significant errors in reference parameters, leading to incorrect management decisions and overexploitation (Lai and Gunderson, 1987; Beamish and McFarlane, 1995). Hence, there is a need for consistent age estimation across populations in order to effectively assess current life history parameters and predict future responses to perturbations.

### 1.1 Traditional age estimation

Age estimation in fish relies on the use of calcified structures or "hard parts" to infer age based on interpretation of growth increments formed within the structure and related to time. In order for a structure to be suitable for use in age estimation, it must meet several key criteria. First, the structure must grow throughout the lifespan of the individual, even if somatic growth ceases, in order to assume age-related material is recorded continuously through life (Campana, 2001). This growth typically occurs as seasonal growth band pairs, with one band being deposited during warmer months during periods of faster growth, and the second being deposited in colder months during periods of slower growth (Cailliet and Goldman, 2004). Second, the pattern of growth increments should be consistent and objectively interpretable. Third, increments should be relatable to a regular time scale, i.e., they should be able to be validated over time (Vitale *et al.* 2019). As part of these criteria, the material comprising the age structure must also not be subject to metabolic reworking, e.g., reabsorption of deposited material during times of low growth or changes to energetic demands (Campana and Neilson, 1985). In some fish, an ageing structure might not exist that possesses all of these characteristics across all life stages. This is a challenge that fisheries management confronts with some regularity, and

is compounded by the fact that validation of ageing methods across the full lifespan of each species for each ageing structure used has not been accomplished (Campana, 2001).

The structures used for age estimation in fish vary both across and within phylogenetic groupings. Skeletal composition tends to dictate which structures are best suited to age estimation, with some exceptions. In the ray-finned fishes (Actinopterygii), ageing is usually accomplished using otoliths (ear stones), although this is generally restricted to teleosts as chondrosteans (e.g., sturgeons) have smaller, more fragile otoliths with diminished utility for age estimation (e.g., Stevenson and Secor, 2000). Among teleosts, otoliths are the preferred ageing structure as they tend to provide the best resolution over the longest age ranges (Secor *et al.* 1995; Campana, 2001), but there are some species whose otoliths are prohibitively small (e.g. gray triggerfish; Allman *et al.* (2018), but see Shervette *et al.* (2021)), are more difficult to age (e.g., albacore, Prince *et al.* 1995), or are difficult to obtain from fishery-dependent or endangered specimens due to the destructive nature of sampling them (e.g., bluefin tuna, Santamaria *et al.* 2009; goliath grouper, Brusher and Schull, 2009). In cases such as these, alternate structures such as fin spines, vertebrae, or occasionally fin rays can be used instead (Casselman, 1987). Scales have also been widely used for age estimation in teleost fish, but validation studies have shown they can underestimate age in older fishes, and can also be subject to resorption, hence their use tends to be confined to short-lived species (Beamish and McFarlane, 1995). Instead of otoliths, cartilaginous fishes such as sharks, rays, and chimaeras possess inner ear structures similar to otoliths known as otoconia, which are composed of microparticles embedded in a gelatinous organic matrix that serve a similar function as otoliths (Carlström, 1963). However, these otoconia are generally small,

brittle, and amorphous, and hence are not useful for age estimation purposes (Schnetz *et al.* 2019). In these fishes, hardened structures including vertebrae and fin spines have instead become preferred for age estimation due to similar deposition of growth bands throughout the various structures (Natanson *et al.* 2018a). However, the functional morphology of skeletal structures used for ageing varies according to their type and location within the body. This inherently impacts the suitability of the structure to age estimation, a fact that should be accounted for in evaluation of their practical use (Campana and Neilson, 1985; Campana and Thorrold, 2001; Natanson *et al.* 2018b).

Traditional age estimation methods using growth increment counts are typically labor intensive and costly. The steps involved to process ageing structures for interpretation typically include the removal of the structure from the fish, cutting or sectioning the structure to expose the growth increments, grinding or polishing the exposed surface to enhance visualization, and mounting of the processed section onto a slide for visual interpretation by counting of the increments (e.g., VanderKooy, 2009). Beyond processing, the interpretation of increments to produce age estimates is also time consuming and is subject to several sources of error. The accuracy of an ageing method may vary across life stages and hence be a source of error in estimation. Consistency of ageing methods should ideally be validated over the entire lifespan of the species, although this is seldom accomplished for all life stages (Campana, 2001; Cailliet and Andrews, 2008). Additionally, the precision of age estimates is important, as a method is not sound if it does not enable consistent estimates given the same criteria (Kalish *et al.* 1995; Campana, 2001). Multiple counts of increments are generally made for each age structure, or a subsample of structures, either by a single reader or multiple readers, so

that counting precision can be estimated and to identify any bias in estimation on the part of the age readers. This process is carried out for essentially all fish species monitored for management purposes, and in some cases thousands of individuals per species are aged annually to inform stock assessment models, with total effort estimated to approach 1 million age structures per year worldwide (Campana and Thorrold, 2001). Given the increasing numbers of species subject to stock assessment and the immense amount of resources required to accomplish age estimation at the production scale, the advent of new methodologies to increase efficiency and decrease costs are sorely needed.

### 1.2 Near Infrared Spectroscopy

Near Infrared Spectroscopy (NIRS) is a relatively new technique for age estimation in fish, but it has been used widely in other fields of research. NIRS falls in the realm of vibrational spectroscopy, which studies the interactions of various molecules with light and uses characteristic vibrational signatures to detect the types and quantities of organic molecular bonds contained within the substance of interest (Siesler *et al.* 2002; Workman and Weyer, 2012). NIRS utilizes light from the near infrared region of the electromagnetic spectrum, between 12,800 – 4000 $cm^{-1}$ (wavenumbers) or 780–2500 nm (wavelength), to evaluate organic chemical bonds (predominantly C-H, C=O, N-H, and O-H bonds) present within a material (Siesler *et al.* 2002; Workman and Weyer, 2012). These bonds vibrate in characteristic ways when irradiated at specific frequencies and thereby absorb light, producing signature absorbance patterns representative of the composition of the sample (Murray and Williams, 1987). Relation of these absorbance patterns to other known variables (such as age) via calibration regression models can be used alongside multivariate statistical analyses to provide a rapid and non-destructive

method of discriminating a variable of interest from spectral data alone (Beebe *et al.* 1998; Siesler *et al.* 2002; Vance *et al.* 2016).

Quantification of molecular bonds in NIR spectroscopy follows the principle of Beer's Law, which essentially states that the amplitude of light absorbance at any given wavenumber is dependent upon the number of molecular bonds present in the sample vibrating at that frequency in the given pathlength of light (i.e., the concentration of bonds in the sample; Ingle and Crouch, 1988). Hence, while some features of the spectral signature of a given substance are broadly attributable to the constituents, the true mechanism of NIRS discrimination among spectral signatures instead focuses on the architecture of the molecular bonds underlying the compounds themselves, which are the product of both the chemical and physical interactions of all molecules in the sample (Williams, 2019). In this way, the interpretation of spectral signatures is complex, and determining the causation underlying NIRS discriminatory capability is often not undertaken for the process-related analyses commonly employing NIRS e.g., those in agriculture and pharmaceuticals (Siesler *et al.* 2002; Workman and Weyer, 2012).

Spectral signatures comprise several distinct areas within the NIR spectrum where molecular bond vibrations of different energy levels are detected. NIRS detects harmonic oscillations in molecular bonds, meaning these vibrations are detected at multiple points along the NIR spectrum, and absorbance intensity decreases as the vibrational mode shifts from fundamental to overtone regions (Siesler *et al.* 2002). Absorption intensity is highest in the mid-infrared region (4000 – 400 $cm^{-1}$) where fundamental bond vibrations are detected. These same vibrational signatures are also present in the NIR region, but at lower intensities. The area from ~5500-4000 $cm^{-1}$ reflects combination bands derived

from bending and stretching of fundamental vibrations, while 9091-5555 $cm^{-1}$ and 12700-9091 $cm^{-1}$ comprise signatures of first and second overtone vibrations, respectively. Absorption intensity in NIR combination bands is roughly 2 orders of magnitude lower than that of the mid-IR fundamental bands, and NIR overtone bands decrease by about 1 order of magnitude for each successive overtone (Workman and Weyer, 2012). Since the relative energy of NIR light is proportional to wavenumber, the penetration depth is also proportional; hence, the optimum pathlength for interrogating samples is longest in the overtone regions and shortest in the combination region. This has implications for sample types and presentations used for various NIRS analyses (Norris and Hart, 1965; Workman and Weyer, 2012).

Sample presentation refers to the physical way in which a sample interacts with the NIR light from the spectrometer and has substantial effects on spectral signatures. In addition to information about the chemical makeup of the sample, NIRS spectral signatures, and especially those from solid samples, also contain information on the physical properties of the sample such as diffuse reflectance, light scattering, polarization, and refraction (Workman and Weyer, 2012). Put another way, information about the architecture of the sample is layered with that of the chemical components to comprise the snapshot of the molecular structure provided via its spectral signature (Williams, 2019). Even samples with the same molecular composition can have different spectral signatures if the patterns of molecular bonding are different due to even small changes at the atomic level. For example, hydrogen bonding is especially well-suited to detection with NIRS, and hydrogen bonds form readily between such constituents as water, proteins, and oils, each themselves comprising various conformational

arrangements depending on the overall molecular structure of the sample. If even a minute change is made at the molecular level, for instance one type of protein changed to another, this would alter the bond arrangements between constituents and hence the shapes of the molecules themselves, resulting in different spectral signatures even though the overall composition of the sample remained the same (Williams, 2019). These principles provide some insight into the mechanism for spectral discrimination of e.g., wheat hardness (Manley *et al.* 2002), cuticular hydrocarbons in mosquito carapaces (Lambert *et al.* 2018) and other applications where NIRS outperforms even wet chemistry; whereas a change in certain constituents at the scale of parts per million is easily discriminated in spectral data (where it would be represented by potentially billions of molecules), differences that finite can be out of range for chemical assays (Williams, 2019).

The routine use of NIRS in process-related roles gained widespread attention beginning in the 1960s for its diagnostic use in agriculture applications and continues to expand today. Much of the early work in mainstreaming NIRS was done by Karl Norris on behalf of the USDA in pursuit of characterizing moisture content and other attributes of cereal grains in agriculture (Norris, 1996). Using methanol extracts from wheat, Hart et al.(1962) demonstrated that a relationship to moisture content could be made based on rapid scans of ground wheat using reflectance measurements, and Norris and Hart (1965) built upon this work to demonstrate the potential for NIRS to predict moisture content in a variety of samples including wheat, soybean, wheat flour, and wheat bran. They also gave important insights into the effects of physical characteristics of samples on NIRS spectra, namely particle size, thickness, and uniformity of samples, and highlighted the

importance of accounting for physical effects in sample presentation. This study was also among the first to develop predictive models for interrogation of intact samples (peanuts and peas), which revolutionized the field to enable non-destructive analysis of key variables of interest, including proteins (e.g., Williams *et al.* 1985). The fast and reliable quantification of protein content by NIRS auto analyzers led to NIRS becoming a workhorse of industrial applications, replacing costly and time-consuming wet chemistry for routine monitoring (Williams, 2019).

The advent of computer modeling and chemometrics has been a driving force in the advancement of NIRS as a widely applicable tool (Burns and Ciurczak, 2007). Chemometrics refers to the overall use of mathematics to analyze complex spectrochemical data and encompasses both the preprocessing of raw spectral data, for enhancement of select features and removal of noise, and the use of multivariate analyses (e.g., principal components analysis and partial least squares regression) to create predictive models for variables of interest. Spectral data are multivariate by nature because the absorbance at each individual wavenumber is related to the absorbance at all other wavenumbers, as well as to the myriad variables correlated to the spectral signature as a whole. Because the overall data matrix for an entire spectral signature is immense, dimension reduction via principal components analysis is invaluable for determining the most important latent variables underlying spectral differences and the proportion of the spectral variance they explain. Preprocessing of spectra encompasses mathematical transformations such as normalization and various derivative transformations, which in conjunction with dimension reduction can help separate true spectral features from surrounding noise (Beebe *et al.* 1998; Burns and Ciurczak, 2007). Preprocessing also

helps to overcome some of the hindrances posed by sample presentation of complex mixtures and variability in solids/diffuse reflection. Common techniques include multiplicative scatter correction for overcoming particle size differences, first derivative transforms to accentuate features, and normalization to overcome sample variability (Beebe *et al.* 1998).

In addition to preprocessing, good experimental design is essential for building robust prediction models. Most NIRS applications, including age prediction in fish, use partial least squares regression and associated calibration models to estimate variables of interest from spectral data alone. Samples comprising calibration models should include all potential sources of sample variation, not only encompassing the full range of the variable(s) of interest, but also the full range of other inherent properties that affect spectral signatures (Burns and Ciurczak, 2007; Workman and Weyer, 2012; Williams, 2019). The sample distribution for the calibration model should also be considered, and sample size should be uniform across the variable range where possible to ensure residuals are minimized equally across the sample set and not weighted to the mean (Burns and Ciurczak, 2007). Generally, a sample size ≥ 10-15 per category value across the full calibration range is considered sufficient in most systems (Burns and Ciurczak, 2007; Williams, 2019), but in complex samples, in those with high inherent spectral variability, or in systems requiring fine resolution of variables, the sample size required for optimizing the calibration model might be much higher (e.g., Lambert *et al.* 2018). The criteria for assessing prediction capability of the calibration model include several metrics: Root Mean Square Error of Cross Validation (RMSECV), Root Mean Square Error of Prediction (RMSEP), coefficient of determination ($R^2$), and the Residual

Prediction Deviation (RPD). The RMSECV and RMSEP metrics should be minimized, the $R^2$ maximized, and RPD > 3 to be considered optimized (Williams, 2019).

The applications for NIRS comprise a rapidly evolving field including pharmaceuticals (e.g., QA/QC of whole tablets; Blanco and Alcalá, 2006), food analyses (e.g., wine characteristics; Cozzolino *et al.* 2006), medical diagnostics (e.g., brain function; Villringer *et al.* 1993), and ecological research (e.g., amphibian reproduction; Vance *et al.* 2016). One of the most prevalent areas of interest in the wildlife literature is the use of NIRS as a tool for mosquito population monitoring for mitigating human parasitic infection (e.g., Lambert *et al.* 2018). This includes the specter of age discrimination, which has been demonstrated successfully across several species and life stages. The underlying mechanism for age prediction in mosquitos is unknown, but age-related changes in proteins have been proposed and successfully measured (Sikulu *et al.* 2015). There are difficulties, however, with resolving age in wild-caught populations using the calibration models created from laboratory-reared specimens, which hinders practical application of the technique and indicates the potential for natural variation in wild specimens to preclude accurate modeling and prediction of age in situ (e.g., Ong *et al.* 2020). These difficulties highlight the secondary nature of NIRS predictive capabilities, which rely solely upon robust calibration models to inform prediction.

Age prediction in fish using NIRS scans of calcified structures has alternatively been quite successful from an experimental standpoint. Wedding *et al.* (2014) first applied NIRS to estimate age from scans of whole otoliths of saddletail snapper (*Lutjanus malabaricus*) with a high degree of accuracy (≤ 1.5 years) relative to traditionally-estimated ages. Additionally, regional and/or seasonal differences in spectral signatures

were also apparent, with distinct separation of principal components for post-wet season versus post-dry season otoliths collected from two locations (Wedding *et al.* 2014). Similar ageing success as well as regional and seasonal discrimination was also demonstrated by Robins et al.(2015) using barramundi (*Lates calcarifer*) and pink snapper (*Pagrus auratus*) otoliths. The geographic differences in spectra were most apparent when using calibration models from one region to predict ages for another region, but full calibration models incorporating all regional variation resulted in age prediction error rates for all samples on par with region-specific models (Robins *et al.* 2015). This study also addressed the effect of storage time on spectral signatures and age prediction, finding that spectra tended to stabilize around 6-11 months and were stable for at least five years after, although between-year variability in spectra was evident and seemingly confounded these results. Finally, sample presentation was experimentally evaluated across several orientations on the scanner and found to be best when otoliths were placed sulcus-side (convex-side) down in a standardized position for each scan, highlighting the importance of sample presentation to optimizing calibrations. In light of these successful proof-of-concept studies, Helser et al.(2019) undertook a case study using walleye pollock (*Gadus chalcogrammus*) otoliths, and reported age prediction resolution to within ≤ 1 year on average and with similar error and decreased bias relative to traditional ages up to 12 years. Although regional differences in condition across the sampled population were apparent, best fit calibration models were those that combined samples across regions and sampling years, which suggests individual spectral variation in otoliths might in some cases outweigh variation due to regional or temporal sources (Helser *et al.* 2019b).

Age prediction with NIRS has also been assessed using vertebrae, dorsal fin spines, and pelvic fins of sharks with some success. Vertebrae of great hammerhead *Sphyrna mokarran*, piked spurdog *Squalus megalops*, and spottail shark *Carcharhinus sorrah* scanned akin to NIRS otolith methods were found to predict ages to within 0.87-1.85 years of traditional ages across age ranges to 25 years (Rigby *et al.* 2014, 2016a). For *S. mokarran* and *C. sorrah*, NIRS predicted ages produced statistically similar length-at-age models as traditional ages, and so NIRS was suggested to be a robust ageing method for these species based on these results (Rigby *et al.* 2016a). The results for the deepwater shark *S. megalops* were especially novel, as vertebrae for this species are poorly calcified and do not possess visually discernable growth bands, and whose traditional ages were estimated using counts of growth bands in dorsal fin spines instead (Rigby *et al.* 2014, 2019). Dorsal fin spines for *S. megalops* and *Squalus montalbani* were also evaluated for age prediction with NIRS, but had higher prediction error (2.4-3 years) and reduced model fit (Rigby *et al.* 2014) relative to vertebrae models. Fin samples for *S. megalops* were also evaluated for age prediction, and surprisingly reflected traditional ages to within 2.7 years (Rigby *et al.* 2014). While error rates across shark age structures were overall higher than those from otolith studies, the sample sizes used for calibration models were lower (n=76-99) relative to those used for otolith models (n=169-306; Wedding *et al.* 2014; Robins *et al.* 2015; Helser *et al.* 2019). Additionally, traditional age estimates for shark species, especially those attained from alternative structures such as dorsal fin spines, tend to be accomplished with lower sample sizes and higher potential bias due to the difficult nature of obtaining and interpreting these tissues (Campana, 2001); hence, the traditional ages used to inform NIRS calibration models for these

tissues might ostensibly have more error included, which could also impact resolution of NIRS prediction models (Rigby *et al.* 2019). Overall, it appears vertebrae provided better resolution among shark age structures for age prediction based on spectral data, but the potential for non-lethally sampled tissues such as fins and fin spines to reflect age via spectral signatures is a revelation with huge potential impacts to wildlife management as a whole (Rigby *et al.* 2014, 2019).

The mechanism behind the NIRS relationship with fish age, and to a lesser degree to regional or environmental inputs, is not explicitly known for any of the structures examined to date. Because growth of the age structure occurs in the form of cyclic deposition of mineral growth on an organic matrix, most have postulated that the changing ratio of mineral to organic material across the lifespan is reflected in spectral signatures. Wedding *et al.* (2014) noted that the spectral features of *L. malabaricus* otolith signatures that remained consistent across regions (and hence were consistent across the lifespan in all otoliths) were reflective of bonds related to carbonate ions present in otoliths, and also suggested a role of microchemistry in delineating regional otolith signatures. Robins *et al.* (2015) likewise suggested the role of water chemistry for influencing spectral signatures due to incorporated changes in trace element concentrations across the lifespan. Helser et al.(2019) proposed the age-related accumulation of covalent organic bonds associated with proteins in the otolith organic matrix as one possibility for further research. Similar mechanisms involving organic constituents were suggested by Rigby *et al.* (2014, 2016a) for age prediction in shark tissues, and (Rigby *et al.* 2019) went on to hypothesize that chondroitin sulfate, a

collagen constituent, is a likely source of age related changes underlying NIRS spectral differences across shark vertebrae, fins, and spines.

In order to fully evaluate the potential for NIRS to be used in place of or as a complementary tool in age estimation using the suite of available fish ageing structures, it is best to have an idea of the chemical and physical makeup of each. Hence, a brief review of known attributes for otoliths, scales, vertebrae, and fin spines and fin rays are discussed herein.

## 1.3 Composition & morphology of ageing structures

### *1.3.1 Otoliths*

Otoliths are the crystalline ear stones located in the inner ear of teleost fish, and are responsible for orientation and hearing through detection of vibrations. Three pairs of otoliths are present in the inner ear of teleosts: the sagittae, lapilli, and asterisci. The size, shape, and composition of otoliths vary across the three otolith types, as well as across species. Generally, the sagittae are the largest otoliths and tend to be preferred for age estimation (e.g., Radtke, 1984). They are typically composed of about 90-98% calcium carbonate, ~0.2-10% organic content in the form of proteins, collagens, and proteoglycans, and < 1% trace elements (Kalish, 1989; Campana, 1999; Dauphin and Dufour, 2003; Thomas *et al.* 2019), although these values are highly species-specific. The calcium carbonate component is present in the form of polycrystalline aragonite for the majority of sagittae and lapilli (Carlström, 1963) but sporadic inclusion of the other common polymorphs vaterite and calcite can be found simultaneously to aragonite in some otoliths (Strong *et al.* 1986; Gauldie, 1993). Entirely vateritic sagittae and lapilli

can also form aberrantly (Mugiya, 1972; Reimer *et al.* 2017) but vaterite seems to be the preferred form in most asteriscii (Lowenstam and Weiner, 1989; Oliveira *et al.* 1996). The organic matrix of otoliths is known to form the template for calcium carbonate mineralization, and calcium binding and crystal formation during mineral accretion of otoliths are protein-mediated. Degens (1969) first characterized the organic matrix of teleost saggitae as being made up of a collagen-like protein deemed otolin, described as a fibrous structure containing characteristic acidic amino acids and hydroxyproline in similar proportions as collagen. This protein was later more fully characterized as a short-chain structural protein containing collagenous domains, important to directing the calcium binding and crystal structure of otoliths, and was renamed otolin-1 (Davis *et al.* 1995; Murayama *et al.* 2002). In recent years, additional otolith proteins have been identified and characterized across species, including OMP-1 (Murayama *et al.* 2000), Starmaker (Söllner *et al.* 2003), OMM-64 (Tohse *et al.* 2008), Starmaker-like (Bajoghli *et al.* 2009), Otoc1 (Petko *et al.* 2008), SPARC (Kang *et al.* 2008), Neuroserpin (Kang *et al.* 2008), and Tectorin, Otogelin, Transferrin, and Myosin Light Chain 9 (Weigele *et al.* 2016). The functions of these proteins vary, with some attributed to forming the structural template for otolith growth while others are thought to directly modulate calcium binding and growth band formation. The recent advent and application of proteomic techniques in otoliths has revealed the presence of an astonishing number of proteins, more than 300 in all, not previously known to occur in otoliths (Thomas *et al.* 2019). Many of these proteins, and to some extent other constituents as well, appear to be derived from endolymph trapped in the interstitial spaces during otolith formation as opposed to being

actively deposited onto the otolith (Thomas and Swearer, 2019; Thomas *et al.* 2019) but nonetheless these substances are present constituents in whole otolith analyses.

The physical structure of otoliths is also of consequence to the use of NIRS for data collection. Otoliths accrete material both daily (Pannella, 1971) and annually (Campana, 2001) throughout the life of the fish according to both circadian and seasonal rhythms, and generally at a rate mirroring that of somatic growth (Campana and Jones, 1992). However, fish otoliths, along with squid statoliths, are the only calcified structures known to grow throughout the whole life of the organism (Campana and Thorrold, 2001), and have been documented to grow even in the absence of somatic growth (Maillet and Checkley, 1990). Alternating translucent and opaque growth increments are deposited in pairs to comprise annuli, with opacity thought to vary due to alternating composition of mineral (translucent) and organic (opaque) components (Wright *et al.* 2002; Hüssy *et al.* 2004a) although Jolivet *et al.* (2013) suggested variation in organic matrix constituents determines opacity instead. Density can also vary across increments due to differential incorporation of mineral and organic fractions (Hoff and Fuiman, 1993). Taken together, incremental changes in opacity and density create repeating patterns of discontinuities that ostensibly affect light penetration and reflective properties depending on the number and patterns of increments the light encountered. These factors can also vary according to age and environmental and nutritional conditions (Hoff and Fuiman, 1993; Hoie and Folkvord, 2006; Høie *et al.* 2008), contributing to individual variability in otolith-light interaction. Spatial heterogeneity in the distribution of elements (Izzo *et al.* 2016a; Hüssy *et al.* 2020b) as well as proteins (Vasconcelos-Filho *et al.* 2019; Thomas *et al.* 2020) have

also been revealed using new tools in 3-D visualization, helping to elucidate the complexity of the molecular architecture underlying otolith composition.

### *1.3.2 Scales*

Teleost scales, which are either ctenoid or cycloid in shape, comprise two distinct layers: the external layer, which is a mineralized layer of calcium phosphate similar to hydroxyapatite, and the basal plate, an inner layer composed of individual lamellar sheets of loosely-packed collagen fibers (Zylberberg *et al.* 1992). Scale growth generally parallels somatic growth rates (Campana and Thorrold, 2001) and occurs on different axes for the two layer types. In the external layer, growth occurs via deposition of concentric growth increments on the outer edge of the scale (i.e., widening), while the basal plate grows subsequently by addition of collagen layers to the interior of the scale from the inner focus to the external edge (i.e., thickening), a process known as underplating (Meunier, 1984; Hutchinson and Trueman, 2006). Hence, scales are thickest at the focus and thin toward the margin, and the depositional chronology of accreted material varies depending on the axis of measurement, i.e., the most recent material in the mineralized layer is deposited at the margin, but the most recent material in the basal plate is formed beneath existing layers and in proportion to the existing scale diameter. This also means that, when considering the scale as a whole, the collagenous fraction will be proportionally biased toward the most recently deposited material; thus analyses that rely on depositional timing of the non-mineral component, e.g., tracers of diet and environment partitioned in the organic fraction, accurately reflect only the most recent year of life (Hutchinson and Trueman, 2006; Kerr and Campana, 2014). Scales can be lost to trauma and regenerated, and can also be subject to resorption during times of poor

nutrition or other sources of stress such as spawning (Carragher and Sumpter, 1991), hence multiple scales must be sampled per fish to ensure the full lifespan of the fish is reflected. Resorption occurs in both the external and basal layers, although the highly-mineralized external layer appears to be resorbed first (Kacem *et al.* 2013). Resorption can cause distinctive marks on the scales, such as "spawning checks", which consist of notable discontinuities in annuli patterns (Shearer, 1992).

The unique accretion dynamics of scales as discussed above have implications for the use of scales with NIRS for age prediction. Because of their high protein content and given that proteins absorb intensely in the NIR spectrum, there is great potential that age-related compositional changes would be easily discriminated using NIRS. Scales are more translucent than otoliths in many cases and might have more uniform structure across ages, making concerns about changes in light penetration and specular reflection less apparent. As with traditional ageing methods, there is a need to sample multiple scales per fish to fully capture inherent individual variability in the calibration model, and to ensure regenerated scales are easily detectable as outliers and not included in age prediction models. Because most scales do not deposit daily growth increments (Campana and Thorrold, 2001), there may be more readily discriminated seasonal trends in scale growth over time. In species for which age estimation using scales has been vetted, NIRS has the potential to be a successful secondary method for production ageing.

*1.3.3 Vertebrae*

Calcified internal skeletal structures such as vertebrae are common alternatives for age estimation in fish species, both for bony fishes and elasmobranchs, without useable otoliths (Campana, 2001). In bony fishes, vertebrae may be cellular (osteocytic) or acellular (anosteocytic), with composition and mechanisms for bone formation and resorption differing between the two. Osteocytic bone is formed by deposition of the organic matrix by osteoblasts, which are subsequently entrapped within the bone matrix and then mineralized as part of the bone, hence comprising a portion of the final structure. The entrapped osteoblasts eventually change into osteocytes, which serve to regulate bone formation and resorption. In anosteocytic bone, the formation process is similar but osteoblasts are not entrapped, hence they are not part of the overall bone structure (Davesne *et al.* 2019). The organic matrix, known as osteoid, is made up primarily of type I collagen fibers, and the mineral component is hydroxyapatite (~ 65%) which calcifies the collagen fiber matrix (Weiss and Watabe, 1979; Mahamid *et al.* 2008). Most vertebrae of extant teleosts are anosteocytic (Moss, 1961; Davesne *et al.* 2019). Vertebrae are formed into cone-shaped (amphicoelous) centra, and generally accrete defined growth layers as the fish grows, much like the growth bands formed in otoliths and scales, although no daily bands are evident in vertebrae (Campana, 2001). Despite outward similarity, the mineral density of vertebral centra in teleosts varies both by bone type as well as spatially within individual centra of the same fish, which affects X-ray and ostensibly other light attenuation (Cohen *et al.* 2012; Ofer *et al.* 2020). Mineral density is also known to vary positionally along individual vertebral columns (Ofer *et al.* 2020), hence the standardization of location within the vertebral column should be taken

into account for any age determination method used (Campana, 2001). There is further spatial heterogeneity in the orientation of collagen fibers within individual vertebral centra, a property that is shared across bone types (Ofer *et al.* 2020). Environmental signatures from incorporation of trace elements are evident in vertebrae, but the potential for metabolic reworking or resorption is high, and more study is needed to fully evaluate their utility as environmental tracers (Kerr and Campana, 2014).

Shark vertebrae are compositionally different from those of bony fishes, and composition also varies across elasmobranch species. The primary mineral component is hydroxyapatite (39-55% by weight), which is deposited within a cartilaginous matrix of proteins comprising mainly type I and II collagens (17-27% by weight) and proteoglycans (12-28% by weight) (Rama and Chandrakasan, 1984; Michelacci and Horton, 1989; Clement, 1992; Porter, 2006). A high concentration of associated water content within vertebrae has also been reported (26-53% by weight; Porter, 2006). The level of mineralization varies across species, from highly mineralized, solid vertebrae like those of Carcharhinids, less mineralized vertebrae with diffuse radials forming the intermedialia such as Lamnids, and some deepwater sharks such as Squalids with poorly mineralized vertebra (Goldman *et al.* 2012). As in bony fish, vertebral growth bands are generally formed in elasmobranch vertebrae incrementally comprising one translucent and one opaque band pair per year (Cailliet, 1990; Cailliet and Goldman, 2004), although in poorly mineralized vertebrae growth bands might not form at all (e.g., Rigby *et al.* 2016b). However, recent studies have highlighted the functional role of elasmobranch vertebrae, i.e. structural support for the organism, in determining the timing and extent of centrum growth, as opposed to simple age-related accretion as in otoliths (Natanson *et al.*

2018b; James and Natanson, 2020); hence the assumptions that underlie the suitability of ageing structures may not be fully met in some species. Most studies that have demonstrated "missing time" in age structures have validated age through early life, and have not documented discontinuous band deposition until later years of life where somatic growth tapers off (Passerotti *et al.* 2014; Harry, 2018; Natanson *et al.* 2018a). For many species, true validation studies have not been accomplished, but these structures are still considered useful through early adulthood during the portion of the lifespan where growth is typically faster and hence growth of the age structure happens accordingly. Elasmobranch vertebrae are thought to be metabolically stable and not subject to reworking (Campana *et al.* 2002; Hale *et al.* 2006; Tillett *et al.* 2011). Elemental signatures linked to diet and environment are evident as in other structures, and are present in higher quantities than in otoliths, but the mechanisms of fractionation and incorporation are not well studied (Campana *et al.* 2002; Kerr *et al.* 2006; Kerr and Campana, 2014).

Overall, NIRS analysis of vertebrae has a high potential for discriminating age related changes simply based on their higher content of organic matrix and proteins relative to otoliths. Additionally, human bone and cartilage have been studied extensively with NIRS for assessment of composition, structural changes with age, and other physical and chemical properties (e.g., Afara *et al.* 2012; Palukuru *et al.* 2014; Ailavajhala *et al.* 2020), which could provide insights into mechanisms involved with NIRS age prediction using similar structures in fish.

*1.3.4 Fin rays and spines*

Fin rays and spines form part of the exoskeleton of fish, and can be useful for age estimation depending on species. In teleosts, fin rays and spines are acellular dermal bone primarily composed of calcium phosphate (Findeis, 1997) and are thought to form through direct mineralization of type I collagen (Bird and Mabee, 2003). Fin rays are formed of multiple calcified segments joined together with collagen fiber bundles (Montes *et al.* 1982), with new growth occurring through the life of the fish both by longitudinal growth at the distal end of segments as well as by thickening of proximal segments. The new growth forms first as a collagen network into which carbonated hydroxyapatite is subsequently deposited (Landis and Géraudie, 1990). Fin spines, of which dorsal or pectoral fin spines are typically used for ageing, are of similar structure. Fin spines vary in size and growth bands vary in their spacing and clarity depending on where along the spine the bands are read (Vilizzi, 2018). The mechanism for increment formation is the successive growth of bone tissue at different seasonal rates, becoming an ordered series of opaque and translucent bands over time (Cort, 1991; Santamaria *et al.* 2009). Opacity differences between the increments corresponds to calcium concentration, with more calcium in translucent bands than in opaque bands (Ferreira *et al.* 1999). Concurrent to growth, resorption occurs in the innermost core of the spine, resulting in a net reduction in the fraction of compact bone of the spine core with age (Santamaria *et al.* 2015). Despite this, fin rays have been used successfully to discriminate stock structure and migration patterns of sturgeons (Kerr and Campana, 2014), although additional work is needed to verify the stability of chemical signatures in spines and rays (Gillanders, 2001).

Elasmobranch fin spines are made up of dentine with differences in structure across taxa. Generally, there are three main layers: 1) an inner layer of cartilage and pulp tissue; 2) a "stem" layer comprising three dentine layers; and 3) the mantle, made up of dentine, pigment, and an external mineralized layer of enamel (Holden and Meadows, 1962; Beamish and McFarlane, 1985). Spines grow longitudinally from the base, and from the core in diameter, depositing dark ridges on the mantle corresponding to annuli (Beamish and McFarlane, 1985; Campana *et al.* 2006). Ageing in some species can be accomplished by polishing and enumerating growth bands on the exterior of whole spines, while others must be sectioned to expose growth bands. For those requiring sectioning, experimental sections must be undertaken to determine the area that contains the full record of growth across the lifespan, as banding pattern can vary longitudinally along the spine (Calis *et al.* 2005; Barnett, 2008). Spines experience wear on the distal tip opposite of the growing axis, which can confound age estimates and lead to underageing (Gillanders, 2001). Bomb radiocarbon validation has verified the conservation of spine tissue in spiny dogfish (Campana *et al.* 2006), but validation in other species is lacking, and radiometric studies have shown that spines are not a closed system in deepwater dogfish species (Cotton *et al.* 2014). Taken as a whole, the potential positional variability in banding patterns inherent in these spines will significantly impact the ability of NIRS to relate age to spectral data, depending on the way in which spines are presented for NIRS analysis (Rigby *et al.* 2014, 2019).

### 1.4 Conclusion

NIRS is a multidisciplinary method for discriminating physicochemical differences among samples, often based on very small differences, and with the ability to

do so without significant sample processing. Organic molecular bonds are the target of NIRS absorption measurements, but physical characteristics of the sample are equally as important in discrimination among samples. The skeletal structures used for age estimation in fish range widely, not only in their chemical composition, but also in their physical structure and morphology. These differences have profound implications for the use of the structures for age prediction using NIRS, and must be considered when undertaking initial proof-of-concept studies and formation of age calibration models. Complete knowledge of the chemistry underlying NIRS discrimination of age groups is not necessary in order to create predictive age models (Siesler *et al.* 2002; Rigby *et al.* 2019); however, understanding the underlying chemistry is key to understanding the experimental system as a whole, as well as for elucidating future applications of the technique to other aspects of research (Siesler *et al.* 2002).

One drawback of the NIRS approach to age prediction is its existence as a secondary method and hence, its dependence on traditional age estimates (and therefore any inaccuracies implicit in the technique) for the calibration of a species-specific model that relates spectral data to age, which is a necessary first-step before spectral data can be used alone to estimate age. NIRS age prediction will only be suitable for species and structures with existing age estimates that have been at least verified as occurring with set periodicity. NIRS cannot be applied to determine novel ages where none exist for model calibration. However, the success of preliminary studies thus far has demonstrated great potential for the application of NIRS as a routine secondary age prediction method, perhaps suitable for production ageing in fisheries management. There is also potential for its application to other aspects of fisheries research.

The focus of this dissertation is a series of studies to evaluate the use and potential mechanisms of NIRS for age estimation using otoliths of red snapper, *Lutjanus campechanus*. Red snapper is a commercially and recreationally important finfish species that is subject to intensive monitoring and management practices in the southeastern United States due to historical overfishing of the populations in both the western north Atlantic Ocean and the Gulf of Mexico. Tens of thousands of red snapper otoliths are aged each year by various fisheries management organizations, and strict regulations over the past 20 years have resulted in the rebound of the populations to harvestable levels.

In Chapter 2, I present a proof-of-concept study to evaluate the capability of NIRS to predict daily ages in otoliths of juvenile red snapper. Using traditional age estimates and NIRS spectral data collected from otoliths aged 39 – 120 days, I 1) demonstrate for the first time that NIRS accurately predicts daily ages from scans of whole otoliths, 2) evaluate the equivalence of data products formulated using NIRS-predicted and traditional ages, 3) evaluate the ability of NIRS to discriminate otolith weight from spectral data, and 4) demonstrate the use of light apertures to optimize spectral data collection from small otoliths and discuss the effects of sample presentation on NIRS analysis.

In Chapter 3, I evaluate the feasibility of using NIRS for production ageing of red snapper otoliths. Using traditional age estimates and NIRS spectral data collected from otoliths aged 0 – 38 years, I 1) evaluate the accuracy of NIRS age prediction from rapid scans of whole otoliths, 2) discuss the potential for discriminating regional signatures from otoliths of different geographical origins, 3) demonstrate the effect of changing otolith size on light attenuation and discuss the implications of this for age prediction in

large otoliths, and 4) discuss the potential benefits and caveats to implementing NIRS for production ageing in a management context.

In Chapter 4, I present the results from a series of experiments to evaluate various age-related physical and chemical aspects of otoliths potentially underlying the use of NIRS to predict age in otoliths. By comparing NIRS spectral signatures acquired from 1) whole ambient otoliths, 2) whole desiccated otoliths, 3) whole ground otoliths, and 4) subsampled fixed quantities of otolith powder, I demonstrate the mechanism of NIRS age prediction based on compositional changes in protein and calcium carbonate concentration. Further, I present novel data on ontogenetic dynamics in protein and amino acid concentrations in otoliths of red snapper. Finally, I also demonstrate the influence of otolith morphometrics and water content on age prediction and discuss the implications of these results on the further use of NIRS analyses in fisheries research.

# CHAPTER 2

# FOURIER-TRANSFORM NEAR INFRARED SPECTROSCOPY (FT-NIRS) RAPIDLY AND NONDESTRUCTIVELY PREDICTS DAILY AGE AND GROWTH IN OTOLITHS OF JUVENILE RED SNAPPER *LUTJANUS CAMPECHANUS* (POEY, 1860)[1]

[1] © Elsevier B.V. 2019. Passerotti, M.S., Jones, C.M., Swanson, C.E., Quattro, J.M. 2020. Fourier-transform near infrared spectroscopy (FT-NIRS) rapidly and non-destructively predicts daily age and growth in otoliths of juvenile red snapper *Lutjanus campechanus* (Poey, 1860). Fisheries Research 223: 105439.

Reprinted here with permission of the publisher (Appendix A).

## 2.1 Abstract

Fourier transform near infrared spectroscopy (FT-NIRS) has shown great promise as a rapid and non-destructive method for predicting age in years from a variety of ageing structures in fish. Herein we assess the utility of FT-NIRS to predict both daily age and otolith weight from whole otoliths of juvenile red snapper *Lutjanus campechanus* collected from the US Gulf of Mexico and southeastern US Atlantic Ocean. Spectral data from whole otoliths (n=153) were collected with a FT-NIR spectrometer while manipulating otolith presentation with an external aperture to maximize signal to noise. Traditional daily age estimates and otolith weights were correlated to spectral data via partial least-squares regression to create age and otolith weight prediction models that were compared across aperture treatments and geographic region. FT-NIRS calibration models using apertured spectra were significantly better at predicting age than models using non-apertured spectra (model rank=5 and 10, respectively) and yielded predicted age to within an average of six days relative to traditional estimates ($R^2$=0.91, RMSECV=6.08 days, bias = −0.04). Exponential growth models produced from FT-NIRS-predicted ages ($L_t=28.3*e^{0.01t}$) were not significantly different (likelihood ratio $\chi^2$=1.05, df=2, p=0.59) from those derived from traditional ages ($L_t=30.7*e^{0.009t}$). Additionally, FT-NIRS models were capable of predicting otolith weights that were not significantly different from direct measurements (t=1.75, df=147, p=0.08). This study is the first to demonstrate successfully the potential of FT-NIRS to predict daily age and otolith weight in juvenile fishes, as well as the first to manipulate external apertures to optimize signal to noise. These findings support the potential for broad application of FT-NIRS in fisheries biology.

## 2.2 Introduction

Estimating the daily age of larval and juvenile fishes as it relates to growth dynamics and environmental correlates is essential to under- standing the ecology of fish species, and these data are of particular value for species of management concern. Since (Pannella, 1971) first recognized daily growth increments in the otoliths of juvenile fishes and related them to age, investigations have pursued the use of daily age estimates for reconstruction of environmental, oceanographic, and feeding conditions, as well as to investigate growth and mortality effects throughout larval settlement and ontogenetic shifts (see reviews in (Campana and Neilson, 1985; Sponaugle, 2010). Where incremental deposition is verified as occurring daily for a given species, otolith microincrements are considered a treasure trove of information for determining early life history dynamics and other downstream effects.

Estimating daily age using counts of otolith microincrements is a challenging and time-consuming process. Preparing otoliths for daily age estimation requires skill with techniques involving dissection, mounting, and polishing of sometimes microscopic structures, often necessitating the use of cross-polarized light for visualization, in order to produce otoliths with discernable microincrements. In addition, expertise in interpreting microincrements as well as multiple reads and/or readers for the same otolith are necessary to achieve accurate and consistent counts (see (Secor *et al.* 1992; Sponaugle, 2010). In some cases, daily age estimates from microincrements are used in adult fish as well, where more uniform environmental conditions preclude formation of annual growth bands at various stages of adulthood. This is the case with several species of tunas, for which daily age estimates are more accurate than annual estimates

at various stages of adulthood (e.g. (Williams *et al.* 2013) presenting further challenges associated with counting large numbers of microincrements over potentially many years of life.

Fourier-transform near infrared spectroscopy (FT-NIRS) has recently been used to rapidly and non-destructively estimate annual age in several species of fish from scans of various tissues, including otoliths (Table 2.1). This technique utilizes light from the near infrared region of the electromagnetic spectrum (12800 – 4000 $cm^{-1}$ wavenumbers, 780 – 2500 nm) to evaluate organic chemical bonds present within a material (Williams, 2008). These bonds vibrate in characteristic ways when irradiated at specific frequencies and thereby absorb light, producing signature absorbance patterns representative of the composition of the sample (Murray and Williams, 1987). Comparison of these absorbance patterns, or spectrograms, among samples as they correlate with other known variables (such as age) can be used alongside multivariate statistical analysis to provide a rapid and non-destructive method of discriminating the variables of interest, e.g., age, from spectral data alone (see (Vance *et al.* 2016) for a review of applications in conservation biology).

Wedding *et al.* (2014) first demonstrated the utility of FT-NIRS for ageing saddletail snapper (*Lutjanus malabaricus*) from FT-NIRS scans of whole otoliths with a high degree of accuracy and precision relative to traditionally-estimated age in years. Robins *et al.* (2015) also investigated use of FT-NIRS for annual age estimation in barramundi (*Lates calcarifer*) and pink snapper (*Pagrus auratus*). Recently, Helser *et al.* (2019) found FT-NIRS could predict age in walleye pollock (*Gadus chalcogrammus*) otoliths with similar precision as traditional methods and, importantly,

with resolution to within less than a year relative to traditional annual age estimates. Each of these studies also demonstrated some degree of environmental or regional specificity for otolith spectra. The mechanism behind the FT-NIRS relationship with age, and to a lesser degree to regional or environmental inputs, in otoliths is not explicitly known, but Helser et al. (2019) proposed the accumulation of covalent organic bonds associated with proteins in the otolith organic matrix as one possibility for further research. One drawback of the FT-NIRS approach is the dependence on traditional age estimates (and therefore any inaccuracies implicit in the technique) for the calibration of a species-specific model that relates spectral data to age, which is a necessary first-step before spectral data can be used alone to estimate age.

Owing to the promising evidence thus far for use of FT-NIRS to predict annual age from whole otoliths, we sought to investigate the use of FT-NIRS to estimate daily ages from whole otoliths of juvenile fish. Red snapper (*Lutjanus campechanus*) is one of the most valuable finfish species in the southeastern United States, with economic impacts of $28 million from commercial landings and $47 million from recreational activities (NMFS, 2018). In addition to directed fisheries, juvenile red snapper in the Gulf of Mexico are also taken in substantial numbers as bycatch in shrimp trawl fisheries (Gutherz and Pellegrin, 1988; Ortiz *et al.* 2000; Gazey *et al.* 2008). As such, species monitoring and stock assessment activities for red snapper are substantial and include a large effort focused on the determination of age from otoliths. Studies of juvenile red snapper life history have confirmed daily growth band deposition in otoliths (Szedlmayer, 1998; Rooker *et al.* 2004), and others have documented regional and habitat-related differences in abundance, growth, and mortality which, when related

to daily age estimates, provide valuable insights for management (Workman *et al.* 2002; Rooker *et al.* 2004; Patterson *et al.* 2005; Jones, 2013; Powers *et al.* 2018). Therefore, red snapper is a worthwhile model species with which to evaluate FT-NIRS as a rapid and non-destructive method of predicting daily age from scans of whole otoliths.

Given the importance of age estimation to fisheries management, the challenges associated with obtaining traditional daily age estimates from otoliths, and the potential for FT-NIRS to improve efficiency of daily age estimation, we investigated the utility of FT-NIRS for estimating daily ages in juvenile red snapper. The objectives for this study were to 1) determine feasibility of using FT-NIRS to estimate daily age from whole otoliths of juvenile red snapper, 2) compare sample presentation methods for optimizing FT-NIRS prediction results, 3) evaluate equivalence of traditional and FT-NIRS generated ages via growth model analysis, and 4) examine factor loadings of resulting FT-NIRS models for potential underlying sources of spectral variation with age.

## 2.3 Methods

### *2.3.1 Traditional age estimation*

Whole otoliths of juvenile red snapper were obtained from archival samples, whose corresponding paired otolith was aged via traditional methods as described in Jones (2013) and Swanson et al. (in prep). Otoliths from the Jones (2013) study were collected from the US Gulf of Mexico off the Texas coast between 2006 and 2008, while those from the Swanson et al. study (in prep) were collected in 2015 and 2016 off the Florida coast in the Atlantic Ocean. For both studies, estimation of daily ages was carried out by a single reader using two independent counts of increments. In cases where

independent counts did not agree but were within 5% CV (Swanson et al. in prep) or 10% CV (Jones, 2013), the counts were averaged to obtain a final age estimate. For counts outside of these respective CV limits, a third count was made and the two counts with CVs within the respective limits were averaged to obtain a final age estimate. Age estimates with CV >10% between the closest two counts were excluded from analysis in all studies. For the purposes of the current study, final increment ages reported in Jones (2013) and Swanson et al.(in prep) are referred to as "traditionally estimated" ages that were subsequently used to inform the FT-NIRS prediction model and to produce "FT-NIRS predicted" ages.

### *2.3.2 FT-NIRS*

NIR spectral data were acquired using a Bruker Matrix-I Near Infrared Spectrometer with a 22-mm diameter sample window and OPUS 7.8 software (Bruker Scientific, Billerica, MA). Whole otoliths, which had previously been cleaned with water and stored dry for archiving, were first scanned by placing them directly on the center of the sample window, convex side down, conventionally positioned so that the rostral axis of the otolith was horizontal in relation to the sample window (e.g., see (Wedding *et al.* 2014; Robins *et al.* 2015; Helser *et al.* 2019b). A 19-mm gold-coated transflectance stamp was placed over the top of each positioned otolith to standardize the path length of NIR incident light. A total of 64 spectral scans were acquired for each otolith in each sample presentation (with and without aperture) at a frequency of 16 $cm^{-1}$ along the entire NIR spectrum (3600 – 12000 $cm^{-1}$). Scans were averaged to produce a single representative spectrogram for each sample in each presentation. Each representative spectrogram took approximately 30 seconds to produce.

Due to the small size of the otoliths in question (approximately 1.5 – 7.0-mm at the widest point), standardizing the presentation of the otoliths on the sample window was a challenge, and we hypothesized that excess stray light might confound results. As such, we designed a custom aperture fitted over the top of the sample window to constrain the light field and facilitate a standardized positioning of otoliths. The custom aperture was made using a 28-mm diameter white Teflon (PTFE) disc of 0.1-mm thickness (US Plastic Corporation, Lima, OH), through which a 2-mm hole was drilled in the center. The disc was laid directly on top of the sample window so that the aperture hole was centered (Figure 2.1), and was secured around the edges with masking tape. Otoliths were positioned on the Teflon aperture identically to the first trial, so that the convex apex of the otolith was in direct contact with the sample window via the aperture hole, and the transflectance stamp was again placed over the top. Scans were repeated as described above.

### ***2.3.3*** *Data Analyses*

All spectral data analysis was conducted using the OPUS software suite (version 7.8, Bruker Scientific). Spectrograms for all samples from both presentation trials were first inspected visually for obvious anomalous or overly noisy spectra. Those that were obviously aberrant based upon visual inspection and could not be rectified by rescanning were removed from the analysis (n = 6). Of the archival otoliths available for this study, we chose to exclude those with estimated ages greater than 120 days in order to constrain the error surrounding traditional age estimates, as well as to standardize the age ranges of the two regional sample groups. Remaining spectrograms (n = 153) and their corresponding, previously estimated increment ages were modeled using partial least

squares regression (PLSR). Background and details for statistical analysis of NIR spectral data related to otolith age, including PLSR, are well described in Wedding (2014) and Helser et al. (2019). Briefly, multivariate spectral data were fitted to traditionally-estimated otolith ages using PLSR, resulting in a calibration model putatively capable of generating a FT-NIRS-predicted age from spectral data alone. After the initial model was fitted, wavenumber selection as well as data preprocessing treatments were trialed to determine treatments and wavenumber ranges that minimized root mean square error (RMSE) of predicted ages. For this study, we determined that a first derivative Savitsky-Golay transform (17 smoothing points, polynomial order = 2) as well as vector normalization (SNV) of mean-centered data with wavenumber selection of 7506 – 4242 $cm^{-1}$ minimized RMSE for all age models. For otolith weight models, the wavenumber ranges selected were 7506 – 6101 $cm^{-1}$ and 4649 – 4242 $cm^{-1}$ with a first derivative Savitsky-Golay transform (17 smoothing points, polynomial order = 2) applied. Models were evaluated using a "leave one out" method of cross validation, whereby calibration models were produced with one sample left out and that sample subsequently tested against the model for goodness of fit. This was repeated, in turn, with each sample tested against the calibration model until all samples had been cross-validated and goodness of fit judged based on the $R^2$ (coefficient of determination), RMSECV (root mean square error of cross validation), and RPD (residual prediction deviation) values. Due to small sample size for our regional models, within-region samples were not split into separate calibration and validation sample sets, as small sample sets might promote over-confidence in validation models (Williams, 2013). For the regional "combined" models, which had more than 120 samples, we split the samples

into calibration and validation sets for a more robust measure of the predictive capability of the calibration model selected.

Prior studies have sometimes demonstrated measurable differences in NIRS predictive capabilities among different populations of the same species, possibly arising due to differences in water chemistry, condition, or growth rate (Wedding *et al.* 2014; Robins *et al.* 2015; Helser *et al.* 2019b). For this reason, we evaluated each regional sample set individually as well as combined into a single calibration model. We also evaluated the effect of the Teflon aperture on model fit for each data set. Best models were selected based upon improvements to $R^2$, RMSECV, RPD, and rank (number of model factors) over other models.

Equivalence of NIRS-predicted ages to traditionally-estimated ages was evaluated by modeling each age estimate relative to fish standard length (SL, mm) using a maximum log likelihood method (Haddon, 2001), which determined that exponential growth models provided the best fit to the length-at-age data. We tested for significant differences between resulting growth models using a likelihood ratio test (Chen *et al.* 1992; Haddon, 2001). Length-at-age models were of the form $L_t = L_0 * e^{kt}$, where $L_t$ = body length at age t, $L_0$ = length at hatch, $k$ = instantaneous rate of growth, and $t$ = age in days.

As a means of evaluating the potential underlying causation of the FT-NIRS-age relationship, we sought to examine the capability of FT-NIRS to predict otolith weight. Otolith weights were collected to the nearest milligram using a Mettler Toledo microbalance (Columbus, OH), and weights were correlated to spectral data via PLSR,

wavelength selection, and data preprocessing as outlined for age models above. Factor loadings from FT-NIRS otolith weight models were compared to those of FT-NIRS age models to determine if age-related spectral differences were driven by an otolith weight-age relationship. Equivalence of NIRS-predicted versus directly measured otolith weights was tested using Student's paired t-test on log-transformed weights, due to non-normality of raw otolith weight data (Zar, 1999). Growth model analyses were performed in Microsoft Excel 2016; all other statistical analyses were performed in R (Version 3.4.3 "kite-eating tree", 2017).

**2.4 Results**

FT-NIRS spectrograms for a total of 153 otoliths were used to evaluate prediction of daily age and the effect of the Teflon aperture (Atlantic: n = 64, age range 39 – 112 days, mean ± SD = 91.5 ± 19.5 days; Gulf of Mexico: n = 89, age range 39 – 120 days, mean ± SD = 74.4 ± 18.4 days; Figure 2.2 and Table 2.2). Overall, FT-NIRS calibration models predicted age well, but there was a strong, positive effect of the Teflon aperture on RMSE and model fit. All models predicted age to within 7.5 days or less relative to traditional ages, on average, based on RMSECV and RMSEP values. Data from Atlantic red snapper otoliths resulted in better prediction models than those from the Gulf of Mexico, especially in terms of model rank. However, the best models both with and without aperture came from the combined region data set, likely due to the increased sample size and thus modeled variability for the calibration. For non-apertured spectra, the Combined model improved $R^2$ and RPD over both regional models, although the rank and bias increased. However, the Combined Teflon model was an improvement over all other models for $R^2$, RMSECV, and RPD. Splitting the combined data set into a

calibration/validation set was not detrimental to the predictive capability of the calibration model, and the validation model produced the best fit of all the age prediction models in terms of $R^2$, RMSEP, and RPD, predicting age to within less than 6 days relative to traditional ages for the majority of samples (Figure 2.3). The Coefficient of Variation (CV) for comparing FT-NIRS-predicted ages versus traditionally estimated ages was 4.3%, which is less than the 5% CV threshold for precision typically considered acceptable for ages generated from traditional methods (Morison *et al.* 1998; Campana, 2001).

Length at age models fitted using traditional versus FT-NIRS predicted age estimates produced the following exponential growth models ($r^2$, residual squared error):

Traditional Age: $L_t = 30.7 * e^{0.009t}$ ($r^2$=0.592, RSE=0.93)

FT-NIRS Age: $L_t = 28.3 * e^{0.01t}$ ($r^2$=0.661, RSE=0.86)

Models did not differ significantly from one another ($\chi 2 = 1.05$, df = 2, p = 0.591; Figure 2.4), suggesting the FT-NIRS predicted ages are not significantly different from traditionally estimated ages for this sample set.

FT-NIRS calibration and validation models successfully predicted otolith weight to within a milligram or less for most otoliths, with excellent fit approximating a 1:1 relationship based on $R^2$, RPD, and bias metrics (Figure 2.5). FT-NIRS predicted otolith weights (mean ± SD = 0.0165g ± 0.0086g) did not differ significantly from directly measured weights (mean ± SD = 0.0163g ± 0.0085g; t = 1.746, df = 147, p = 0.082), suggesting FT-NIRS predicted otolith weights are equivalent to directly measured otolith weights for this sample set.

Use of the Teflon aperture improved the fit of FT-NIR age prediction models, especially with regard to the rank of the calibration models, and reduced RMSECV by 10 – 16% relative to models using non-apertured spectra (Table 2.2). The resulting spectral signatures of otoliths scanned with the aperture were different than those scanned without it, presumably due to the interaction of the Teflon with NIR light (Figure 2.2). However, evaluation of the spectral regions most important to the respective Combined calibration models, as identified from the composite PLSR loadings (Figure 2.6A), show that the regions that were most influential (i.e., highest amplitude in positive or negative direction) for model results are similar between aperture and non-apertured models, although the relative amplitude of peaks was different in most cases due to reduced variation in the Teflon spectra. This indicates that the use of the aperture did not change which putative molecular bonds contributed to the modeled relationship with age, but instead enhanced the signal to noise ratio to improve resolution around informative regions.

Loadings for factor 1 (describing the majority of the variance explained for each respective model) of age and otolith weight models overlapped in range and amplitude at various points (Figure 2.6B); however, specific differences are also evident. A large portion (6100 – 4650 $cm^{-1}$) of the informative range for age was not included in the model for otolith weight. Additionally, the loadings for the peak centered near 4350 $cm^{-1}$ were in opposite directions for the age model (positive) versus the otolith weight model (negative), indicating opposite associations of this spectral band to the respective predictive models.

## 2.5 Discussion

Previous studies on the use of FT-NIRS to predict age in otoliths have demonstrated capabilities in age estimation on an annual scale (Table 2.1). This study is the first to demonstrate the capability of FT-NIRS to predict age on a daily scale from juvenile fish otoliths, as well as the first published use of an aperture for improving otolith presentation to the spectrometer. Our results indicate that FT-NIRS provides a rapid, non-destructive method of accurately estimating daily age parameters but also otolith weight from whole juvenile otoliths, which has broad implications for fisheries applications and management. The ability of FT-NIRS to also predict otolith weight is also highly relevant to the further application of FT-NIRS in fisheries management, because examining the mechanism behind this capability helps shed light on the drivers of the FT-NIRS: age relationship.

Root mean square error of cross validation (RMSECV) is generally the primary diagnostic parameter, amongst others, used to select best fit FT-NIRS calibration models, where minimizing the RMSECV value is desired to achieve the highest precision of FT-NIRS predicted ages to traditional ages. However, evaluating RMSE values as a percentage of the dependent variable range gives a more standardized way to evaluate resolution and assess error across models of different ranges (Couture *et al.* 2016). Of the species investigated for annual age prediction with FT-NIRS in otoliths thus far, the best age resolution based on RMSECV values was in *L. calcarifer* with an RMSECV of 0.75 years, or 9 months (Robins et al. 2015). Based upon % RMSE, which we calculate here for all previously published NIRS age prediction models in fish (Table 2.1), the *G. chalcogrammus* age model (maximum age = 15 years) has the best age resolution at

5.2%, to which our daily age calibration model %RMSE (6.08 days/120 days maximum age = 5.1%) is equivalent despite a much smaller sample size for daily ages. While a threshold RMSE value for accepting FT-NIRS predicted ages as equivalent to traditional ages has not been discussed in published work on otolith ageing to date, the ~ 5% RMSECV resolution presented here and in Helser et al. (2019) are the lowest in the published literature thus far. Given that daily age model resolution improved when regional data sets were pooled and sample size increased, it is likely that larger sample sizes would give even better resolution of daily ages. Thus, it is apparent that FT-NIRS is capable of predicting age at a scale fine enough to be suitable for use in determining daily age from juvenile otoliths.

The use of an aperture to improve resolution of FT-NIRS age prediction in otoliths has not previously been demonstrated. A Teflon aperture has, however, been used in other applications as a means to increase resolution by reducing unwanted background exposure and improve consistency of sample presentation to the spectrometer. Min and Lee (2005) used a Teflon sheet of 3.175 mm thickness with aperture of 25 mm to reduce background interaction and standardize positioning of citrus leaves on the sample window for NIR spectroscopy to predict nitrogen content. That study also provided a correction factor to be applied to apertured-spectra in order to correct for Teflon-induced changes to absorbance signatures. This step was not necessary in our study as we did not seek to integrate spectra obtained both with and without the aperture into a single calibration model. Our results suggest that experimentation with sample presentation is important in pursuit of new applications of FT-NIRS in fisheries, especially when dealing with small samples, and that sample

presentation is likely a considerable source of variation among spectrometers and laboratories. When the sample is small relative to the sample window, it appears excess background signal can negatively impact calibration results. When using an aperture, care should be taken to properly account for its impact on spectral patterns and, if necessary, correction factors should be calculated to allow for integrating apertured and non-apertured data. The aperture used in this study was not large enough to permit scanning of the entire otolith for the largest otoliths in our sample set. As such, it might have been more advantageous to use successively larger apertures that scale with individual otolith size. However, minute differences in the characteristics of each aperture are unavoidable and could likely be a considerable source of error; for this reason, we did not manipulate aperture size per se in this study. There exist telescoping aperture fittings for use with NIR spectrometers that could overcome this concern and perhaps provide even better resolution of daily ages in small otoliths.

The potential of FT-NIRS to predict otolith weight has not been previously investigated. It seems intuitive that this correlation should exist given the known correlation of otolith weight with age owing to the incremental accretion of growth bands (e.g., Lou *et al.* 2005). The ability to predict fish length using FT-NIRS has been demonstrated in two species of shark, however, based upon scans of fin tissues (Rigby *et al.* 2014). Since FT-NIRS measures quantities and types of organic chemical bonds in materials, we expect that at least some of these quantities change in proportion to size as well as with age, although these changes might not necessarily occur in the same magnitude and/or direction.

The capability of FT-NIRS to predict age in juvenile red snapper otoliths does not appear to be solely based upon its ability to predict weight, and this 'decoupling' has manifold implications for fisheries biology. FT-NIRS age prediction models for juvenile red snapper result in better fit and lower RMSE (mean $R^2 = 0.91$, mean RMSE = 6.00; Table 2.2) than the best-fit model produced from regression of daily age with otolith weight alone ($R^2 = 0.76$, RMSE = 10.01). FT-NIRS models were also found to be better predictors of annual age than were otolith weight-at-age models in *P. auratus* (Robins et al. 2015). Examination of the first factor loadings (Figure 2.6B) for FT-NIRS predictive models for both age and otolith weight show that, while the overall range of loadings (and thus the areas of the light spectrum with highest importance to the model) are similar between the age and otolith weight models, there are differences in several important regions of the NIR spectrum. The most obvious divergence occurs between approximately 6094-5454 $cm^{-1}$, a region that factors heavily in the age model but is excluded in the otolith weight model altogether. This region is associated with O-H bonds from absorbed water within the interstitial spaces of the aragonite matrix (5160 $cm^{-1}$; Gauldie *et al.* 1998) as well as C-H and N-H bonds possibly originating from the protein matrix (Wedding, 2014; Helser et al. 2019). Loadings in opposite directions around 4350 $cm^{-1}$ also suggests there are changes in number or type of these bonds (likely C-H, N-H, or O-H bonds; (Brown *et al.* 2011, 2012; Palukuru *et al.* 2014; Roberts *et al.* 2017) occurring with age that are not associated with changes in otolith weight.

Previous studies have examined otolith weight as a more efficient and less biased corollary of age than estimates from enumerated growth bands (Boehlert, 1985; Pawson, 1990; Worthington *et al.* 1995; Matić-Skoko *et al.* 2011; Britton and Blackburn, 2014).

While most have found otolith weight to have the highest correlation with age among all otolith size measurements, generally otolith weight alone is not entirely discriminatory in its correlation with age (Francis and Campana, 2004; Steward *et al.* 2009). Indeed, multivariate models incorporating several indices of size at age (i.e., otolith weight and fish length; Brander, 1974) tend to be better corollaries of age (Fossen *et al.* 2003; Francis and Campana, 2004; Francis *et al.* 2005; Hanson and Stafford, 2017), which complements our results in suggesting other dynamics are at work in the relationship between otolith characteristics and age. More study in this area is needed, utilizing larger sample sizes and expansion of analyses to include identifying chemical constituents as they relate to age, as well as expanding investigation to include annual age classes, to better understand the dynamics and specific drivers of the relationships between FT-NIRS, otolith chemistry and age, as well as the interaction of these relationships with otolith size.

Daily incremental otolith growth occurs as alternating deposition of a translucent calcium carbonate layer (as twinned aragonite crystals) with an opaque layer of organic protein matrix rich in acidic amino acids (*e.g.* Gauldie, 1999; Morales-Nin, 2000; Hüssy and Mosegaard, 2004). While aragonite may be substituted for its polymorphs calcite or vaterite under certain conditions (Gauldie, 1993; Campana, 1999; Parmentier *et al.* 2007), this substitution is relatively rare and was not observed in otoliths used in this study based on visual inspection. The protein matrix, however, has been shown to change ontogenetically (Morales-Nin 1986a, 1986b) and also varies in composition according to the environment (Campana and Thorrold, 2001; Elsdon *et al.* 2008; Sturrock *et al.* 2012; Chang and Geffen, 2013). In addition to changes in amino acids relative to age (Morales-

Nin, 1986a; 1986b), relative protein content and the ratio of soluble: insoluble proteins have been shown to undergo ontogenetic changes (Hussy and Mosegaard, 2004). Helser et al. (2019) also posited that the accumulation of proteins within the organic matrix was a likely mechanism for age prediction with FT-NIRS spectral data of walleye pollock otoliths. Thus, the protein matrix seems the most likely driver for age-related, but not necessarily weight-related, chemical changes on a daily scale in juvenile red snapper.

The results of our study have broad application to fisheries science as well as the further use of FT-NIRS in management applications. Estimation of hatch date from increment counts in otoliths of larval and juvenile fishes is routinely used in conjunction with other metrics for evaluating fisheries recruitment dynamics over a range of time scales and influencing factors (Wright and Trippel, 2009; Buckley *et al.* 2010; Sponaugle, 2010; Johnson *et al.* 2014). Especially for species like red snapper, which are protracted spawners, the ability to discriminate among cohorts is key when evaluating the role of seasonal and environmental effects on recruitment. Given the time-consuming nature of producing daily increment counts at a production scale, the capability of FT-NIRS to generate age predictions in a fraction of the time and with improved repeatability relative to traditional methods would save significant costs and improve turnaround time for analyses while maintaining standards for age precision. Beyond larval and juvenile fish, this technique also has application to species that do not deposit easily discernable annual increments but instead must be aged via daily microincrement counts, as has been the case with tuna species such as skipjack *Katsuwonus pelamis*, yellowfin *Thunnus albacares*, albacore *T. alalunga*, bigeye *T. obesus* and Pacific bluefin tuna *T. orientalis* (*e.g.* Williams *et al.* 2013). The non-destructive nature of FT-NIRS analysis also allows

for both otoliths to be available for further study beyond simple age determination and opens opportunities for comparative analyses utilizing destructive techniques. Insights from this study regarding the relationship of FT-NIRS to both age and otolith weight further the discourse related to broader use of FT-NIRS in fisheries applications. The basis of using FT-NIRS for age determination does not lie in knowledge of the underlying chemical constitution of the tissues being analyzed; rather, it simply relies upon detection of small differences in the types and concentrations of various molecular bonds present in the sample relative to age, which could be associated with any number of molecular compounds (Siesler *et al.* 2002; Helser *et al.* 2019b; Rigby *et al.* 2019). However, as with any new method, results must be vetted and, ideally, underlying drivers understood so that any potential shortcomings can be identified. Additionally, deeper investigation into age-related changes in structural chemistry may opportunistically provide insights into new primary chemical methods for age determination not previously known to the field. Future work involving FT-NIRS application to fish age should include examination of underlying chemistry as it relates to spectral data in pursuit of understanding on both fronts, as well as continued experimentation to optimize sample presentation and determination of best practices for comparing data and results across spectrometers and laboratories.

## 2.6 Acknowledgements

We extend thanks to Joshua Brennan, Jason Erickson, Irina Benson, Dr. Thomas Helser, and Dr. Michael Myrick for helpful guidance and discussion surrounding FT-NIR methods. Allen Andrews provided insightful discussion about otolith weight and otolith chemistry. Alex Chester provided useful edits to an earlier version of the manuscript.

Funding: This work was supported by South Carolina Sea Grant [R/CF-23], an equipment grant from the College of Arts and Sciences, University of South Carolina, and funds from a SPARC Graduate Research and an ASPIRE-I grant from the Office of the Vice President for Research at the University of South Carolina.

**Table 2.1**. Calibration model results for all previously published FT-NIRS age prediction studies in fish. Unless denoted by *, results were those from the best fit model of the publication for each species. Models denoted with * were full sample models reported for the species. Wavenumber ranges ($cm^{-1}$) were taken from text where specifically outlined by the authors; otherwise, general ranges were given based upon figures within publications. $R^2$ = coefficient of determination; RMSECV = Root Mean Square Error of Cross Validation; % RMSE = RMSECV/maximum age included in cross validation model*100; Rank = number of factors in final model.

| Study | Species | Age range | Structure | n | $R^2$ | RMSECV | % RMSE | Bias | Rank | $cm^{-1}$ range |
|---|---|---|---|---|---|---|---|---|---|---|
| Wedding et al. 2014 | *Lu. malabaricus* | 1-23 yrs | Otolith | 169 | 0.93 | 1.35 | 5.8 | -0.005 | 4 | 7400 – 4000 |
| Rigby et al. 2014 | *Sq. megalops* | 5-25 yrs | Vertebrae | 97 | 0.89 | 1.85 | 7.4 | -0.004 | 4 | 9300 – 8200<br>7800 – 6800<br>4600 - 4000 |
| | | 5-25 yrs | Dorsal fin spine | 97 | 0.82 | 2.41 | 9.6 | -0.008 | 3 | 9300 – 8200<br>7800 – 6800<br>4600 - 4000 |
| | | 5-25 yrs | Fin clip | 97 | 0.76 | 2.67 | 10.7 | -0.058 | 7 | 9300 – 8200<br>7800 – 6800<br>4600 - 4000 |
| | *Sq. montalbani* | 3-31 yrs | Dorsal fin spine | 95 | 0.73 | 2.96 | 9.5 | 0.052 | 4 | 9300 – 8200<br>7800 – 6800<br>4600 - 4000 |
| Robins et al. 2015 | *La. calcarifer* * | 2-12 yrs | Otolith | 298 | 0.86 | 0.75 | 6.3 | 0.300 | 3 | 4832 – 4327 |
| | *P. auratus* * | 3-25 yrs | Otolith | 306 | 0.88 | 1.53 | 6.1 | -0.060 | 2 | 6160 – 4580 |
| Rigby et al. 2015 | *Sp. mokarran* | 0-10 yrs | Vertebrae | 76 | 0.89 | 0.87 | 8.5 | 0.012 | 5 | 9200 – 4000 |
| | *C. sorrah* | 0-10 yrs | Vertebrae | 99 | 0.84 | 0.88 | 8.9 | -0.007 | 5 | 9200 – 4000 |
| Helser et al. 2018 | *G. chalcogrammus* | 1-15 yrs | Otolith | 202 | 0.95 | 0.78 | 5.2 | 0.002 | -- | 6821–5269<br>5022–4171 |

**Table 2.2**. Results of FT-NIRS calibration/validation models for red snapper age and otolith weight prediction. SA = South Atlantic; GOM = Gulf of Mexico; Combined = SA and GOM regions combined; Teflon = samples scanned using Teflon aperture; $R^2$ = coefficient of determination; RMSECV = Root Mean Square Error of Cross Validation; % RMSE = RMSECV/maximum age included in cross validation model*100; Rank = number of factors in final model.

| **Calibration Model** | **Sample size** | **Rank** | **$R^2$** | **RMSECV** | **% RMSE** | **Bias** | **RPD** | **Slope** | **Offset** |
|---|---|---|---|---|---|---|---|---|---|
| SA | 64 | 5 | 0.87 | 6.62 | 5.9 | -0.127 | 2.76 | 0.93 | 5.23 |
| SA_Teflon | 64 | 2 | 0.90 | 5.92 | 5.3 | -0.024 | 3.08 | 0.90 | 7.41 |
| GOM | 89 | 9 | 0.85 | 7.52 | 6.3 | -0.034 | 2.58 | 0.89 | 9.71 |
| GOM_Teflon | 89 | 5 | 0.89 | 6.31 | 5.3 | -0.019 | 3.07 | 0.90 | 8.83 |
| Combined | 153 | 10 | 0.88 | 7.13 | 5.9 | -0.152 | 2.91 | 0.92 | 7.10 |
| Combined Teflon | 153 | 5 | 0.91 | 6.08 | 5.1 | -0.042 | 3.41 | 0.92 | 6.72 |
| Combined_Teflon_Calibration | 108 | 5 | 0.91 | 6.33 | 5.3 | -0.033 | 3.28 | 0.93 | 6.45 |
| Combined_Teflon_Otolith Weight_Calibration | 105 | 4 | 0.99 | 0.001 | | 1.66 e-5 | 9.51 | 0.99 | 0.00 |
| **Validation Model** | **Sample size** | **Rank** | **$R^2$** | **RMSEP** | | **Bias** | **RPD** | **Slope** | **Offset** |
| Combined_Teflon_Validation | 45 | 5 | 0.92 | 5.61 | | -0.343 | 3.64 | 0.90 | 8.88 |
| Combined_Teflon_Otolith Weight_Validation | 44 | 4 | 0.98 | 0.001 | | 0.001 | 7.78 | 0.96 | 0.00 |

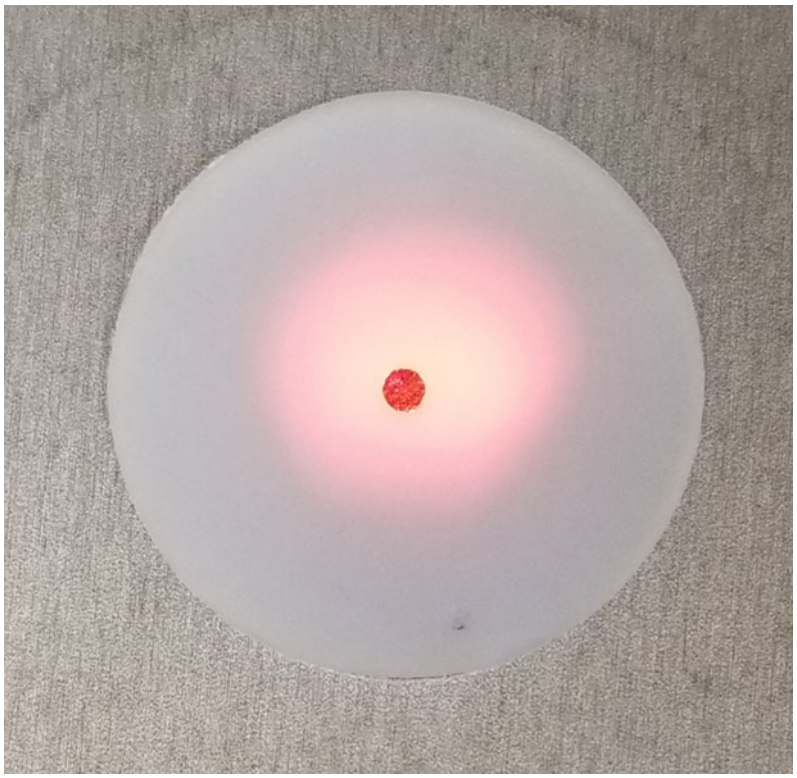

**Figure 2.1**. Teflon disk with 2mm aperture aligned over spectrometer window. Otoliths were placed in aperture opening and a transflectance cap placed on top for scanning.

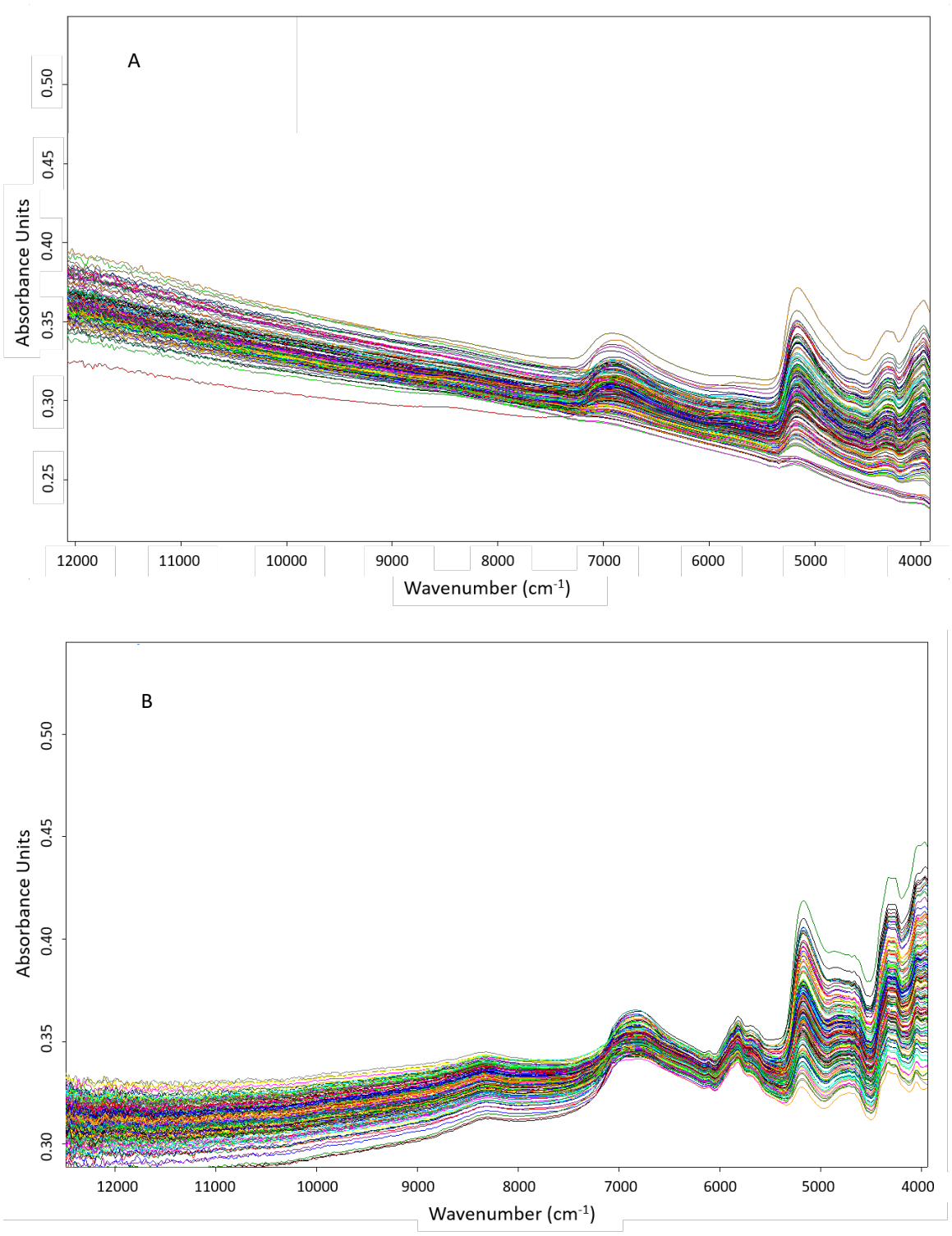


**Figure 2.2.** Spectrograms of 153 red snapper otoliths collected with A) no aperture and B) Teflon aperture.

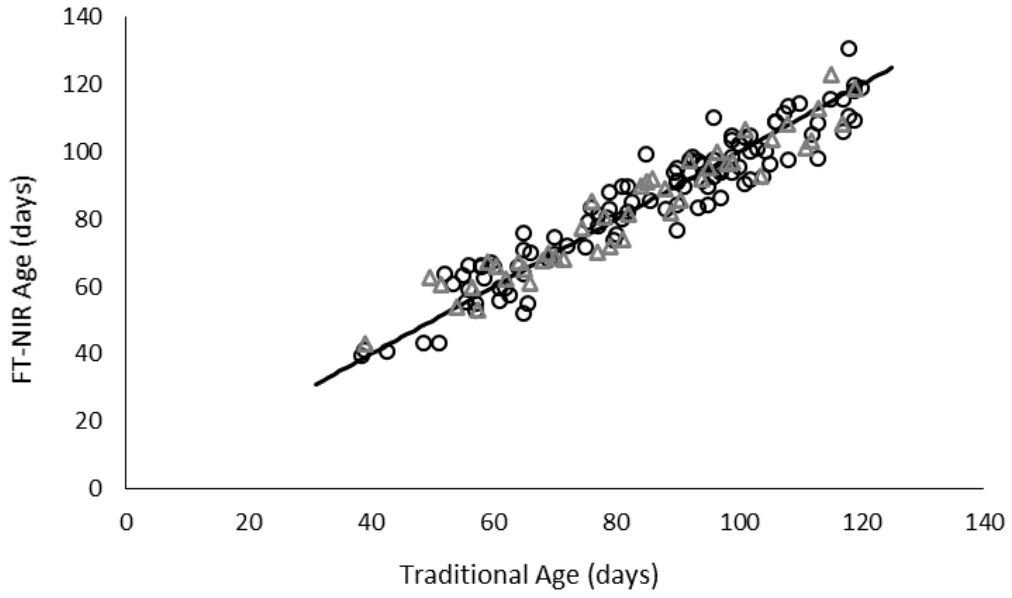


**Figure 2.3.** Calibration (black circles) and validation (grey triangles) model results of FT-NIR predicted ages relative to traditional ages. Black line is 1:1 line for reference.

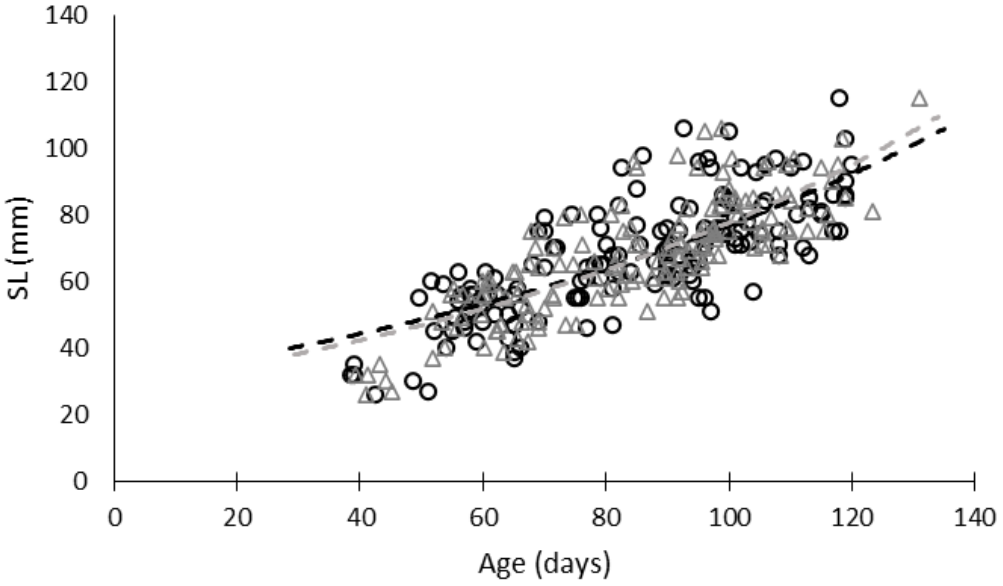


**Figure 2.4.** Length-at-age models calculated from traditional (black dashes) and FT-NIRS predicted (grey dashes) ages plotted against observed standard length (SL) at traditional (black circles) and FT-NIRS predicted (grey triangles) ages.

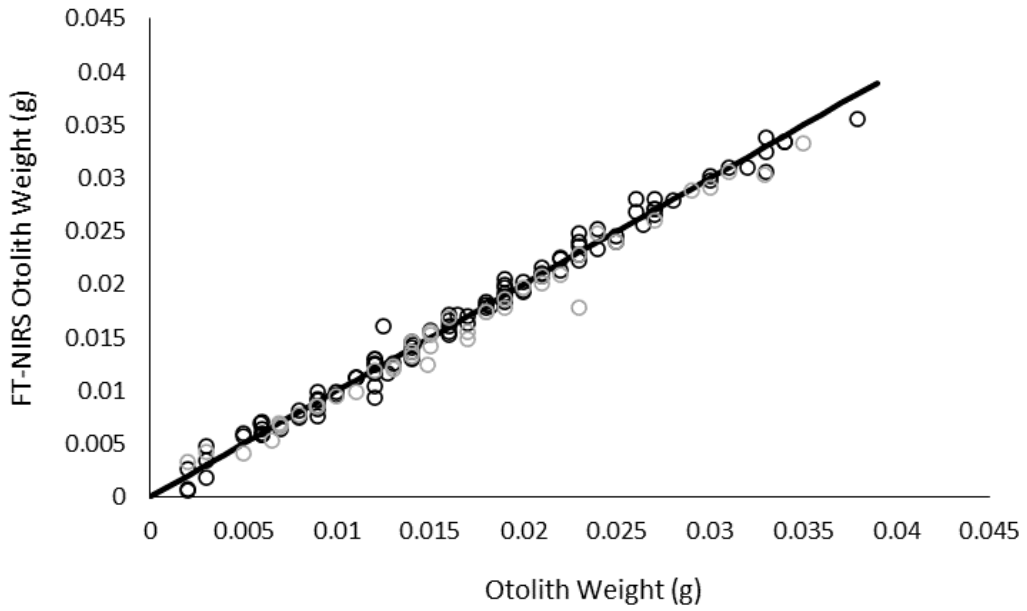


**Figure 2.5.** Calibration (black circles) and validation (grey circles) model results of FT-NIR predicted otolith weights relative to directly measured otolith weights. Black line is 1:1 for reference.

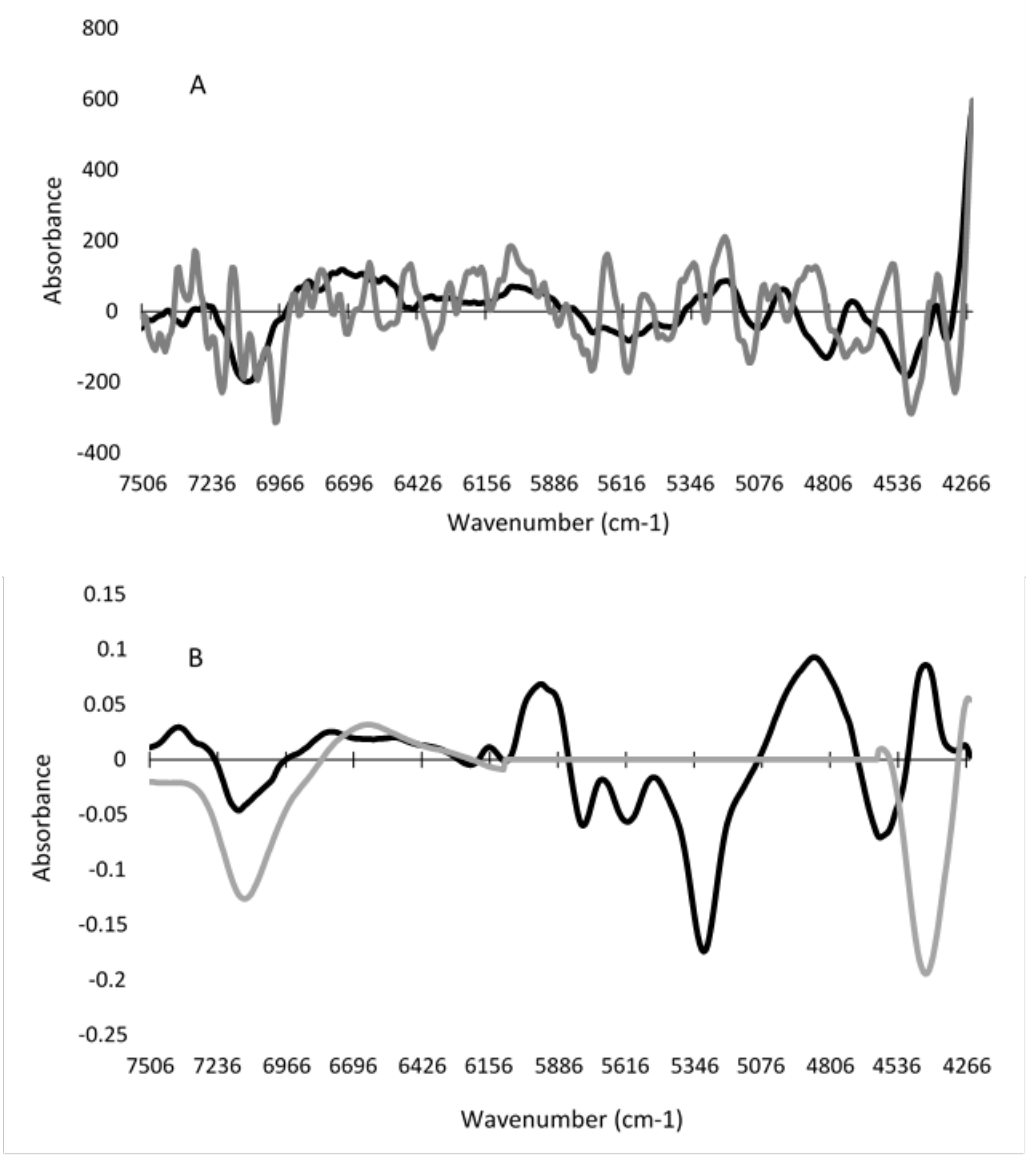


**Figure 2.6**. Loadings plots of preprocessed FT-NIRS prediction models corresponding to A) overall regression coefficients for non-apertured (gray line) and Teflon-apertured age (black line) for Combined regional models, and B) Factor 1 loadings for age (black line) and otolith weight (grey line) models for the Combined Teflon model.

# CHAPTER 3

# AGE ESTIMATION OF RED SNAPPER (*LUTJANUS CAMPECHANUS*) USING FT-NIR SPECTROSCOPY: FEASIBILITY OF APPLICATION TO PRODUCTION AGEING FOR MANAGEMENT[2]

[2]  Passerotti, M. S., Helser, T. E., Benson, I. M., Barnett, B. K., Ballenger, J. C., Bubley, W. J., Reichert, M. J. M. 2020. Age estimation of red snapper (*Lutjanus campechanus*) using FT-NIR spectroscopy: feasibility of application to production ageing for management. ICES Journal of Marine Science 7(6): 2144-2156.

Reprinted here with permission of the publisher (Appendix A).

## 3.1 Abstract

Recent application of Fourier transform near infrared spectroscopy (FT-NIRS) to predict age in fish otoliths has gained attention among fisheries managers as a potential alternative to costly production ageing of managed species. We assessed age prediction capability of FT-NIRS scans in whole otoliths from red snapper, *Lutjanus campechanus*, collected from the US Gulf of Mexico (GOM) and US Atlantic Ocean (SA). Otoliths were scanned with a FT-NIR spectrometer and resulting spectral signatures were regressed with traditionally estimated ages via partial least squares regression to produce calibration models, which were validated for predictive capability against test sets of otoliths. Calibration models successfully predicted age with $R^2$ ranging 0.94-0.95, mean squared error ≤ 1.8 years, and bias < 0.02 years. Percent agreement (PA) between FT-NIRS and traditional ages was lower than within-reader agreement for traditional estimates, but average percent error (APE) was similar and Kolmogorov-Smirnov (K-S) tests were not significantly different ($p \geq 0.06$) between traditional and FT-NIRS predicted ages for optimal calibration models. Ages > 31 years were not well predicted, possibly due to light attenuation in the thickest otoliths. Our results suggest FT-NIRS can improve efficiency in production ageing for fisheries management while maintaining data quality standards.

## 3.2. Introduction

Age estimation of marine fishes for use in management is one of the costliest elements of the fisheries stock assessment process in terms of both money and time expenditures. In the US, production ageing of hundreds of managed species is carried out on a continuous basis by both federal and state agencies, often comprising numerous age

readers and methodologies to compile estimates for hundreds of thousands of fish per year (Campana and Thorrold, 2001; Helser *et al.* 2019b). Processing of ageing structures, usually otoliths, might entail embedding in resin, thin sectioning, mounting sections on slides, and enumerations of growth bands by multiple readers to generate age estimates. The total time expenditure can average hours per specimen and be subject to reader bias on varying scales depending on the methodology, experience, and training of readers (Campana, 2001).

Fourier transform near infrared spectroscopy (FT-NIRS) is a non-destructive light spectroscopy technique that has been used in agriculture and pharmaceuticals for several decades (Reich, 2005) and more recently has been applied to wildlife biology (Vance *et al.* 2016). FT-NIRS passes light from the near infrared (NIR) region through a sample, and the interaction of this light with the sample over the length of the NIR spectrum forms a "spectral signature" of absorbance measurements at each wavelength (or wavenumber), which indicates the presence and quantity of organic chemical bonds contained within the sample, namely CH, -OH, -NH, and -SH (Murray and Williams, 1987; Williams, 2008). In biological applications, spectral signatures acquired from various species have been correlated with variables such as age in mosquitos (Mayagaya *et al.* 2009; Sikulu-Lord *et al.* 2016; Lambert *et al.* 2018), sex in frogs (Vance *et al.* 2014), and fecal content in mammals (Tolleson *et al.* 2005; Wiedower *et al.* 2012), enabling diagnostic tools for predicting these metrics based on spectral data alone.

Rapid age estimation in fish using FT-NIRS scans of whole ageing structures has the potential to revolutionize the way age estimates are produced for fisheries stock assessment (Rigby *et al.* 2014; Wedding *et al.* 2014; Robins *et al.* 2015; Rigby *et al.*

2016a; Helser *et al.* 2019b; Passerotti *et al.* 2020b). Application of FT-NIRS technology to fish age estimation uses a calibration set of otoliths with associated traditionally-estimated ages to "train" a predictive model using NIR spectral data as a response. The set of spectral data is then evaluated using multivariate partial least squares (PLS) regression to correlate spectral signatures with age. This process produces a linear correlation model to predict age of a fish based on a rapid scan (usually ≤ 60 seconds) of a whole otolith. Ideally, the calibration model should incorporate as much age-related spectral variation as possible, so that its subsequent prediction ability is robust. In order to evaluate the predictive capability of the calibration model, both an internal cross-validation and an external validation using a separate test set of otoliths is ideal (Williams, 2008). The potential impact of this technology on the production ageing process for fisheries stock assessment, both in turnaround time and cost, is significant (Robins *et al.* 2015; Helser *et al.* 2019b). To this end, US federal management entities are actively vetting incorporation of FT-NIRS into current stock assessment processes (Helser *et al.* 2019b) and recommendations have been made to pursue use of FT-NIRS for improving the scope and timing of production ageing for managed species (SEDAR, 2020).

While published FT-NIRS age estimates suggest prediction error rates similar to traditional age estimation, further comparison of FT-NIRS predicted ages to traditional ages in the context of age data products used in fisheries stock assessment models has not been published. Comparisons of percent agreement and bias from FT-NIRS-acquired data and traditional age readers are similar in scale and have been reported by Helser *et al.*(2019a) and Rigby *et al.* (2014, 2016a). Similarly, Rigby *et al.* (2016a), and Passerotti

*et al.* (2020) used FT-NIRS predicted ages to create growth models for comparison to traditional age-length data. Further translation of FT-NIRS ages, for example to age composition for use in catch-at age models, has not been published. Additionally, basic information as it relates to the physical properties of ageing structures interrogated by the approach (depth of NIR light penetration, for instance) is lacking.

Red snapper *Lutjanus campechanus* are a long-lived (50+ years) sub-tropical reef fish species found in the western Atlantic Ocean and throughout the Gulf of Mexico (GOM) (Nelson and Manooch, 1982; Manooch and Potts, 1997) for which ageing methods have been validated with the bomb radiocarbon $\Delta^{14}C$ chronometer (Baker and Wilson, 2001; Barnett *et al.* 2018; Andrews *et al.* 2019). In the southeastern United States, it is one of the most commercially and recreationally important marine finfish species, accounting annually for over $20 million in commercial landings and nearly $50 million in economic impacts from the recreational fishery, mostly in the US GOM (NMFS, 2018). This species is federally managed as two separate stocks, the US GOM and southern US Atlantic Ocean (SA), with the GOM stock further subdivided into eastern and western subunits with a line of demarcation at the Mississippi River (Figure 1, modified from SEDAR, 2008). The regulatory history of red snapper has been complex, contentious, and costly (Cowan, 2011), requiring a large investment of effort and time to collect and process increasing numbers of biological samples to be used as assessment model inputs. In the most recent GOM red snapper stock assessment (SEDAR 52; SEDAR, 2018) nearly 50,000 new age estimates were produced over four years from fish collected from the US GOM region alone (Lombardi, 2017) at an enormous cost in terms of time and money. Though fewer red snapper are collected in

the Atlantic region (SEDAR, 2017; NMFS, 2018), over 10,000 SA ages have been produced in the last five years (M. Reichert, personal communication).

Given the high costs of producing age estimates on the scale and timeline needed for management of red snapper, and the potential of FT-NIRS to generate ages for use in management, we evaluated the capability of FT-NIRS to predict age from whole otoliths of red snapper in the context of production ageing across regional stocks. Further, we report novel experimental results evaluating the depth of NIR light penetration in otoliths of varying size and age, which has not been previously documented but represents a necessary step forward to determining the physical focus (or foci) of the NIRS/age correlation.

## 3.3. Methods

### *3.3.1 Sample selection*

Sagittal otolith samples used in this study were compiled from archival fishery-independent collections of red snapper collected from the US Gulf of Mexico (GOM) and southeastern US Atlantic Ocean (SA). GOM samples were collected for the NOAA Southeast Fisheries Science Center, Panama City Laboratory, and herein are further subdivided into eastern GOM (EGOM) and western GOM (WGOM) sample sets according to catch location and geographic designations for subunits of the GOM stock as defined by federal stock assessments (SEDAR, 2008; Figure 3.1). SA samples were collected by the South Carolina Department of Natural Resources (SCDNR), Marine Resources Research Institute, as part of the Southeast Reef Fish Survey (SERFS) and Marine Resources Monitoring Assessment and Prediction (MARMAP) sampling

programs. Generally, fishery-independent sources collect both right and left sagittal otoliths; left otoliths are typically sectioned for ageing, leaving the right otolith available for FT-NIRS. For this study, otoliths were selected to equalize sample sizes across regions while maintaining a similar range of collection years (GOM: 2011-2016, SA: 2011-2017). A notable exception was the inclusion of the two oldest otoliths aged 35 and 38 years, both from the SA. These otoliths were collected in 1997, but because otoliths of advanced age (generally 30+) were not available within the constrained collection years, we included them for evaluation of FT-NIRS age prediction for long-lived individuals.

We selected separate calibration and test sets of otoliths from each geographic region for comparison: EGOM, WGOM, and SA. Calibration sets were selected to approximate a uniform distribution within regions, with relatively even numbers of samples (n~10 per age class) across all available age classes, where possible. Test sets of otoliths for each region were chosen at random from the same sampling years to mirror a typical age structure for each population (Figure 3.2). Otoliths were stored dry in coin envelopes after collection, and were wiped clean with ethanol and air dried for at least 48 hours prior to FT-NIR data acquisition.

### *3.3.2 Traditional Age Estimation*

For each otolith used in FT-NIRS analysis, a traditional calendar age estimate, or reference value, was available from the paired otolith and was generated using methods as outlined in (SEDAR, 2015) for GOM otoliths and in Wyanski *et al.*(2015) for SA otoliths. All otoliths were independently aged by at least two age readers. Only those ages obtaining consensus were included in this analysis. For GOM age estimates, three independent age readings were available for each otolith, and only estimates where at

least two of three counts agreed were used. For SA age estimates, two age readers performed independent counts, and for those that did not initially agree, consensus was subsequently obtained or else the sample was excluded from the analysis. Because red snapper are protracted spawners, calculation of calendar age requires information on increment count (i.e., number of annuli), month of capture, edge type, and month of increment formation using the conditional formula (Potts, 2009; Allman *et al.* 2012):

$$\text{Calendar Age} = \begin{cases} \text{Increment \#} & \text{Month} \geq \text{July} \\ \text{Increment \#} & \text{Month} < \text{July and Narrow Translucent Edge} \\ \text{Increment \#} + 1 & \text{Month} < \text{July and Wide Translucent Edge} \end{cases}.$$

*3.3.3 Spectral Data Collection*

Spectral data were collected with a Bruker Matrix I FT-NIR spectrometer (Bruker Scientific, Billerica, MA). Whole otoliths were positioned convex-side down in the middle of the sample window with the rostral axis positioned horizontally relative to the sample window (see Robins et al. 2015, for detailed description and pictures of scanning setup). A gold-coated transflectance cap was placed over the top of the otolith to reduce stray light entering the detector. A total of 64 spectral scans were acquired for each otolith at a frequency of 16 $cm^{-1}$ along the entire NIR spectrum (3,600 – 12,000 $cm^{-1}$) and scans were averaged to produce a single representative spectrogram for each sample. Each spectrogram took approximately 30 seconds to produce. Principal components analysis (PCA) was used for data visualization and outlier detection within the PLS regression process. Spectral data analysis was conducted using the OPUS software suite (version 7.8, Bruker Scientific, Billerica, MA).

*3.3.4 Data pre-processing and model selection*

For each calibration model, multivariate spectral data were fitted to traditionally-estimated otolith ages using PLS regression (Chen and Wang, 2001). Models were evaluated for age prediction capability using a "leave one out" method of cross validation, whereby calibration models were produced with one or more samples left out and those samples subsequently tested against the model for goodness of fit. This was repeated, in turn, with each sample tested against its calibration model until all samples had been cross-validated and goodness of fit was judged based on the $R^2$ (coefficient of determination), RMSECV (root mean square error of cross validation), and RPD (residual prediction deviation) values. RPD values of 3 or higher are generally accepted as "good" from a chemometrics standpoint (Williams, 2008). Wavenumber selection and data preprocessing treatments were compared to determine treatments and wavenumber ranges that minimized RMSECV of predicted ages, resulting in an optimized model capable of generating FT-NIRS-predicted ages from spectral data alone. Loadings plots were evaluated and noisy regions of the spectrum were excluded to yield optimized wavenumber selection. In addition to standalone regional calibration models (EGOM, WGOM, SA), we also tested combined GOM (WGOM and EGOM) and All Regions Combined (WGOM, EGOM, and SA combined) calibrations. Once final calibration models were chosen for each region, calendar ages for test sets of otoliths were predicted by each calibration model in turn, and model fits compared to determine the optimal prediction model for each test set. We also calculated % RMSE = (RMSE/maximum age*100) to evaluate standardized model error in the context of the maximum age included in the model (Couture *et al.* 2016; Passerotti *et al.* 2020b).

Samples in the oldest age classes were underrepresented as our pooled samples contained only two samples beyond 31 years. In forming calibration models, including these rare, older otoliths in the SA and All Regions Combined models caused differences in both model performance and in the pre-processing required to yield optimum age prediction. This could be due to one or more factors: the different collection year for older otoliths, some physical or chemical difference in the otolith-NIR light interaction for these samples, or simply reduced model performance due to inconsistency of sample distribution. As such, we compared optimized calibration models that either included ("SA Complete" and "All Regions Complete") or did not include ("SA Truncated" and "All Regions Truncated") the oldest two samples to assess how their inclusion affected the subsequent models' predictive capability. For all models except the two "Complete" models, spectral data were preprocessed by mean-centering followed by transformation using the Savitsky-Golay first derivative with 17 smoothing points (polynomial order = 2), which corrects for baseline shifts due to light scatter from differences in particle size and perhaps other physical differences among samples. "Complete" models, those including the two oldest fish, were optimized using only wavelength selection with no further preprocessing, as this data treatment yielded better model results than any preprocessing regime in which spectral data were transformed.

*3.3.5 Bias estimates*

Relative bias was compared between FT-NIRS predicted ages and traditional age estimates (FT-NIRS bias), as well as between individual reader ages comprising the traditional age estimates (reader bias). FT-NIRS ages predicted from calibration models are produced as continuous numbers rather than integer ages, hence comparison of

calendar age estimates between methods required rounding raw FT-NIRS ages to the nearest integer. Relative Bias (B) was calculated for FT-NIRS ages as $B^{FT\text{-}NIRS} = Age^{FT\text{-}NIRS} - Age^{Traditional}$ and for traditional ages as $B^{Trad} = Age^{Reader1} - Age^{Reader\,2}$ (Helser *et al.* 2019b). Percent agreement (PA) and average percent error (APE, Beamish and Fournier, 1981) were calculated for both types of ages for comparison using the FSA package in R (Ogle *et al.* 2018). To further evaluate the capability of FT-NIRS to generate age compositions similar to those used to inform management, we tested for differences ($\alpha = 0.05$) in test-set sample age distributions derived from FT-NIRS predicted- and traditional-age data using a two-sided Kolgomorov-Smirnov (K-S) test on ages output for each test/calibration set combination.

*3.3.6 Light Penetration*

Given the differences in model performance and preprocessing requirements for the oldest samples, and the constraint given sample availability that we could not experimentally change collection year or sample distribution to test for their effects on model performance, we chose to evaluate whether NIR light penetration is attenuated in older, thicker otoliths, which could lead to age underestimation and differences in preprocessing requirements for best predicting age in these otoliths. We selected a subset of 58 otoliths from the SA ranging 1 - 38 years in age, measured thickness of the otoliths through the core region using calipers, and tested for a distinct chemical signature (polystyrene) on the distal concave surface of the whole otolith as detected by NIR light penetration through the otolith core. Otoliths were positioned on the sample window as previously described and a 5-mm diameter polystyrene disc was placed on top of the otolith, directly over the core area. Polystyrene was chosen because it provides a distinct

FT-NIR signature detectable even in the presence of otolith signatures. Otoliths were scanned as described earlier and spectra were evaluated for differences in signatures with and without polystyrene. Spectra were transformed using a Savitsky-Golay first derivative with 17 smoothing points (polynomial order = 2) and wavelength range was reduced to select the regions where the polystyrene spectral signature was most easily differentiated from that of otoliths based on their respective individual signatures. PCA was used to discriminate presence or absence of a polystyrene signature. Analyses were carried out using the Conformity package within OPUS (version 7.8) and The Unscrambler 10.2 (Camo Analytics).

### 3.4 Results

A total of 1,357 otoliths were included in FT-NIR age prediction analyses across all regions (WGOM: n = 354, EGOM: n = 311, SA: n = 692). PCA analysis of preprocessed spectral data for all otoliths showed no discernible separation due to region (Figure 3.3a). The first two principal components (PCs) explained 98% of the spectral variation among otoliths; in contrast, the first two PCs explained only 84% of the spectral variation amongst age groups (Figure 3.3b). Most FT-NIRS age calibration models required 6 – 8 PCs (model rank) to maximize predictive power (Table 3.1), suggesting spectral differences explaining less than 2% of the overall variance played a substantial role in successful age prediction.

All calibration models performed well, predicting traditional calendar age with $R^2$ = 0.94 – 0.95, RMSECV ≤ 1.8 years, bias < 0.02, and RPD > 4 (Table 3.1; Figure 3.4). Although some differences in prediction capability were apparent among regional calibrations, the All Regions Combined models generally performed at or above the level

of the regional models and predicted age to within about 1.5 years with minimal bias and favorable RPD scores. Additionally, % RMSE for the All Regions Combined Complete model was lower than nearly all other calibrations, owing to the larger age range included in the Complete models. Informative spectra did exhibit some variation between the two regions, but overall were similar to each other in range (Figure 3.5).

The lack of regional spectral differentiation and the equivalence of calibration models is compelling; hence for clarity and brevity, we will discuss test set results for all regions combined as predicted by the All Regions Combined calibration models only, although full results from pairwise validation of regional test set/calibration model combinations are provided in Table S1 for reference. Combined test set ages were predicted well by both All Regions Combined models, with $R^2 = 0.92$ and RMSEP ~ 1.00, meaning at least 67% of ages were predicted to within a year or less relative to traditional age (Table 3.2, Figure 3.6). Of the two models, the All Regions Truncated calibration optimized all parameters for combined test set ages.

Bias between FT-NIRS and traditional ages was similar overall for all test sets (Tables 3.2, 3.S1), therefore only results for the All Regions Truncated model are plotted. Mean FT-NIR bias ± SD by age class overlapped reader bias across most ages (Figure 3.7). FT-NIRS bias increased at older ages over that of traditional age estimates, but otherwise mean bias was equivalent between ageing methods. Overall, percent agreement (PA) was lower for FT-NIRS ages relative to between-reader agreement for traditional ages (Figure 3.8), with FT-NIRS PA ± 1 year = 87.1% and traditional between-reader PA ± 1 year = 93.4%. Between-reader APE varied by region (GOM = 4.71%, SA = 9.70%, Combined = 6.97%), and was lower than FT-NIRS generated values

(Tables 3.2, 3.S1). Age distribution of FT-NIRS ages did not differ significantly from that of traditional ages for validations where RMSEP was minimized and PA maximized (Tables 3.2 and 3.S1, Figure 3.9). For nearly all test sets, this corresponded to validation with the All Regions Truncated calibration model. Combined test set ages predicted with the All Regions Complete calibration were significantly different than traditional estimates ($p = 0.004$).

### *3.4.1 Light Penetration*

Ages up to 38 years were cross-validated in the SA Complete and All Regions Combined Complete calibration models, comprising the oldest otoliths assessed for FT-NIR age estimation to date, and the lowest % RMSE for annually aged otolith calibrations published to date (Table 3.1, Figure 3.4e and g; Passerotti *et al.* 2020). Optimization of Complete age prediction models was achieved by using raw spectral data, that is, spectral data that had undergone no data transformations or smoothing algorithms (preprocessing). Conversely, all other models presented were optimized using mean-centering and first derivative Savitsky-Golay transformations. Preprocessed Complete calibration models were characterized by higher offset (SA: 0.70, All Regions: 0.59), lower slope (SA: 0.90, All Regions: 0.93), reduced RMSECV (SA: 1.68, All Regions: 1.67), and greater bias at age classes ≥ 28 years (i.e., mean bias ± SD: SA preprocessed = 7.1 ± 3.6 years, SA no preprocessing = 4.3 ± 3.1 years) relative to the un-preprocessed models ultimately used for cross-validation (Table 3.1). Despite excellent predictive ability based on PLS regression model metrics, ages of the oldest two otoliths (35 and 38 years old) were under-predicted in both Complete calibration models, in the SA Complete by 7.9 and 4.5 years and All Regions Complete by 6.6 and 3.3 years,

respectively. Given that these un-preprocessed models used physical differences in light scatter to improve predictive capability, light penetration may have played a role in FT-NIR age prediction of the 35 - and 38 – year-old otoliths.

Otolith thickness ranged from 2.1 – 5.9 mm and increased with age (Figure 3.10). Raw spectra for otoliths both with and without the polystyrene disc, as well as the raw spectrum for polystyrene, are plotted in Figure 3.11a. The polystyrene spectrum has a unique and characteristic peak at 5950 $cm^{-1}$ which is easily discernable relative to the typical otolith spectrum in both position and magnitude. Generally, otolith spectra increase in magnitude with increasing fish age (although not absolutely), and the polystyrene signal at 5950 $cm^{-1}$ became attenuated as the magnitude of raw spectra increased. Preprocessing improved spectral differentiation between treatments (Figure 3.11b), and a PCA of preprocessed spectra by treatment is presented in Figure 3.12. Differentiation is apparent between disc and no-disc spectra, except for SA239, the 38 – year old fish with the thickest otolith, for which the "disc" spectrum overlaps the "no-disc" grouping as segregated along PC 1. While there was some separation of SA239 disc vs SA239 no-disc scores, the fact that the SA239 disc spectrum could not be distinguished from other no-disc scores suggests the polystyrene signal is not detectable, hence NIR light penetration is likely attenuated in this otolith.

**3.5 Discussion**

These results provide a baseline of understanding for application of FT-NIRS to otolith age prediction across multiple stocks of red snapper and make a compelling case for the feasibility of incorporating FT-NIRS estimated ages into fish stock assessments for management. Calibration models predicted ages that were highly correlated to and

within a year or less for the majority of test set samples relative to traditionally estimated ages in fish ranging 0 – 31 years, lending further credibility to use of FT-NIRS for ageing based on the example of shorter-lived pollock in Helser *et al.*(2019a). When translated into error terms more typically associated with age estimation error in fisheries, absolute PA for red snapper FT-NIRS predicted ages ranged 43 - 53%, with PA within ± 1 year of 87 - 89% and APE values ≤ 10% relative to traditional ages. While PA was lower than most published between-reader values (i.e., Baker and Wilson, 2001; Wilson and Nieland, 2001; White and Palmer, 2004), PA ± 1-year herein approached the ~90% ± 1-year agreement reported for sub-sampled production ages in the GOM (Allman *et al.* 2002). APE values were typical relative to between-reader error in production ageing. In many cases for typical production ageing in the GOM, only one age estimate might be generated for an otolith due to time constraints. As such, the only measure of error for a given set of production ages might be those derived from counts of reference collections shared between ageing facilities. In the most recent assessment (SEDAR 52; SEDAR, 2018), a GOM reference collection was reported to have within-lab APEs ranging 1 – 7% for ageing facilities across the region (Lombardi, 2017), and APEs ranging 2.5 – 11.6 % were reported in other calibration studies of the region (Allman *et al.* 2002, 2005). A similar reference collection of Atlantic red snapper otoliths aged across three production ageing laboratories produced an APE of ~11% (SFB-NMFS, 2015). Because we only used otoliths with available consensus ages for this study, bias estimates for traditional ages herein are likely underestimated relative to ages typically supplied for management. Further, age class distribution was not significantly different for FT-NIRS ages relative to traditional estimates, which solidifies the potential use of FT-NIRS ages to generate stock

assessment information such as mortality estimates. In all, FT-NIRS shows overt promise to improve efficiency in production ageing for fisheries management by greatly reducing time and effort while maintaining data quality standards.

Improvements in efficiency for FT-NIRS age estimation over traditional methods are substantial, particularly because as long as otoliths are clean and dried to ambient conditions, little preparation is required to collect spectral data (Robins *et al.* 2015). In contrast, traditional age estimation protocols for red snapper require thin sectioning, mounting, and polishing of sections before band enumeration can be performed (VanderKooy, 2009). Realistically, a few hundred otoliths can be processed and aged in a typical work week using traditional methods. With FT-NIRS, each scan takes approximately 30 seconds using the spectrometer and settings in the current study. Depending on the setup of the scanning system, manipulating samples on and off the spectrometer can add about 1 additional minute. Under optimized efficiency, spectral data collection for the 1,357 otoliths analyzed in this study could be accomplished in 34 hours. Some spectrometers have sample wheels that can be automated to rotate a series of samples over the sample window, which might further improve efficiency of scanning (Robins *et al.* (2015) provides more details regarding spectrometer cost and setup options). Model building and selection of optimum calibration models based on reference collections add additional time considerations to implementation of the FT-NIRS method. Because outcomes benefit from having calibration models encompassing the full range of spectral variability possible, one potential scenario for operationalizing FT-NIRS might be to scan all archival specimens to develop initial optimized calibrations on a species/region/temporal case-by-case basis, and then re-evaluate models on a rolling

basis as new years of otolith collections are added. Estimating ages traditionally for a subset of collections each year would provide calibration data for model comparisons and create a checkpoint for quality control.

Current understanding of the underlying drivers of FT-NIRS age prediction are lacking, but it has been suggested that age-related changes to the otolith protein or organic matrix are a likely mechanism (Helser *et al.* 2019a). Red snapper age prediction models generally relied on spectral regions between 7600 – 4100 $cm^{-1}$, a reduced region relative to the entire spectrum interrogated (12000 – 4000 $cm^{-1}$), with some model-specific variation in importance of different signals occurring throughout that range. These reduced regions roughly correspond to various -CH, -OH, and -NH bonds, and are similar to important age-predictive regions from other otolith age prediction models (Wedding *et al.* 2014; Robins *et al.* 2015; Helser *et al.* 2019b) including juvenile red snapper (Passerotti *et al.* 2020b). Ostensibly, otoliths record variability in both environment and fish physiology, and chemical changes might be associated with the crystal lattice, deposition of the organic layer, or both, depending on the molecule (i.e., Campana, 1999; Izzo *et al.* 2016; Thomas *et al.* 2017; Thomas and Swearer, 2019). The assumption that FT-NIRS detects all chemical changes, and that the changes are definable with age, requires further confirmation. Environment and physiology can interact with otolith morphometrics to create spatial heterogeneity in otolith chemistry within individual structures (Sturrock *et al.* 2015; Limburg and Elfman, 2017; Vasconcelos-Filho *et al.* 2019), which could also play a role in age-related patterns in FT-NIRS signatures. Further work is needed to define age-related physicochemical patterns in otoliths as related to changes in the FT-NIRS signature.

Region did not explain most of the variation in otolith spectral signatures based on PCA, although age prediction model outcomes did vary by region. Hence, the regional differences in calibration model performance likely stem from an interaction of regional differences in sample size and ageing precision for traditional reference ages, and temporal variation included in the growth history of otoliths. Environmental variability between regions could also play a role in regional model performance, despite best efforts to minimize this by constraining of sampling years. The SA sample sets included an additional year of collections (2017) as well as the two oldest otoliths collected in 1997, which might have added variability not accounted for by the GOM samples. Preliminary analysis of GOM red snapper showed that RMSEP was lower in a single year (2012) calibration than for multiple years combined (Barnett *et al.* 2019), although this is based on a small sample size. For some test set validations herein, age prediction improved when spatial variability and sample size of the calibration model increased (Table 3.S1) and the All Regions Truncated model optimized RMSEP and PA in most test sets. All other published studies have found similar evidence. Helser *et al.* (2019) found similar results in walleye pollock *Gadus chalcogrammus*, where some annual and regional variation in spectral data was evident, but combined year models performed best when considering test set results across all groupings. Wedding *et al.* (2014) and Robins *et al.* (2015) also found seasonal and geographic differences in spectral signatures and resulting age calibration models for coastal snapper and barramundi species, and again found it preferable to combine calibrations to accommodate variation for optimizing prediction capability. Studies of red snapper otolith chemistry have found regional differences in stable isotope and trace element

profiles within the GOM (Patterson *et al.* 2008; Nowling *et al.* 2011; Sluis *et al.* 2012, 2013, 2015) and the Atlantic (Barnett *et al.* 2016), but no comparative studies between the GOM and Atlantic exist. Further chemical profiles of otoliths from both regions are lacking. Additionally, while trace elements can be bound to organic matrix in otoliths (Izzo *et al.* 2016a; Thomas *et al.* 2017; Thomas and Swearer, 2019), it is not clear whether FT-NIRS can detect trace elements in otoliths, although the lack of regional spectral variation suggests they are not detectable at a diagnostic level in whole otoliths.

In addition to spatial and temporal variation among spectra, the age structure of sample sets varied across regions despite efforts to standardize that of calibration sets. Constraining the collection years included in calibration models might control for some temporal variation in water quality and other environmental variables; however, the age composition of sample sets will inherently affect the temporal variability included in the model since otoliths from older fish include more years of environmental variation than do those from younger fish. For populations with mostly young fish, e.g., EGOM, modeled variation might differ significantly from populations with older fish sampled in the same years and in the absence of regional variability. This idea has potential ramifications for ages estimated from single-gear surveys, where gear biases in catch-at-size by age might affect age distributions and thus any resulting FT-NIRS calibration models. Future effort should include the collection of FT-NIRS data for all archived otoliths to further explore dynamics in spectral variation across time and regions, as well as the effects of age distribution on model performance.

Model performance in terms of PA, APE, and age composition presented herein relative to the PLS regression metrics typically reported in FT-NIRS feasibility studies

demonstrates that additional considerations are necessary to select optimal calibration models for otolith age data. Despite satisfactory model performance for nearly all models presented here based on $R^2$, RMSEP, and RPD values as defined in previous FT-NIRS age prediction studies (Rigby *et al.* 2014; Wedding *et al.* 2014; Robins *et al.* 2015; Rigby *et al.* 2016a; Helser *et al.* 2019b; Passerotti *et al.* 2020b), the resulting translation to integer ages for management use did not always yield optimal PA and APE values (Table 3.S1), which are typically used to judge quality of age estimates in fisheries research. Differences among prediction performance metrics might stem from the rounding convention used to transform the decimal ages output from FT-NIRS prediction models to integers for use as calendar ages. We compared several rounding methods and found none worked better than conventional rounding, however further investigation into best practices might very well lead to improvements in this area. There might also be some "regression effect" or "regression toward the mean" occurring differentially among calibration/test set pairings, whereby the mean age of the calibration model, and thus the age for which model prediction error is least, differs from that of the test set, thereby increasing prediction error disproportionately in age classes as they progress sequentially further from the calibration model mean (Williams, 2013). Regional differences in otolith chemistry aside, this regression effect could have contributed to differential prediction ability of calibration models, as mean age of the GOM Combined test set was 5 years old compared to 3 years old in the SA test set. Hence, using calibration models with similar age composition to targeted test sets may result in lower prediction error (Williams, 2013). Future investigation should further assess this phenomenon, as well as

issues of rounding convention and regression effects, and explore potential mitigation techniques.

Spectral variation in red snapper otoliths older than 31 years of age were not modeled similarly to their younger counterparts, which might indicate further changes underlying otolith growth that affect FT-NIRS analysis at advanced fish age. That optimal cross-validation models used no preprocessing means there is no correction in spectral signatures for changing particle size or baseline correction for light scatter occurring due to size differences of the otoliths and their inherently different presentation on the sample window of the spectrometer. As such, it is possible that the SA Complete and All Regions Complete calibration models rely more on these physical otolith differences than other preprocessed models, in addition to any chemical differences. It is also possible that chemical changes underlying age prediction might taper off with age and/or size. These results suggest that multiple factors could affect spectral variation in thick, old otoliths which has implications for their use with FT-NIRS applications.

This idea led us to evaluate the relationship of NIR light penetration with otolith size as a way of testing one of many potential sources of spectral variation. Size of red snapper otoliths range widely across age classes and are large relative to other fish species. Williams *et al.* (2015) demonstrated otolith thickness to be a diagnostic metric in morphometric indices for predicting otolith increment age in deepwater snappers and we found red snapper otolith thickness likewise to increase with age to a maximum of almost 6 mm in the oldest fish used in this study. Sample thickness alters NIR light penetration in cartilage at several wavenumber regions (Padalkar and Pleshko, 2015) and although the aragonite matrix of otoliths is less opaque and less proteinaceous than that of

cartilage, the behavior of light with the otolith organic matrix might be similar. Indeed, spectral differences between 6280 – 6080 cm $^{-1}$ indicate that NIR light signal was attenuated in the oldest, thickest red snapper otolith, and additional regions of potential variation in spectral signature may exist that were not identified in our preliminary analysis. Thus, the effects of even gross otolith morphometrics on NIR light penetration and resulting spectral signatures are unknown and should be fully explored.

There is a great need for more understanding of how underlying otolith chemistry affects FT-NIRS age estimation in order to assess additional fine details of age prediction using FT-NIRS. Future otolith chemistry research should also consider adding FT-NIRS data collection to the methodology prior to additional destructive analyses, so that there are directly measured "wet chemistry" values for various constituents of interest to pair with spectral data for further investigation. Further, best practices must be developed to ensure that ages are predicted consistently and repeatably for each species should this technology be operationalized for management. A process for model updating will also need to be implemented to incorporate additional age-related uncertainty into spectral data to ensure continued prediction improvements. Given that the next US red snapper stock assessment is scheduled for 2021, it provides an important opportunity to develop sensitivity analyses comparing use of traditional and FT-NIRS ages in assessment models and resulting management benchmarks.

### 3.6 Acknowledgments

The authors wish to thank the staff at the NMFS Southeast Fisheries Science Center Panama City Laboratory and the SC DNR Marine Resources Research Institute for providing age and other meristic data for this study, especially L. Thornton, N.

Willett, D.B. White, J. Evans and M. Willis. C. Kastelle at the Alaska Fisheries Science Center, and N. Earl, B. Robertory, and J. Weeks at the University of South Carolina provided assistance with FT-NIRS data collection. A. Andrews contributed valuable insights on otolith size and light penetration as it pertains to FT-NIRS age prediction. We also wish to thank J. Erickson for providing expertise on FT-NIRS equipment and light penetration experimental design. This work was supported by South Carolina Sea Grant [R/CF-23], an equipment grant from the College of Arts and Sciences, University of South Carolina, and funds from a SPARC Graduate Research and an ASPIRE-I grant from the Office of the Vice President for Research at the University of South Carolina.

This is contribution #826 of SCDNR's Marine Resources Research Institute.

The findings and conclusions in the paper are those of the author(s) and do not necessarily represent the views of the National Marine Fisheries Service.

**Table 3.1.** Calibration model results for red snapper FT-NIRS age prediction, by region. The "complete" models for SA and All Regions Combined (indicated by a *) are those including the two oldest fish in the study aged 35 and 38 years, while "truncated" models exclude these samples. RMSECV = root mean square error of cross validation, % RMSE = % root mean square error, RPD = residual prediction deviation, WGOM = western Gulf of Mexico, EGOM = eastern GOM, SA = south Atlantic.

| Calibration Model (Calendar Age) | n | Maximum Age | Rank | $R^2$ | RMSECV | % RMSE | Bias | RPD | Slope | Offset |
|---|---|---|---|---|---|---|---|---|---|---|
| WGOM | 150 | 31 | 6 | 0.94 | 1.84 | 5.94 | -0.002 | 4.16 | 0.95 | 0.56 |
| EGOM | 105 | 18 | 4 | 0.95 | 0.85 | 4.72 | 0.009 | 4.67 | 0.95 | 0.31 |
| GOM Combined | 255 | 31 | 6 | 0.94 | 1.6 | 5.16 | 0.000 | 4.14 | 0.94 | 0.50 |
| SA, truncated | 253 | 28 | 8 | 0.94 | 1.35 | 4.82 | 0.019 | 4.12 | 0.95 | 0.38 |
| SA, complete* | 255 | 38 | 8 | 0.94 | 1.52 | 4.00 | 0.011 | 4.02 | 0.94 | 0.49 |
| All Regions Combined, truncated | 508 | 31 | 8 | 0.94 | 1.54 | 4.97 | -0.004 | 4.02 | 0.94 | 0.49 |
| All Regions Combined, complete* | 510 | 38 | 9 | 0.94 | 1.58 | 4.16 | 0.001 | 4.06 | 0.94 | 0.51 |

**Table 3.2.** Validation results for age prediction of regional test sets of red snapper otoliths relative to the corresponding calibration model used to test (in parentheses). Percent agreement (PA), Average Percent Error (APE), and results of two-sided Kolmogorov-Smirnov (K-S) tests (D statistic and p-value) are also given for each test-set/calibration model combination. RMSEP = root mean square error of prediction, % RMSE = % root mean square error, RPD = residual prediction deviation.

| Test Set (Calibration tested against) | n | Maximum Age | $R^2$ | RMSEP | % RMSE | Bias | RPD | Slope | Offset | PA | APE | K-S D | p |
|---|---|---|---|---|---|---|---|---|---|---|---|---|---|
| All Regions Combined (All Regions, truncated) | 847 | 30 | 0.92 | 0.99 | 3.30 | -0.04 | 3.32 | 1.01 | -0.01 | 45.8 | 10.4 | 0.07 | 0.056 |
| All Regions Combined (All Regions, complete) | 847 | 30 | 0.92 | 1.02 | 3.40 | 0.16 | 3.29 | 1.01 | 0.22 | 44.2 | 11.3 | 0.09 | 0.004 |

**Table 3.S1.** Validation results for red snapper FT-NIRS age prediction of regional otolith test sets relative to the corresponding calibration model used to test (in parentheses). Countershading added to facilitate viewing of regional groupings.

| Test Set (Calibration) | n | Max Age | $R^2$ | RMSEP | % RMSE | Bias | RPD | Slope | Offset | PA | APE | K-S D | p |
|---|---|---|---|---|---|---|---|---|---|---|---|---|---|
| WGOM (WGOM) | 204 | 30 | 0.94 | 1.05 | 3.50 | 0.37 | 4.01 | 1.01 | -0.43 | 37.8 | 15.0 | 0.10 | 0.230 |
| WGOM (GOM Combined) | 204 | 30 | 0.95 | 0.92 | 3.07 | 0.16 | 4.4 | 1.03 | -0.29 | 46.6 | 14.4 | 0.08 | 0.478 |
| WGOM (AR, T) | 204 | 30 | 0.95 | 0.89 | 2.97 | -0.24 | 4.61 | 0.96 | 0.42 | 53.4 | 7.50 | 0.07 | 0.723 |
| WGOM (AR, C) | 204 | 30 | 0.95 | 0.97 | 3.23 | -0.34 | 4.34 | 0.97 | 0.49 | 44.1 | 8.92 | 0.08 | 0.478 |
| EGOM (EGOM) | 206 | 14 | 0.84 | 0.89 | 6.36 | -0.30 | 2.37 | 0.97 | 0.48 | 42.7 | 6.84 | 0.15 | 0.019 |
| EGOM (GOM Combined) | 206 | 14 | 0.81 | 1.08 | 7.71 | -0.20 | 1.86 | 1.09 | -0.23 | 35.4 | 12.0 | 0.15 | 0.025 |
| EGOM (AR, T) | 206 | 14 | 0.81 | 0.94 | 6.71 | -0.26 | 2.2 | 0.94 | 0.56 | 47.1 | 7.02 | 0.13 | 0.058 |
| EGOM (AR, C) | 206 | 14 | 0.82 | 0.94 | 6.71 | 0.30 | 2.22 | 0.94 | 0.02 | 45.6 | 8.98 | 0.09 | 0.345 |
| SA (SA truncated) | 437 | 26 | 0.92 | 0.96 | 3.69 | -0.01 | 3.56 | 0.96 | 0.19 | 42.1 | 10.9 | 0.05 | 0.580 |
| SA (SA complete) | 437 | 26 | 0.89 | 1.16 | 4.46 | -0.03 | 2.93 | 0.95 | 0.22 | 34.6 | 15.3 | 0.06 | 0.525 |
| SA (AR, T) | 437 | 26 | 0.92 | 1.07 | 4.12 | 0.16 | 3.22 | 1.04 | -0.31 | 41.7 | 13.3 | 0.15 | 1.7E-04 |
| SA (AR, C) | 437 | 26 | 0.93 | 1.07 | 4.12 | 0.34 | 3.35 | 1.04 | -0.50 | 43.5 | 13.5 | 0.18 | 2.6E-06 |
| GOM Combined (GOM Combined) | 410 | 30 | 0.91 | 1.00 | 3.33 | -0.02 | 3.12 | 1.04 | -0.18 | 41.0 | 13.2 | 0.07 | 0.222 |
| GOM Combined (AR, T) | 410 | 30 | 0.92 | 0.91 | 3.03 | -0.25 | 3.56 | 0.96 | 0.45 | 50.2 | 7.30 | 0.08 | 0.140 |
| GOM Combined (AR, C) | 410 | 30 | 0.91 | 0.96 | 3.20 | -0.02 | 3.27 | 0.96 | 0.216 | 44.9 | 8.95 | 0.04 | 0.824 |

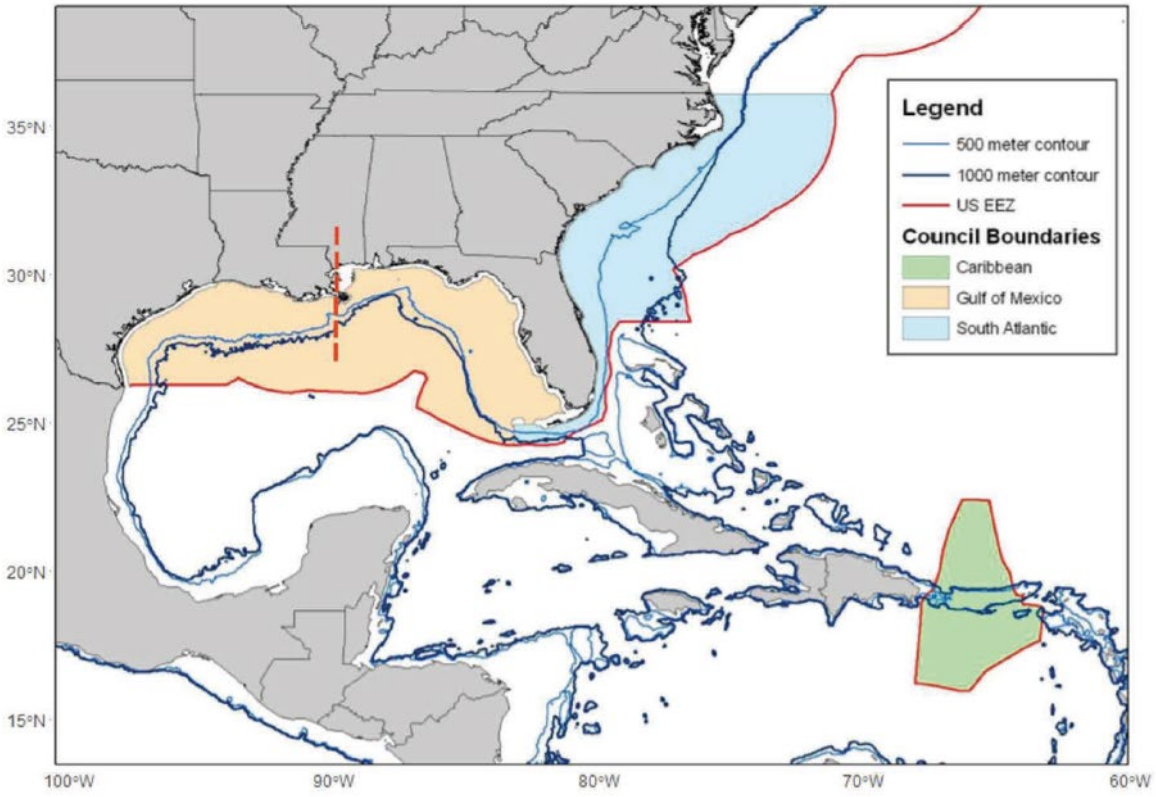


**Figure 3.1.** US federal management regions for red snapper, adapted from SEDAR (2008). The Gulf of Mexico (GOM) is divided into eastern (EGOM) and western (WGOM) subunits roughly along the Mississippi River boundary as indicated by the orange dashed line. Samples for this study were grouped into three regions for testing: EGOM, WGOM, and south Atlantic (SA).

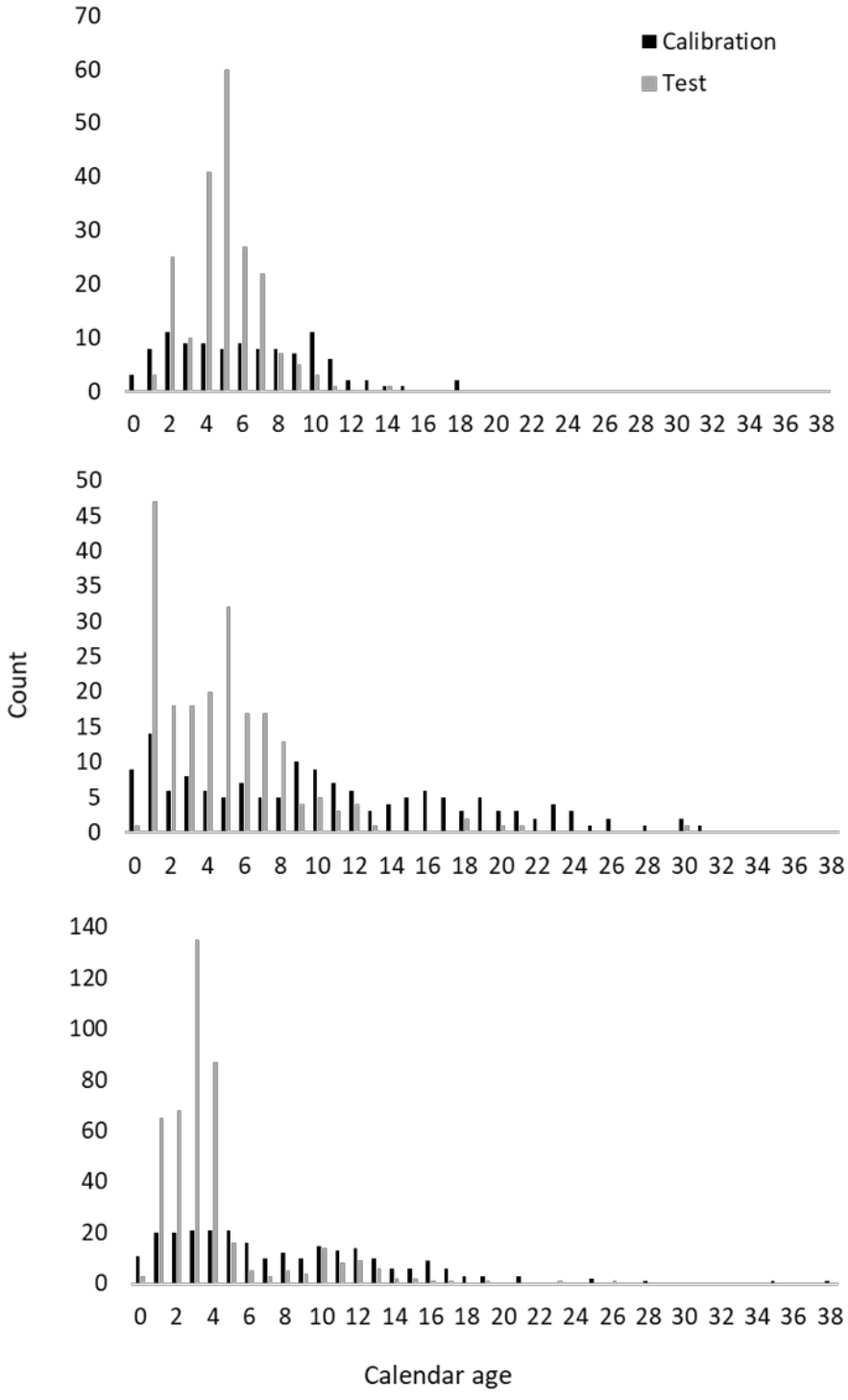


**Figure 3.2.** Red snapper sample age distributions for calibration and test sets for the (top) EGOM, (middle) WGOM, and (bottom) SA.

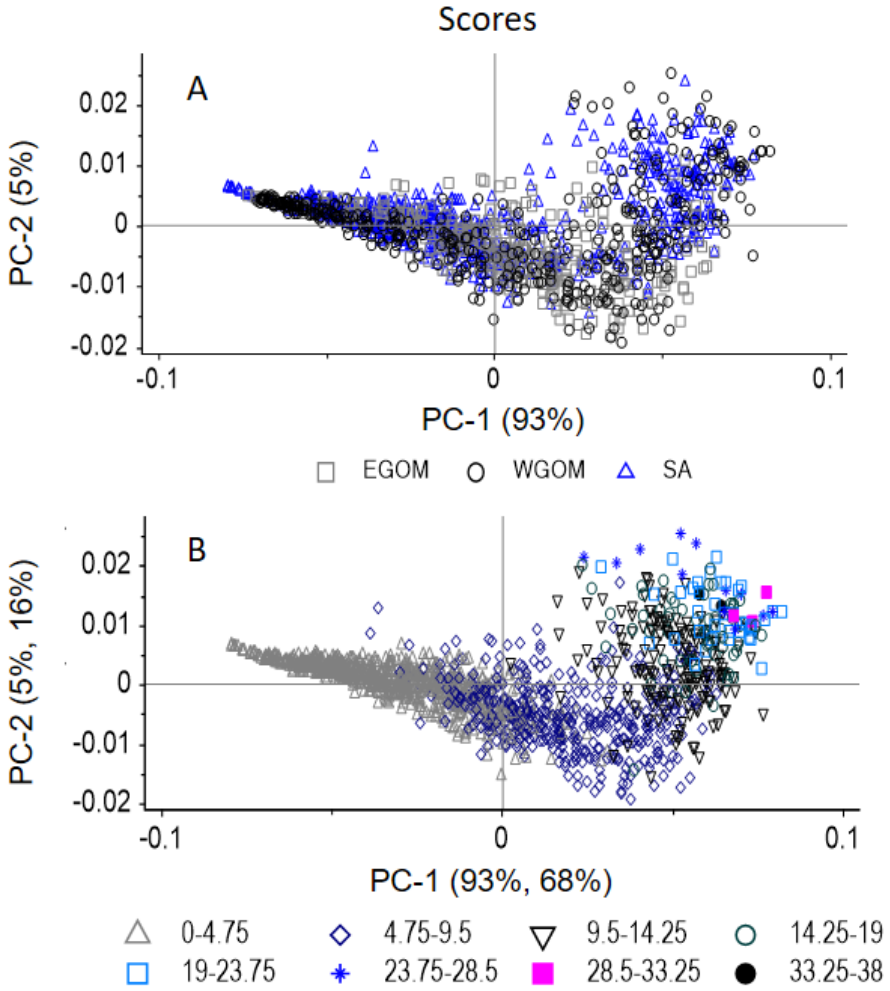


**Figure 3.3.** PCA of first-derivative transformed spectral data for all red snapper otoliths coded by (A) region and (B) age group. Additional scores for PCs in (B) correspond to the first two factors of a combined region age prediction model explaining 68% and 16% of variation in predicted calendar ages, respectively.

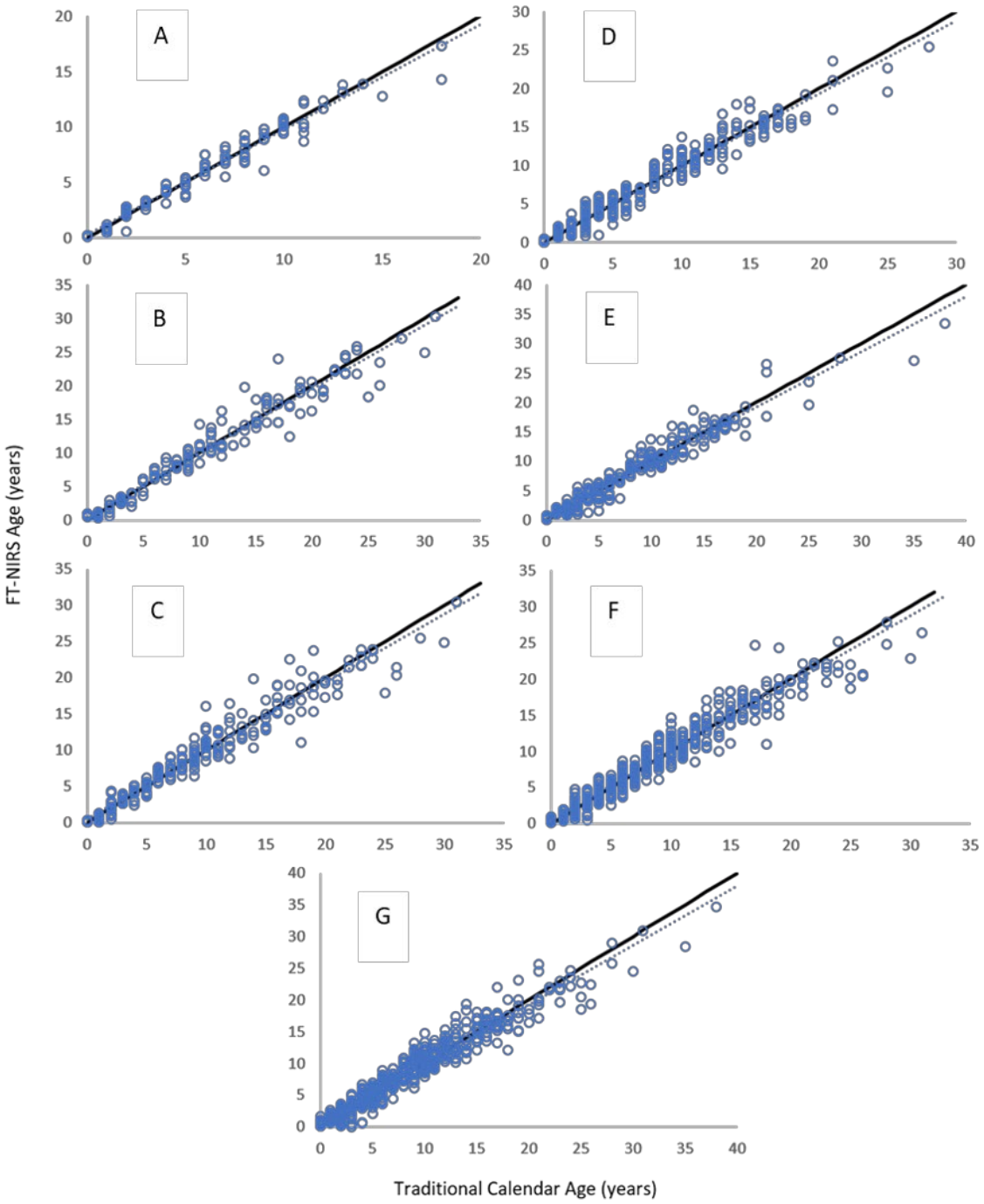


**Figure 3.4.** Plots of red snapper FT-NIRS age calibration model results for the A) EGOM, B) WGOM, C) GOM Combined, D) SA Truncated, E) SA Complete, F) All Regions Combined Truncated, and G) All Regions Combined Complete calibrations. Dashed line is the linear regression, solid line represents a 1:1 regression line.

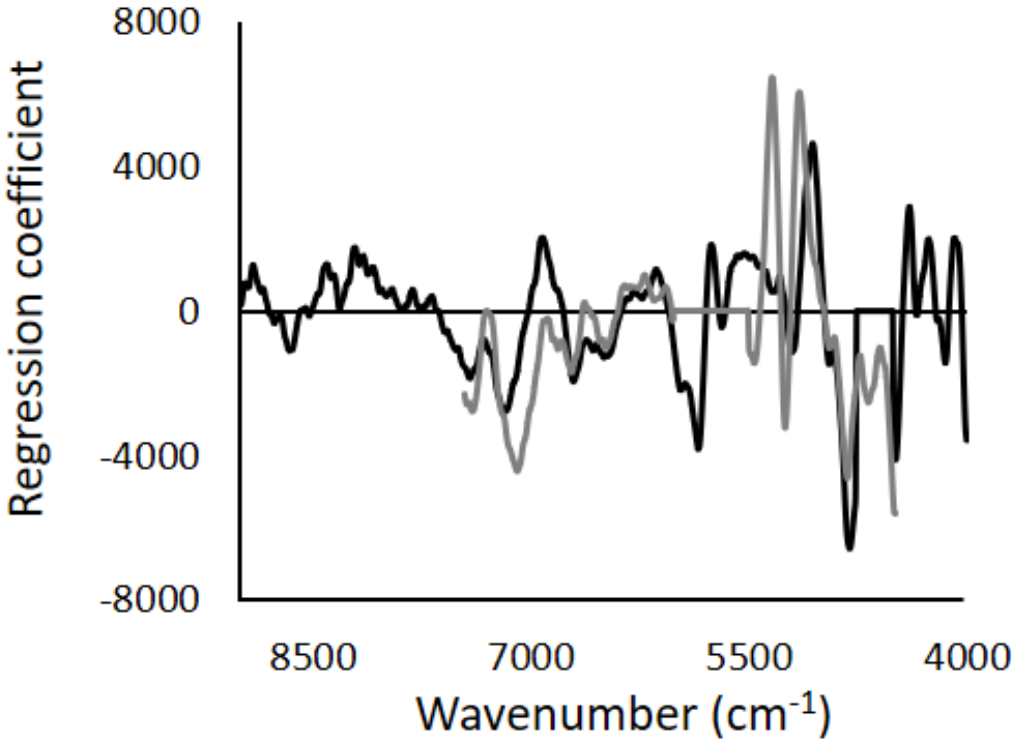


**Figure 3.5**. Loadings plot of regression coefficients for the GOM Combined (grey) and SA Truncated (black) age calibration models for red snapper.

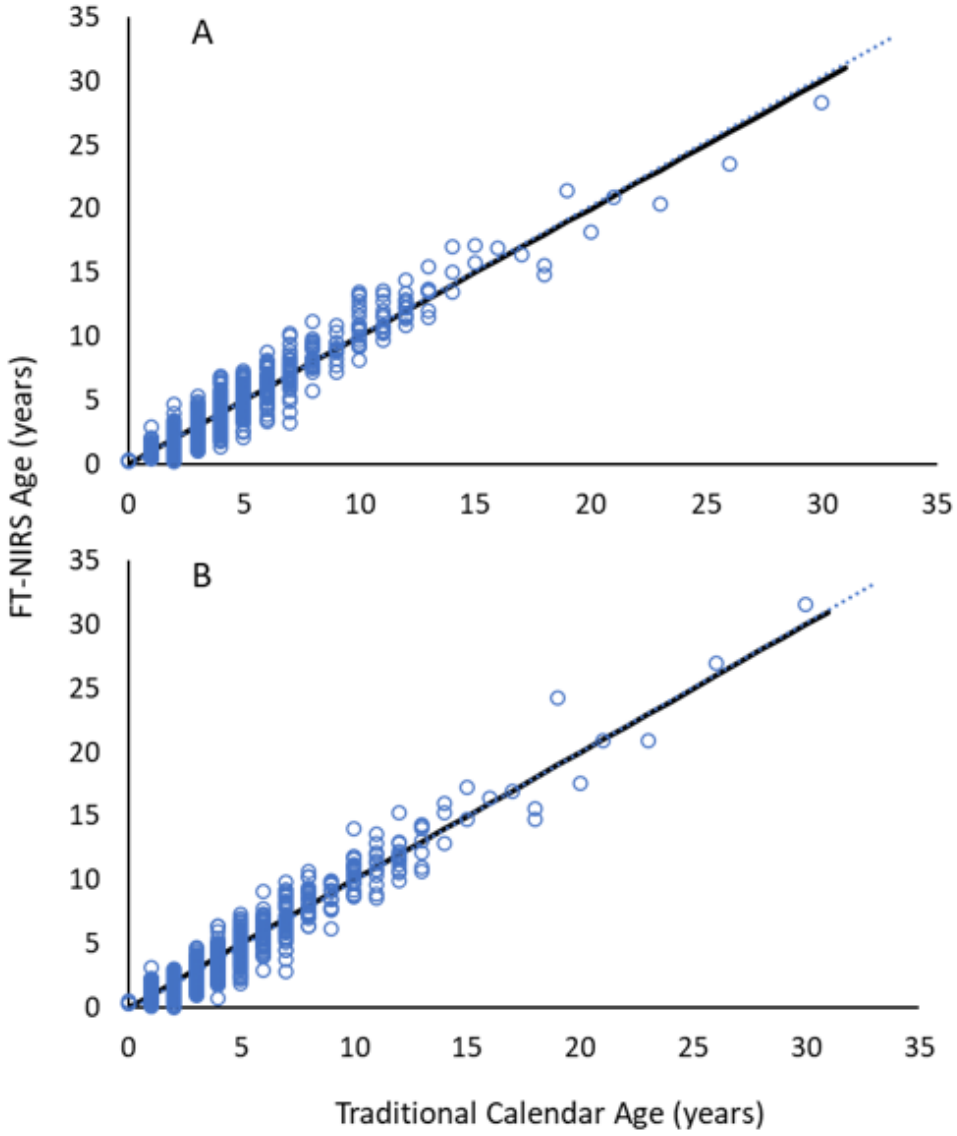


**Figure 3.6.** Plot of red snapper FT-NIRS test set results for the (A) All Regions (All Regions Truncated) and (B) All Regions (All Regions Complete) validations. Dashed line is the linear regression, solid line represents a 1:1 regression line.

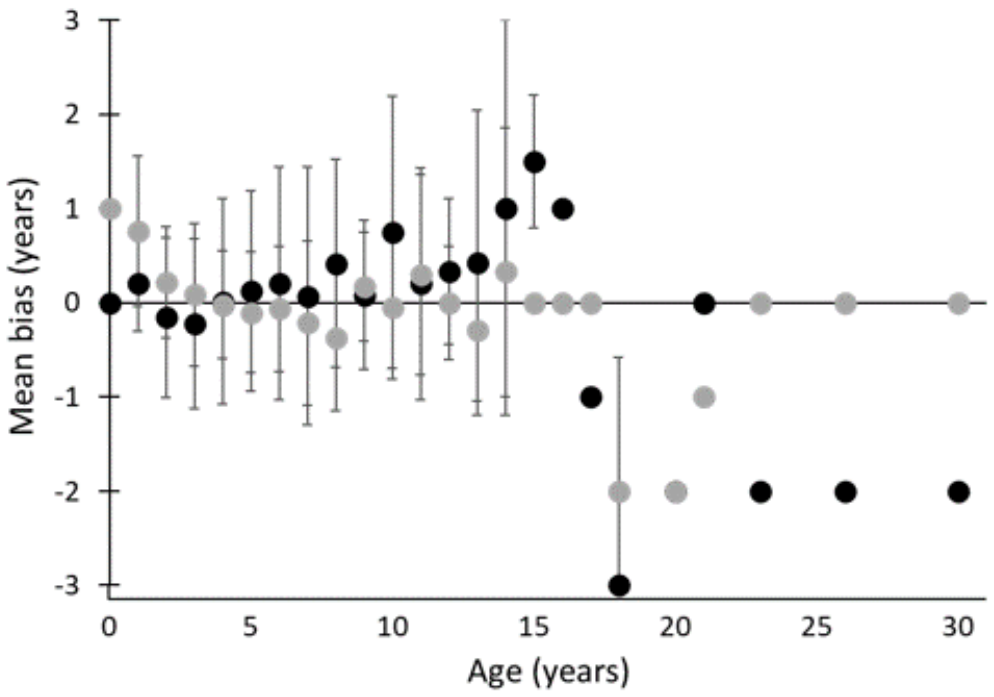


**Figure 3.7.** Mean bias ± SD for red snapper FT-NIRS (black circles) and traditional (grey circles) ages by age class for all test sets combined, as predicted by the All Regions Combined Truncated calibration model.

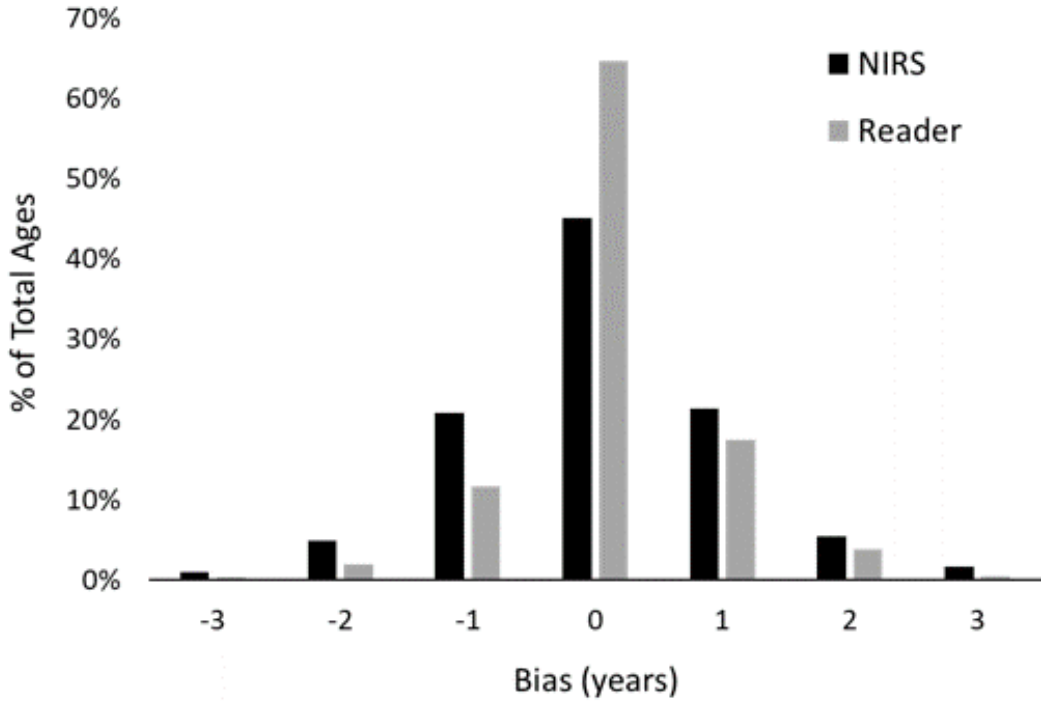


**Figure 3.8.** Frequency of relative bias (B) by method for all red snapper ages across all test sets combined as predicted by the All Regions Truncated calibration model. Raw FT-NIRS ages were rounded to the nearest integer before bias calculation to facilitate comparison with traditional ages.

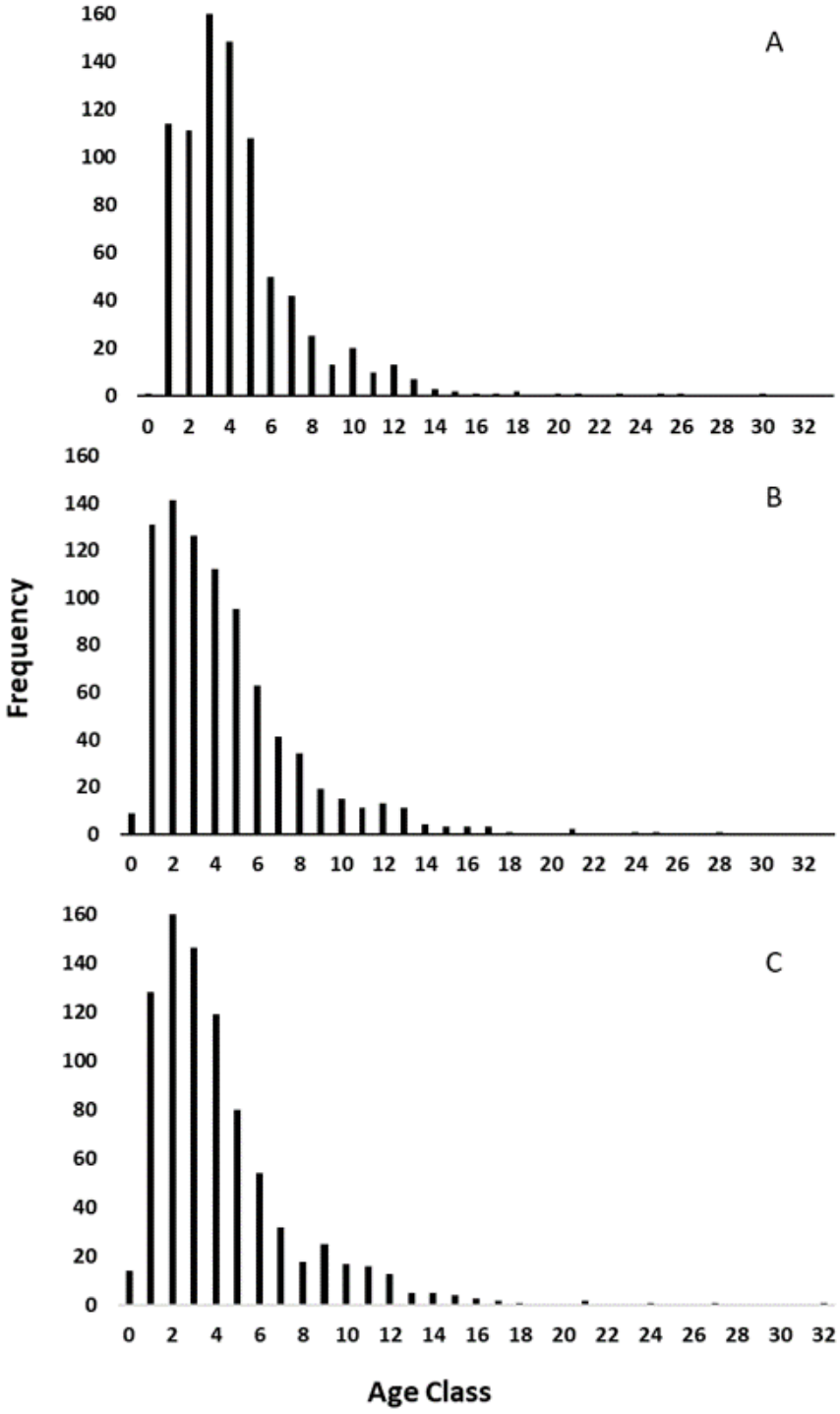


**Figure 3.9.** Age distributions for all red snapper test set samples using (A) traditional ages and predicted ages output by the (B) All Regions Combined Truncated (Band All Regions Combined Complete (C) calibration models.

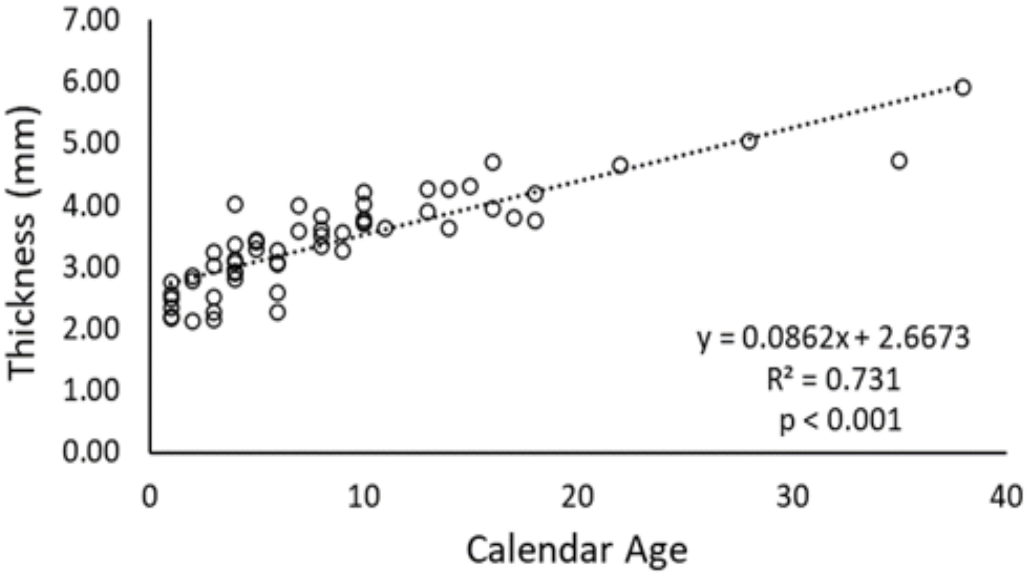


**Figure 3.10.** Otolith thickness (mm) at age (years) for 58 red snapper otoliths assessed for NIR light penetration.

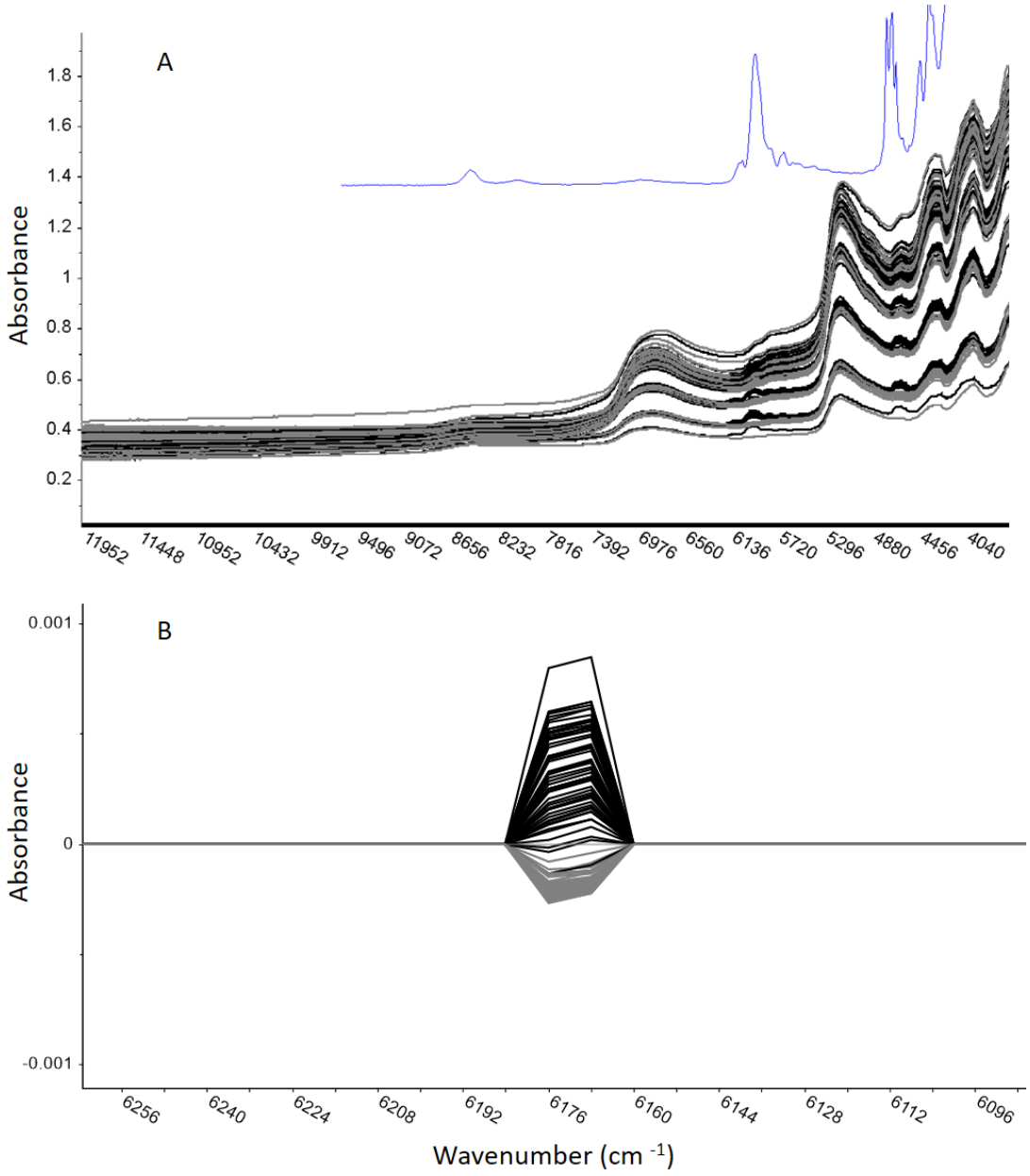


**Figure 3.11.** Raw (A) and first-derivative transformed (B) spectra of red snapper otoliths scanned for light penetration trial with no disc (grey) and polystyrene disc (black). The raw spectrum for polystyrene is overlaid in blue in (A). Differentiation was judged based on wavenumber range 6280 – 6080.

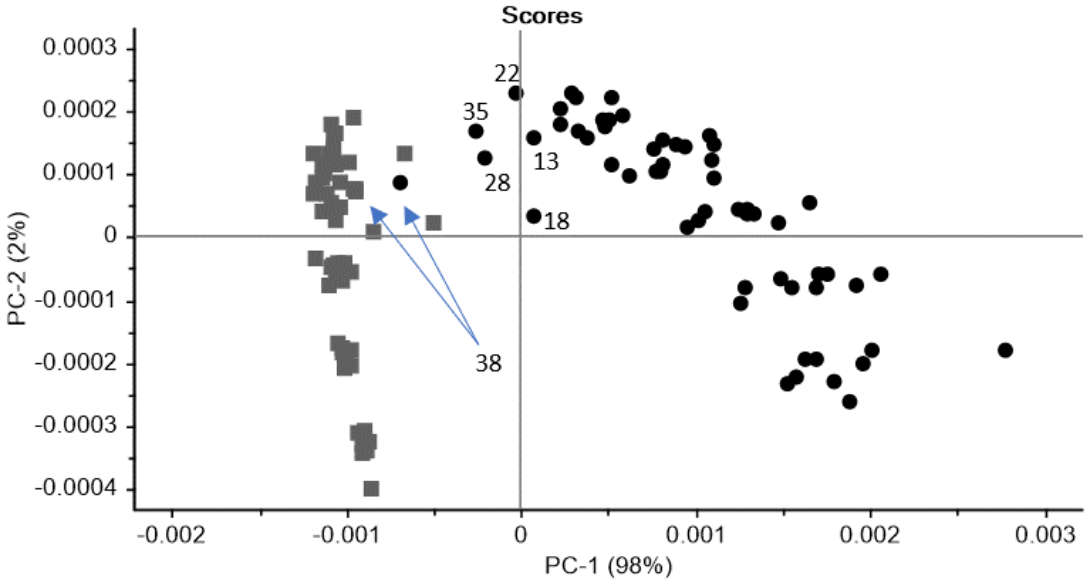


**Figure 3.12.** PCA of red snapper otolith light penetration spectra with no disc (grey squares) and polystyrene disc (black circles). Selected proximal 'disc' samples are labeled with age to show spatial trends.

# CHAPTER 4

# PHYSICOCHEMICAL MECHANISMS OF FT-NIRS AGE PREDICTION IN FISH OTOLITHS[3]

[3] Passerotti, M. S., Reichert, M. J. M., Robertory, B., Marsh, Z., Stefik, M., Quattro, J. M. Physicochemical mechanisms of FT-NIRS age prediction in fish otoliths. *In preparation.*

## 4.1 Abstract

The recent advent of Fourier transform near infrared spectroscopy (FT-NIRS) as a tool for rapid age prediction in fish otoliths has gained the attention of fisheries managers and is actively being vetted for implementation on a production scale for management. The chemical basis for FT-NIRS age prediction has not been established, although age-related changes in organic content have been hypothesized to underlie the method. We used otoliths of red snapper *Lutjanus campechanus* to evaluate the relationship of FT-NIRS spectral signatures and age prediction capability relative to ambient moisture content, sample presentation, sample mass, and protein content. Spectral data were collected from otoliths (n=84) ranging in age from 0 – 28 years at ambient conditions, and again subsequently at each step after oven drying, grinding to powder, and subsampling a fixed mass of each otolith. Crystal structure was also evaluated with Xray diffraction at ages 2, 8, and 17 years, and did not vary systematically with age. Ambient moisture content was low (0.22 ±0.89%), did not change significantly with age, and there was no difference in ages predicted from ambient and dehydrated otoliths. Grinding of otoliths reduced the accuracy of age prediction models, but both full mass and subsampled ground otoliths still yielded predicted ages to within approximately 2 years of traditional ages, suggesting otolith structure contributes minor improvement to age prediction, but that true compositional changes to constituent concentrations underlie age prediction. Acid-hydrolyzed protein concentration ranged from 0.43 – 0.92% of dried otolith weight and increased significantly with age. FT-NIRS models predicted otolith protein content to within 0.04% by weight in optimized models, but wide variability in protein content with age hindered model optimization. Superficially, otolith signatures

resemble a combination of pure calcium carbonate and type I collagen signatures, and individual absorbance patterns at characteristic wavenumbers for each can be correlated to otolith age, providing a foundation for the FT-NIRS age-prediction mechanism.

## 4.2 Introduction

Fourier transform near infrared spectroscopy (FT-NIRS) has recently gained the attention of the fisheries management community as a potential alternative to costly age estimation of fish, which traditionally relies on visual counts of growth bands in otoliths to estimate age (e.g., Campana, 2001). Rapid, non-destructive scans of otoliths using FT-NIRS and subsequent regression modeling of spectral data with traditional age calibration data has resulted in age predictions deemed mostly equivalent, from an experimental standpoint, to traditional estimates for both daily and annual ages across various species for age ranges common in archived collections (Wedding *et al.* 2014; Robins *et al.* 2015; Helser *et al.* 2019; Passerotti *et al.* 2020a, 2020b). In light of these results, US federal fisheries management recommendations have been made to pursue the use of FT-NIRS for improving the scope and timing of production ageing for managed species (SEDAR, 2020), and the National Marine Fisheries Service (NMFS) is in the process of vetting FT-NIRS for production ageing nationwide (e.g., Helser *et al.* 2019b). The case has also been made that FT-NIRS has potential to be useful in ecological studies, including discrimination of geographical differences manifested in otolith chemistry (Wedding *et al.* 2014; Robins *et al.* 2015), among other potential fisheries applications.

No studies to date have provided corroborating evidence of the chemical and/or structural basis for FT-NIRS age prediction in fish. Wedding *et al.* (2014) found that

bonds related to carbonate ions were apparent in spectral data underlying otolith age calibrations, and Robins *et al.* (2015) hypothesized that water chemistry influences otolith spectral signatures due to incorporated changes in trace element concentrations across the lifespan. Helser *et al.*(2019) alternatively suggested that age-related changes in the otolith organic matrix are a likely driver of spectral differences across age groups. Beyond otoliths, mechanisms involving organic constituents were also suggested by Rigby et al. (2014, 2016a, 2019) as underlying the age prediction capability of FT-NIRS in shark tissues.

Sagittal otoliths (those typically used for age determination) have been described as comprising calcium carbonate ($CaCO_3$) in the form of aragonite (≥ 90%, but see caveats below), organic matrix consisting of proteins, collagens, and proteoglycans (≤ 10%), and trace elements (≤ 1%) (Campana, 1999; Payan *et al.* 1999; Borelli *et al.* 2001; Chang and Geffen, 2013). Unfortunately, beyond this general understanding, otolith composition is species-specific (e.g., Degens, 1969; Dauphin and Dufour, 2003) and incompletely described for many species of management concern. An illustration of this is the recent study by Thomas *et al.* (2019), which used proteomics to identify more than 300 proteins in otoliths of black bream *Acanthopagrus butcheri* that were previously unknown to occur in otoliths. Of the proteins that have been described, many can be segregated into the broad categories of structural proteins (collagens and proteoglycans) or biomineralization regulators or substrates (e.g., fibronectin, laminin) (Thomas *et al.* 2019). Collagens and collagen-like proteins (sometimes referred to as water-insoluble proteins) appear to form the majority of the otolith organic template, including a large role of otolin-1, a collagen-like protein unique to otoliths that putatively forms the basis

of the organic matrix upon which $CaCO_3$ is precipitated (Degens, 1969; Dunkelberger *et al.* 1980; Davis *et al.* 1995; Murayama *et al.* 2002; Thomas *et al.* 2019). The daily alternating deposition of organic matrix and $CaCO_3$ forms the concentric growth bands associated with age estimation, a process governed by the other non-collagenous (i.e., water soluble) regulatory proteins which are either deposited within the otolith matrix or entrained into interstitial spaces during otolith accretion (Thomas *et al.* 2019; Thomas and Swearer, 2019; Hüssy *et al.* 2020b). This accretion pattern creates cyclic changes in composition, density, and opacity (e.g., Hoff and Fuiman, 1993; Hüssy et al. 2004a; Jolivet et al. 2008, 2013) and the mechanism for accretion of material from the saccular epithelium creates gradients in the endolymph fluid that can translate to corresponding protein gradients along the accretion axis (Payan et al. 1999; Borelli et al. 2001; Thomas et al. 2020). There is also heterogeneity in elemental distribution patterns (Izzo et al. 2016; Limburg and Elfman, 2017; Hüssy et al. 2020), although it is unclear whether FT-NIRS detects elemental differences at the concentrations (low parts per million) present in otoliths.

Age-related differences in both organic and inorganic otolith constituents have been documented. Otolith cores appear to be more proteinaceous than subsequent growth bands (Jolivet *et al.* 2008, 2013) and ontogenetic declines in relative protein content have been demonstrated (Morales-Nin, 1986a, 1986b; Hoff and Fuiman, 1993; Hüssy *et al.* 2004). Variations in the ratio of water-soluble to water-insoluble proteins are also apparent (Hoff and Fuiman, 1993; Hüssy *et al.* 2004b). To our knowledge no study has investigated protein dynamics over continuous, multi-year time scales. Otolith trace element dynamics are more well-studied because of their utility as life history and

ecological tracers (e.g. Campana and Thorrold, 2001; Elsdon *et al.* 2008; Sturrock *et al.* 2012; Izzo *et al.* 2016b). Trace elements are deposited into both organic and mineral fractions (Izzo *et al.* 2016a) and vary with environmental and metabolic influences; hence, they also vary ontogenetically (Hüssy *et al.* 2020b), and temporal depositional patterns for some elements have recently been proven as useful age chronometers (Heimbrand *et al.* 2020; Hüssy *et al.* 2020a). Overall, it is unclear how these compositional dynamics might influence or underlie FT-NIRS age prediction.

Beyond the impacts of chemical composition, additional questions surround the relationship of FT-NIRS spectral data to other otolith-associated variables, such as the physical effects of otolith size and crystal structure, as well as the influence of bound and unbound water content within the otolith. The effects of otolith size relative to age prediction have been indirectly evaluated by Robins *et al.* (2015), who compared ages predicted from direct regressions of otolith weight with age to those of FT-NIRS prediction models and found FT-NIRS models were more accurate, concluding that FT-NIRS cannot be solely reliant on otolith weight for informing age prediction. Passerotti et al.(2020a) found that FT-NIRS models predicted otolith weight better than age based on PLS model metrics, but that different spectral signatures were responsible for the two models. However, Passerotti et al. (2020b) found that light penetration was attenuated in large, thick red snapper otoliths, potentially hindering accurate age prediction in older individuals of this species. This finding also has implications for how physical light interaction with the otolith (i.e., sample presentation) affects age prediction. NIR light is known to penetrate substrates more deeply than other types of infrared light (up to 10 cm; Workman and Weyer, 2012), but this is highly dependent upon physical and chemical

makeup of the substance and varies according to wavenumber region (Workman and Weyer, 2012; Williams, 2019). The ability to detect chemical signatures under the surface layers of the otolith is of paramount interest given the structural heterogeneity of constituents (described above) and crystal size/orientation (described below), and the unknown origins of FT-NIRS age prediction overall.

Water content and its effects on otolith spectral signatures was investigated long before FT-NIRS was first used for age prediction. Water is known to be a strong absorber of NIR light (Libnau *et al.* 1994; Workman and Weyer, 2012; Williams, 2019) and is generally characterized in any material as free (present in liquid state in pores or spaces within solids) or bound (covalently- or hydrogen-bound to proteins or other molecules) (Padalkar *et al.* 2013). Gauldie *et al.*(1998) used NIRS to examine the movement of water in and out of otoliths by examining known water-associated spectral peaks at 5160 and 6840 $cm^{-1}$ (i.e., Luck, 1984). In Gauldie *et al.* (1998), the peak near 6840 $cm^{-1}$ was associated with O-H bond stretching from both water and other hydroxyl groups contained within organic molecules within the otolith, and did not vary with soaking of otoliths in water; hence, it was used as a proxy for "bound" water within the otolith matrix. The peak at 5160 $cm^{-1}$ was found to reflect the O-H bond stretch overtone as well as the $H_2O$ vibration combination mode, and reflected the moisture absorbed during soaking of otoliths; hence, it was used as a proxy for interstitial water movement into and out of otoliths (Gauldie *et al.* 1998). Alternatively, the majority of other studies evaluating these regions in organic tissues have instead evaluated the effects of drying and found that the peak near 6840 $cm^{-1}$ reflects free water and the peak near 5160 $cm^{-1}$ reflects a combination of free and bound water (Ressler *et al.* 1976; Luck, 1984;

Bagratashvili *et al.* 1997; Palukuru *et al.* 2014). The peaks at 5160 and 6840 $cm^{-1}$ are among the most prominent features seen in all otolith spectral signatures published to date and have been included in wavenumber ranges informing most published FT-NIRS otolith age prediction models (see Wedding *et al.* 2014; Robins *et al.* 2015; Helser *et al.* 2019; Passerotti *et al.* 2020a). Robins *et al.* (2015) evaluated changes to NIR spectra relative to time since collection and found that stabilization varied by species ranging from approximately six months to several years, and attributed the phenomenon to potential moisture acclimation to ambient conditions, pH changes, or protein denaturization. Hence, water content in otoliths potentially affects FT-NIRS age prediction models with unknown consequence.

Near infrared spectroscopy is useful for discriminating crystal structure and polymorphs, including $CaCO_3$ polymorphs (aragonite, vaterite, and calcite) found in otoliths (e.g. Gaffey, 1987; Wang and Becker, 2009; Hopkinson and Rutt, 2016; Hopkinson *et al.* 2017), which could impact FT-NIRS age prediction. Recent studies suggest that multiple polymorphs of $CaCO_3$ occur in sagittal otoliths more frequently than previously thought, although relatively few studies have used quantitative methods such as Xray diffraction to investigate whole otolith crystal structure (Loeppky *et al.* 2019; Pracheil *et al.* 2019). Further, crystal structure can influence otolith composition including differential binding of trace elements (e.g. Melancon *et al.* 2005; Tzeng *et al.* 2007) and polymorphs might vary ontogenetically (Loeppky *et al.* 2019). Crystal size and orientation also vary across the otolith surface (Cook *et al.* 2018), but it is unknown how these change with ontogeny or their overall effect on FT-NIRS spectral signatures.

Defining the causation underlying correlation of FT-NIRS otolith age prediction is desirable, but linking causation to empirical analyte properties is difficult. The use of FT-NIRS for standardized predictive analyses requires the evaluation of critical key assumptions, such as the fact that concentrations of components of interest are in some way related to the spectral data generated from the technique (Chen and Wang 2001). This is a daunting task given otoliths are composites of potentially many measurable components. FT-NIRS is used in various industries such as agriculture and pharmaceuticals to passively monitor sample composition for constituents of interest, e.g., moisture or protein content (Williams, 1975; Norris, 1992; Iwamoto et al. 1995; Workman and Weyer, 2012). Assigning specific features of NIR signatures to individual constituents is not always possible, and often multiple similar constituents, such as different types of proteins, are grouped together and detected using combination bands found to correlate with the overall content of broader constituent categories (Norris, 1978; Workman and Weyer, 2012). Hence, preliminary evaluation of the constituent changes underlying otolith age prediction with FT-NIRS logically begins with attribution of broad constituent groupings, i.e., mineral/inorganic and protein/organic components, with age-specific otolith spectral signatures. Further correlation of age model regression coefficients with wavenumber regions attributable to constituent groups would further help define the relationship, if only superficially.

Towards this end, we herein raised and tested several fundamental null hypotheses regarding the relationship of otolith constituents and structure to FT-NIRS spectral signatures in pursuit of an improved, albeit basic, understanding of the NIR spectral correlation with age in fish otoliths:

Hypothesis 1: Otolith crystal structure does not vary with age.

Hypothesis 2: Bound (chemically-bonded) and free (interstitial) water content in otoliths do not vary with age or after desiccation.

Hypothesis 3: There are no differences in spectral signatures or resulting age prediction models between whole and ground otoliths, i.e., the inherent age-related structural changes in whole otoliths do not underlie age related spectral differences.

Hypothesis 4: Age-related changes in otolith mass do not underlie age-related spectral differences.

Hypothesis 5: There is no relationship between otolith protein content and age-related spectral differences.

Hypothesis 6: There is no relationship between inorganic $CaCO_3$ content and age-related otolith spectral differences.

## 4.3 Methods

### *4.3.1 Otolith collection and age estimation*

Red snapper otoliths for this study were sourced from archival fishery-independent collections taken from the southeastern US Atlantic Ocean by the South Carolina Department of Natural Resources (SCDNR), Marine Resources Research Institute, as part of the Southeast Reef Fish Survey and Marine Resources Monitoring Assessment and Prediction (MARMAP) sampling program between 2011-2016. Generally, left otoliths were sectioned for ageing, leaving the right otolith available for FT-NIRS. A traditional calendar age estimate was generated from the left otolith using

methods outlined in Wyanski *et al.* (2015). These ages were used as reference points to inform FT-NIRS age prediction models as well as for other age correlation models in this study. The paired right otoliths corresponding to these ages were used for the subsequent analyses below.

*4.3.2 FT-NIRS data collection/analysis*

FT-NIR spectral data for otoliths were collected and preprocessed according to the methods outlined in Passerotti *et al.*(2020a). Whole otoliths were positioned convex-side down in the middle of the sample window of a Bruker Matrix I FT-NIR spectrometer (Bruker Scientific, Billerica, MA, USA), with the rostral axis positioned horizontally relative to the sample window. A gold-coated transflectance cap with a black rubber collar was placed over the top of the otolith to reduce stray light entering the detector. Spectral scans were acquired for each otolith at a frequency of 16 $cm^{-1}$ along the NIR spectrum (12,000-4,000 $cm^{-1}$), and a total of 64 scans were averaged to produce a single representative spectrogram for each sample. Spectral data analysis was conducted using the OPUS software suite (version 7.8; Bruker Scientific, Billerica, MA, USA). Spectral data were fitted to traditionally estimated otolith ages using partial least square (PLS) regression (Chen and Wang, 2001). Models were evaluated for age prediction capability using a "leave one out" method of cross-validation, and goodness of fit was judged based on the $R^2$ (coefficient of determination), root mean square error of cross validation (RMSECV), and residual prediction deviation (RPD) values.

For the purposes of this study, otolith age prediction models for each experimental treatment group were constructed in two forms: 1) "standardized" models

used a standardized wavenumber range of 6104-4200 $cm^{-1}$ to facilitate comparison based on commonly important wavenumber regions for predicting age in previous publications (Passerotti *et al.* 2020a, 2020b) ; and 2) "optimized" models in which wavenumber regions were optimized to fit the unique data set and treatments applied in our study, which might facilitate identification of potentially unique spectral features arising from these variables. The same process was also used to fit PLS regressions for predicting otolith protein content and calcium carbonate "layer age" as described below.

Preprocessing for all otolith models except the Fixed Mass Ground (FMG) models consisted of a Savitsky–Golay first derivative transformation with 17 smoothing points (polynomial order = 2), whereas FMG models also underwent vector normalization using the Standard Normal Variate (SNV) function in addition to the Savitzky-Golay transform. Calcium carbonate signatures were also preprocessed using Savitsky-Golay transformation and SNV. Savitsky-Golay transformation is typically used to correct for baseline shifts due to light scatter from differences in particle size and/or other physical differences among samples, while SNV normalizes the data to a mean of 0 and standard deviation of 1. Analyses of absorbance patterns at specific wavelengths was done using preprocessed data for consistency with age prediction models; given that all spectra were subject to first derivative transform, this means that changes associated with peaks in raw spectral data will be offset to either side of the original peak in the transformed data. Hence, changes to specific features in absorbance patterns, e.g., water bands, were evaluated across a small range of nearby wavenumbers and denoted with approximate wavenumber location (e.g., water bands near 5200 and 6900 $cm^{-1}$).

*4.3.3 Spectral comparison*

To explore the relationship of the inorganic and organic fractions of otolith composition to the red snapper otolith FT-NIRS spectral signature, we visually compared a spectrum from a whole red snapper otolith to those of other analytes representative of the two fractions. The inorganic portion was modelled using powdered $CaCO_3$ in the form of precipitated calcite (Amresco, CAS# 471-34-1), and the organic portion was modelled using a Type I collagen signature described in Kandel *et al.*(2020). In addition, we compared individual vibrational mode peak assignments mapped by Hopkinson *et al.*(2017) for $CaCO_3$, which are driven mostly by activity of the $CO_3^{2-}$ anion, to help visualize the complexity of the molecular interactions underlying the relatively broad NIR signatures of composite materials. Alignment of peaks underlying the $CaCO_3$ signature with perceived features in the otolith signature were considered to represent areas of inorganic influence, and those aligned with the Type I collagen signature were considered to represent areas of organic influence, with the understanding that there are numerous additional and potentially unknowable molecules present in otoliths that could also influence the NIR signature. The form of $CaCO_3$ in otoliths is aragonite, but calcite is used here for comparison because it is commercially available in purified form and, in comparison, presents only minor variations in NIR signature (Gaffey, 1987; Hopkinson and Rutt, 2016).

*4.3.4 Crystal structure: Xray Diffraction (XRD)*

Thin sections of three otoliths aged 2, 10, and 17 years were analyzed using XRD to evaluate potential age-related differences in crystal structure. Whole, clean otoliths

were embedded in epoxy and cross-sectioned in the transverse plane through the otolith core according to the methods described in VanderKooy (2009). Resulting thin sections (~ 0.5 mm thick) were individually irradiated with a GeniX 3D microfocus copper k-alpha source (0.154 nm wavelength) focused at a standardized position on the convex surface near the sulcus for each section (Figure 4.2). Xray diffraction patterns were detected on a Hybrid Pixel Array Pilatus detector (Dectris). To identify potential effects of particle size or crystal orientation on thin section results, we also evaluated ground otolith powder with XRD for comparison. Following evaluation of in-tact thin sections, the approximate area of focus for each otolith was excised from the sections and ground gently with a mortar and pestle to a uniform particle size. A subsample of each powdered otolith was then evaluated again with XRD using the settings outlined above. Resulting intensity measurements were normalized across samples before plotting for comparison relative to 2 theta. Peaks were compared to published standards for aragonite (PDF# 0000233), and its polymorphs vaterite (PDF# 0004854) and calcite (PDF# 0000098), as well as hydrated forms ikaite (PDF# 0010853) and monohydratecalcite (PDF# XXXX) to assign crystal lattice identification.

*4.3.5 Interstitial water content: Desiccation experiment*

A set of 84 otoliths ranging in age from 0 to 28 years were selected for evaluation of the effects of ambient moisture content, as well as subsequent evaluation of sample structure (whole vs ground) and sample mass on FT-NIRS spectral signatures and age prediction. Structure and mass experiments are further described below. Otoliths were stored dry in paper coin envelopes under ambient conditions from time of collection to time of experiments, and were first weighed to the nearest 0.001 mg on a Mettler Toledo

microbalance before being scanned for FT-NIRS analysis as described above to provide a baseline spectral signature. Next, the whole otoliths were dried at 55°C for 24 hours in a sealed oven containing an excess of desiccant. After 24 hours, otoliths were allowed to come to room temperature inside the oven, and were then individually removed immediately prior to a second round of FT-NIRS scanning as outlined above. After scanning, otoliths were weighed a second time, and moisture content under ambient conditions ($M_A$) was calculated as

$$M_A = ((Wt_A - Wt_D)/Wt_A)*100$$

where $Wt_A$=ambient otolith mass and $Wt_D$=dried otolith mass. Differences in $M_A$ as a function of age were tested using a Spearman rank correlation. Preprocessed FT-NIRS spectral data were evaluated via regression analysis to identify effects of drying on absorbance signatures across the NIR spectrum, specifically near 6900 $cm^{-1}$ and 5200 $cm^{-1}$ and which have been identified in otoliths and elsewhere as corresponding to either free or bound water (e.g., Luck, 1984; Gauldie *et al.* 1998). Differences in FT-NIRS age prediction between ambient and dried otolith spectra were evaluated by comparing PLS regression parameters between the two treatments, as well as examining regression coefficients and factor loadings for changes in importance of spectral regions to age prediction models.

*4.3.6 Sample structure: Grinding*

Subsequent to the desiccation experiment, the 84 otoliths were individually ground to powder using a tungsten-carbide ring mill until the entire sample easily passed through a 250-micron sieve. Grinding time was standardized among samples to help

ensure uniform particle size, and the ring mill was thoroughly cleaned between samples to avoid cross-contamination. The full mass of each powdered otolith was loaded into a 22 mm cylindrical borosilicate glass cuvette, which was placed onto the FT-NIRS sample window for scanning using a microsample collar fitted to the sample window (Bruker Scientific). Samples were scanned at settings identical to those for whole otoliths as described above. Spectral signatures and FT-NIRS age prediction were evaluated and compared to that of whole otoliths based on differences in PLS regression parameters between whole dried and whole ground otoliths.

*4.3.7 Sample mass: Fixed-mass ground samples*

Following scanning of the full, ground otoliths, a 300 mg subsample was taken from each ground otolith. Only otoliths aged ≥ 3 years were included in the fixed-mass analysis (n=71), since most of the otoliths aged 0-2 years were smaller than 300 mg. The subsampled otolith powder from each was placed into a clean cuvette and scanned in an identical manner to the full ground otoliths. Spectral signatures and FT-NIRS age prediction were evaluated and compared to that of whole and ground otoliths based on differences in PLS regression parameters.

*4.3.8 Calcium carbonate analysis*

To evaluate the effects on age prediction of increasing sample mass without associated increases in analyte (i.e., age-related organic compound) concentration, powdered $CaCO_3$ (Amresco, CAS# 471-34-1) was scanned in quantities ranging from 100 – 1000 mg in 100 mg intervals. Spectra were obtained in the manner identical to that of otolith powders as outlined above, with the exception that each quantity was scanned

in triplicate. To model the effect of increasing otolith mass on age prediction, each quantity of $CaCO_3$ powder was assigned a dummy variable of "layer age" ranging in value from 1 to 10 years according to its sample mass (e.g., 100 mg = 1 year old, 200 mg = 2 years old, etc.). An age prediction model was created using PLS regression as described for otoliths above, and resulting regression parameters were evaluated for goodness of fit. Optimized wavenumber regions, regression coefficients, and factor loadings for the $CaCO_3$ "layer age" model were compared to those from otoliths in all preparations to infer signatures related to mineral $CaCO_3$ content and increasing sample size in the absence of otolith organic components.

*4.3.9 Protein & amino acid content*

To test the hypothesis that protein content is not related to FT-NIRS age prediction in otoliths, acid-hydrolyzed amino acid content was measured and used to estimate total protein content in otoliths ranging in age from 0 – 25 years. Subsamples of ground otoliths (n=26), for which spectral data were previously collected as above, were analyzed for amino acid content at the Molecular Structure Facility, University of California – Davis Genome Center (Davis, CA) using the acid hydrolysis methods described in Cooper *et al.*(2000). Protein content for each otolith was calculated by summing the total AA residues quantified for each sample, after correction for recovery of standards analyzed simultaneously with otolith samples (average correction = 1.9%). During acid hydrolysis, asparagine and glutamine are converted to aspartic acid (ASX) and glutamic acid (GLX), respectively, hence the reported totals for ASX and GLX reflect these combined residues.

To evaluate the ability of FT-NIRS to detect and predict protein content from otoliths, PLS regressions were fit to spectral data from all otolith preparations and related to protein content as measured above. Data preprocessing was carried out as noted for age prediction models, and optimization performed to identify best-fit protein prediction models. Optimized wavenumber regions, regression coefficients, and factor loadings for protein prediction models were compared to those from otoliths in all preparations and $CaCO_3$ models to identify spectral signatures unique to otolith protein content.

Changes to individual amino acid concentration (% otolith weight) were plotted graphically as a function of age, and linear trends were evaluated by calculating Pearson product-moment correlation coefficients for each. Amino acid concentrations as a percentage of total protein weight were also plotted as a function of age and fitted with LOESS curves (span = 2) in order to visualize age-related trends in protein composition. All regressions and associated analyses were performed using R (Version 3.4.3 "kite-eating tree", 2017).

## 4.4 Results

### *4.4.1 Spectral comparison*

Comparison of representative spectral signatures from $CaCO_3$ and type I collagen identified features from each that potentially contribute to the otolith signature, and curve deconvolution for the $CaCO_3$ signature from Hopkinson *et al.*(2017) provides additional insight into the underlying vibrational modes of the $CO_3^{2-}$ anion contributing to the overall shape of the $CaCO_3$ and potentially the otolith spectrum (Figure 4.1). In the raw otolith signature, water features near 6840 $cm^{-1}$ and 5160 $cm^{-1}$ are evident, and similar

but broader, more flattened peaks are apparent in the collagen signature. These peaks are notably absent from the $CaCO_3$ signature, which instead contains a smaller peak near 7200 $cm^{-1}$ and narrow peaks near 5334 $cm^{-1}$ and 5008 $cm^{-1}$. Additional $CaCO_3$ peaks near 4630 $cm^{-1}$ and 4501 $cm^{-1}$ are offset from any visible features in the otolith signature, but the most prominent $CaCO_3$ peak near 4268 $cm^{-1}$ aligns with the leading edge of the broader otolith peak near 4310 $cm^{-1}$. This broader peak might also be influenced by the $CaCO_3$ peak at 4346 $cm^{-1}$. Collagen features that align with those in the otolith signature occur near 5924 $cm^{-1}$ and 5778 $cm^{-1}$, corresponding to known methyl ($-CH_3$) and methylene ($-CH_2$) group vibrations, respectively (Workman and Weyer, 2012), as well as smaller peaks near 4898 $cm^{-1}$ and 4596 $cm^{-1}$.

*4.4.2 XRD*

All observed diffraction patterns from whole sections and corresponding ground powders were consistent with an expected polycrystalline aragonite structure, with no evidence of vaterite, calcite, or hydrated crystal structures. There were variations in relative peak intensity across samples in both preparations (Figure 4.2), which were atypical based on reference structures. As these variations were not reconciled by grinding the otolith sections, they might be associated with other features (e.g., atomic substitutions) rather than crystal orientation or size. Atomic substitutions, such as those of strontium for calcium, are well-documented in otoliths (e.g., Doubleday *et al.* 2014) and are not necessarily age-related. One peak in the ground sample from V_SA_0036 was not consistent with any reference evaluated, and is assumed to be an artifact of the analysis. Overall, the XRD results do not indicate any predictable, age-related changes to the

crystal lattice, and confirm that any water molecules present in the otoliths are extra-crystalline in nature.

*4.4.3 Desiccation experiment*

Ambient otolith weights ranged from 0.0009g – 3.868g (Figure 4.3A) and increased with age in a manner best described by a linear quadratic regression ($y = -0.0033x2 + 0.2097x + 0.0067$, $r^2 = 0.94$, $p<0.0001$). Mean moisture content ($M_A$) for all otoliths was 0.22 ±0.89% and was highest in age-0 otoliths but overall did not vary significantly with age (Spearman rho = -0.03, p= 0.78) (Figure 4.3B). Spectral differences between dried and ambient otoliths were minor over the entire range (Figures 4.4 and 4.5, A-B), with a slight increase in average magnitude of the water peak near 5200 $cm^{-1}$ in dried otoliths relative to ambient otoliths and no difference in magnitude near the 6900 $cm^{-1}$ peak (Figure 4.6 A-B). Drying reduced variability in absorbance values at age at both peaks (Figure 4.6 C-F). Regardless of drying treatment, water-associated peaks near 5200 and 6900 $cm^{-1}$ were present in all otolith signatures, but changes in absorbance at both of these wavenumbers declined drastically after about 10 years of age. Hence, some degree of bound water is reflected at both wavenumbers, and the importance of these regions to age prediction models in whole otoliths could change depending on the age distribution being predicted with the model. Of note is that the 5200 $cm^{-1}$ region is not included in 3 of the 4 optimized otolith age prediction models, and the 6900 $cm^{-1}$ region is absent from 2 of the 4 optimized models herein (Table 4.1).

Ages predicted using the standardized region models were similar between drying treatments based on regression model parameters (Table 4.1, Figure 4.7 A-B). Regression

coefficients between drying treatments varied in magnitude at some wavenumbers e.g., near 5800, 5200, and 4700 $cm^{-1}$, and some shifting of peaks was evident near 5200 $cm^{-1}$ and 4800 $cm^{-1}$ (Figure 4.11A), which is a known effect of drying on NIRS spectra (e.g., Chakravartula *et al.* 2019; Williams, 2019). Overall, however, desiccation appears to have had no significant effect on age prediction in whole otoliths. The persistence of the strong peaks near 5200 $cm^{-1}$ and 6900 $cm^{-1}$ despite desiccation suggests the majority of water detected in red snapper otoliths originates from tightly-bound (i.e. chemically adsorbed e.g., Ailavajhala *et al.* 2020) water molecules, which either accumulate or absorb light differentially according to age or physical characteristics, respectively.

### *4.4.5 Grinding experiment*

Raw absorbance signatures of ground otoliths were similar to those of whole otoliths, but absorbance was overall lower and with apparently reduced effects of light scattering and baseline drift (i.e., the "fanning" effect in spectra across age groups in whole otoliths) (Figure 4.4C). The relative magnitude of individual spectral features also appears somewhat reduced or flattened, e.g., the -OH overtone peak near 6900 $cm^{-1}$ and smaller features between 4600-5000 $cm^{-1}$. Preprocessed absorbance signatures were also similar in shape to those of whole otoliths (Figure 4.5C), but differences in signature of age-0 otoliths are much more apparent than in whole otoliths, especially near 7200 $cm^{-1}$ and ~4600-4500 $cm^{-1}$. A more linear ordering of absorbance magnitude with age is also evident across the spectrum in ground otoliths, demonstrated by the relationship of absorbance with age at the water peak near 5200 $cm^{-1}$ (Figure 4.8A).

Ages predicted with the standardized model were less accurate for ground otoliths than whole otoliths based on RMSE (Table 4.1, Figure 4.7C), with increased deviation in the youngest and oldest ages. Nonetheless, the ground otolith standardized model approached an RPD of 3 and $R^2$ of 0.88, and the optimized model, which overlapped whole otolith optimized regions and added the region at ~7450-6770 $cm^{-1}$, improved to an RPD = 3.15 and $R^2$ ~ 0.90. Regression coefficients were similar between the whole ground and whole dried models for the regions near 5800 $cm^{-1}$ and 5200-4900 $cm^{-1}$, but all other peaks occurred at similar locations but were of opposite direction (Figure 4.11B). Based on comparisons of transformed spectra in Figure 5, these differences could stem from broadening of absorbance peaks in ground spectra which would shift the inflection points highlighted in the transformed spectra and hence the regression coefficients.

*4.4.6 Fixed mass experiment*

Raw absorbance signatures of fixed mass ground (FMG) otolith samples were similar in pattern but were relatively flattened and with fewer prominent features relative to the other otolith preparations (Figure 4.4D). Preprocessed spectra were likewise similar in shape to those from the other otolith preparations but with far less variation in magnitude among age groups as evidenced by spacing of absorbance values under peak curves (Figure 4.5D). Contrary to whole ground and similar to whole dried/ambient otoliths, the oldest FMG samples had lower absorbance values at many points along the spectrum than those of some younger age groups (Figure 4.8B), meaning this non-linear absorbance pattern at various wavenumbers reflects true concentration-related changes

and not an artifact of physical sample structure e.g., increasing sample thickness with age.

Age prediction models for FMG samples had diminished resolution relative to those from other preparations (Table 4.1, Figure 4.7D), but age was nonetheless predictable from fixed mass samples and hence not reliant on otolith size or morphology to inform age models. Standardized region models had the lowest $R^2$ and RPD of all the age models, but also used fewer factors (rank = 3) to explain the age relationship, with factor 1 explaining ~67% of the spectral variance (Figure 4.9). The optimized model performed well in terms of previously published FT-NIRS age prediction models, predicting age to within ~ 2 years and with RPD > 3. In the optimized model, the number of explanatory factors increased to n=8, but the variance explained by factor 1 was the highest of all models at 79%. Regression coefficients for FMG samples generally followed the patterns of whole ground otoliths but with minor changes in magnitude near 6000-5800 $cm^{-1}$, 5150 $cm^{-1}$, and 4700 – 4300 $cm^{-1}$. Peak shifting was also evident near 5300 $cm^{-1}$ and 4550 $cm^{-1}$ (Figure 4.11C). Hence, grinding appears to have had the largest overall effect on regression coefficients across all otolith treatments, ostensibly due to changes in the interaction of NIR light with whole relative to ground otoliths.

### *4.4.7 Calcium carbonate experiment*

Layering of the $CaCO_3$ powder resulted in predictable "layer age" using a PLS regression model (Table 4.1, Figure 4.10) despite preprocessing of spectral data, which is generally used to remove effects from physical variations in samples occurring secondarily to the primary analyte of interest (Rinnan *et al.* 2009). Preprocessed spectra

for “layer ages” highlight features of interest for comparison to otoliths: the absence of prominent peaks between ~5960-5700 $cm^{-1}$, the less prominent but more numerous features in the 5400-5000 $cm^{-1}$ range, and the two small peaks near 4600 and 4500 $cm^{-1}$ that lead up to the prominent peak near 4300 $cm^{-1}$, which is much less broad than that seen in otoliths. Layer age models predicted increasing sample mass/thickness in the standardized region to within one layer (RMSECV=1 or 100 mg sample mass), and with an RPD approaching 3. When optimized for wavenumber region, RMSECV declined to < 1 with RPD > 3, and wavenumber region 6104-4600 $cm^{-1}$. Regression coefficients for the layer age standardized model differed from ground otolith age patterns in distinctive ways (Figure 11D). Primarily, the regression coefficient pattern consisted of mostly broad features with few prominent, recognizable peaks, and did not follow otolith age coefficients in any predictable manner. There were areas that showed some similarity such as those near 5850 - 5600 $cm^{-1}$, 5200 – 5050 $cm^{-1}$, and 4800 – 4600 $cm^{-1}$, but remaining regions were all of opposite magnitude for otolith age models relative to layer age. Hence, where regression coefficient patterns between these models overlap, we can hypothesize that the mineral component of the otolith composition is contributing to the otolith age model, and where coefficients differ in direction, other factors e.g., organic constituents might be more influential.

*4.4.8 Protein/amino acid concentration*

Protein comprised a relatively small proportion of red snapper otoliths, ranging from 0.43 – 0.92% composition by weight, and protein concentration increased linearly with age ($r^2 = 0.651$, $p < 0.0001$; Figure 4.12). Corresponding amino acid (AA) concentrations (% otolith weight) were positively correlated with age in all cases ($r \geq$

0.478, $p \leq 0.014$), but individual variation in measured concentration was also apparent to varying degrees depending on the AA (Figure 4.13). As a proportion of total protein weight, a varying AA-specific age-related trends are apparent and 9 of the 15 were significantly correlated, suggesting the relative quantities and specific types of proteins present in otoliths vary significantly with age (Figure 4.14).

Prediction of otolith protein concentration from spectral data was not as successful as that for age prediction and varied with otolith preparation (Table 4.2). Protein prediction using the standardized region model was poor (RPD=1.58) and was only slightly improved by utilizing the optimized region model (RPD=1.76, Figure 4.15A). Protein concentration for three otoliths stood out as outliers as identified in Figure 4.16, and are also visibly distinct in several AA plots (e.g., GLY) in Figure 4.13. In most protein prediction models, one or more of these otoliths were identified as outliers via Mahalanobis distance calculations of spectral data and were consistently underpredicted by models as indicated in Figure 15A and C. Hence, these points were removed and prediction models recalculated (reduced models, Table 4.2 and Figure 4.15B and D). Reduced models were successful at predicting protein concentration to within ~ 0.04% in whole otoliths and ~0.02% in FMG samples. Wavenumber regions used in optimized models were narrow, focusing on 4688-4600 $cm^{-1}$ in whole otolith and 4600-4544 $cm^{-1}$ in FMG samples. These regions are documented as useful for protein prediction (Workman, 2001) and encompass various vibrations of N-H, C-N, and C=O bonds (Workman and Weyer, 2012). Regression coefficients for the optimized region FMG protein prediction model overlap with prominent features in both the standardized and optimized FMG age models (Figure 4.17). Agreement between FMG age models is

best between about 5000-4550 $cm^{-1}$, encompassing the optimized protein region for both FMG and whole reduced protein models.

Protein prediction models suggest protein is detectable in whole and FMG otoliths using FT-NIRS, but the low percent composition and wide variability with age make direct prediction challenging. Because protein concentration increased with age independent of sample mass in FMG samples, we can hypothesize that the $CaCO_3$ component likewise decreased in concentration with age. Because of its relatively higher concentration and ostensibly easier detection, correlation of $CaCO_3$ dynamics might be more easily modeled with age, which would manifest in negative correlation of regression coefficients at organic (i.e., collagen)-specific wavenumbers, or in positive correlation at $CaCO_3$-specific wavenumbers. When coefficients were compared between the standardized $CaCO_3$ layer age and FMG otolith age models, most collagen-specific wavenumbers were positively correlated with age, including the 4688-4544 $cm^{-1}$ region encompassing optimized protein prediction models, while $CaCO_3$-specific wavenumbers were not overtly influential (Figure 4.11D). Although regression coefficients can be difficult to interpret when based on transformed data, this analysis solidifies the complementary relationship of these peaks with age and demonstrates that both inorganic and organic signatures can be used concordantly to predict age-related changes in percent composition independent of sample mass.

## 4.5 Discussion

Typically, the first step in establishing a calibration model for spectroscopic prediction of an analyte is to identify all potential variables impacting the system under

investigation (Beebe et al. 1998). In the case of fish otoliths, there are potentially hundreds of individual components comprising the structure itself assuming individual organic matrix constituents (e.g., proteins, proteoglycans; Thomas *et al.* 2019), trace elements, and the remaining inorganic fraction act individually to alter the NIR signature. The various types of vibrations that each molecule within the constituents will undergo in the presence of NIR light, and how these molecules interact with all others must also be considered (Siesler, 2008; Workman and Weyer, 2012). The superficial comparison of the otolith spectral signature with that of individual constituents such as collagen and $CaCO_3$ is a first attempt to understanding the primary factors influencing FT-NIRS age prediction. NIR spectral signatures generally comprise broad, overlapping peaks in the combination and overtone regions of the NIR electromagnetic spectrum, which can be difficult to assign to specific chemical bond vibrational modes even when all constituents are known at the molecular level (Alm *et al.* 2007; Workman and Weyer, 2012). A telling visualization is the number of individual peaks underlying the $CaCO_3$ signature presented herein (Figure 1), which encompass at least seven features demonstrating characteristic types of vibrational modes stemming from a single carbonate ion (Hopkinson et al. 2017). With that in mind, we can then consider the complexity that must underlie the type I collagen ($C_{65}H_{102}N_{18}O_{21}$) signature (Kandel *et al.* 2020), the full complement of vibrational modes for which, to our knowledge, have not been fully resolved in the literature. There are also necessary considerations for physical variables related to the otolith and its presentation to the NIR light, such as varying shape, particle size, specular reflection, opacity, and density (Workman and Weyer, 2012), at least some of which are not constant within individual otoliths (e.g., growth bands of different composition and

optical properties) nor across otoliths of different ages. To put it simply: it's complicated. Hence, the spectral signature comparisons herein are not meant to be all-encompassing, but rather attempt to relate the basic relationship between mineral and organic fractions of the otolith to FT-NIRS age prediction, with the understanding that there are numerous other possibilities for constituents and physical interactions to shape the otolith spectral signature.

The results of this study confirm the ability of FT-NIRS to detect age-related chemical changes in otoliths, independent of concomitant changes in otolith size with age, and that these chemical changes do not arise from any systematic differences in crystal structure with age, although the random occurrence of atomic substitutions in the crystal lattice and any associated effect on FT-NIRS signatures cannot be addressed with the current data. We also confirm the presence of tightly-bound water molecules in red snapper otoliths and explore their contribution to the FT-NIRS otolith signature, and confirm that ambient interstitial moisture does not affect age prediction at storage times reported herein. However, some effects of physical changes - arising from the inherent characteristics of the whole otolith structure and how it changes with age - are evident in contributing to age prediction, and are important in understanding the impacts of sample presentation for future FT-NIRS applications. Finally, otolith protein content and associated age-related amino acid dynamics reported herein provide insights into the complexities of the otolith organic matrix and its potential to inform FT-NIRS applications for age prediction and beyond.

Our results indicate interstitial (free) water at ambient storage conditions for otoliths stored for 3 – 8 years comprises a negligible amount of the otolith by weight,

with implications for storage practices associated with otoliths intended for use in FT-NIRS analysis. Typically, otoliths collected and archived for age estimation are stored dry at ambient conditions, but some are preserved in glycerin thymol (e.g., Helser *et al.* 2019) or potentially other liquid preservatives. Robins et al.(2015) documented "storage effects" in the FT-NIRS spectra, attributed to the potential equilibration of otoliths to ambient conditions. Given the evidence herein of spectral effects from small quantities of interstitial water, it is feasible that these storage effects include the loss of interstitial water over time to the atmosphere.

Desiccation induced some shifting of spectral peaks in red snapper otoliths, which is a well-known effect of drying on NIR spectra (e.g., Chakravartula *et al.* 2019; Williams, 2019). The change in magnitude of some regression coefficients with desiccation also suggests that interstitial moisture content altered the contribution of some areas to the age prediction model, e.g., the 5960-5800 $cm^{-1}$ range assigned to $-CH_3$ and $-CH_2$ bond vibrations. These bonds are associated with the organic component; hence this might indicate that the small amount of unbound water in otoliths is more closely associated with the organic matrix than the mineral component. Bound water was evident in spectral signatures from all otolith preparations despite initial desiccation, hence it is not susceptible to changing ambient conditions or to alteration due to the change in otolith structure. NIRS has been used extensively in biomedical studies to assess water content in cartilage and other tissues, of which many have demonstrated an association between bound water and cartilage (Jaffe *et al.* 1974; Bagratashvili *et al.* 1997; Padalkar *et al.* 2013), and even more specifically, collagens and proteoglycans (Mankin and Thrasher, 1975). Free water molecules vibrate with higher frequency than bound water

molecules, which could be useful for elucidating the matrix binding sites of various molecules associated with water, including those of cartilage and collagens (Walling and Danbey, 1989; Padalkar *et al.* 2013) . In light of these considerations, future NIRS studies of otoliths should account for molecular water dynamics, and storage methods using preservation solutions should be evaluated for effects on FT-NIRS age prediction relative to storage at ambient conditions. Conversely, adoption of standard practices including routine desiccation before acquiring spectral data would preempt these effects in unequilibrated otoliths.

Protein made up a small but measurable portion of red snapper otoliths by weight and was not well predicted from spectral signatures without the removal of outliers to reduce variability in the sample set. However, the positive correlation of protein concentration with age provides a potential chemical basis for age prediction beyond simple correlation of overall spectral absorbance with increased otolith size. To our knowledge, estimates of red snapper otolith total protein content are not published elsewhere. Lueders-Dumont *et al.* (2020) documented increasing intracrystalline nitrogen content with otolith weight in three red snapper otoliths (~ 600 – 1100 mg otolith weight, ~ 1 – 6 years old based on otolith weight-at-age reported herein), but did not report total protein content. However, this study found that red snapper otoliths had much lower otolith:muscle $\delta^{15}N$ ratios relative to other species evaluated, and concluded that the large size and hence rapid growth of red snapper otoliths leads to reduced nitrogen enrichment in the organic matrix. The adult otoliths of another Lutjaniid, *Lutjanus ehrenbergii,* averaged ~ 0.6 ± 0.1% protein by weight, which also corroborates the low percent composition we report herein (McMahon *et al.* 2011). Protein content for other species

reported in the literature range from 0.16% to over 10% by weight, but most reported concentrations are below 3% (Degens, 1969; Morales-Nin, 1986a, 1986b; Baba *et al.* 1991; Sasagawa and Mugiya, 1996; Hüssy *et al.* 2004). Ontogenetic comparisons of otolith protein concentration are rare, but those in existence have found juvenile otoliths to contain higher protein concentrations than adults (Morales-Nin, 1986a, 1986b). Jolivet *et al.*(2008) likewise showed organic fractions to be higher in otolith cores than in subsequent growth bands. We did not see this trend in red snapper otoliths. We hypothesize that the rapid otolith accretion occurring in species with large otoliths results in high mineral-to-protein ratios through all life stages, a mechanism which has been suggested to explain low protein content in other species with large otoliths (McMahon, personal communication; Lueders-Dumont *et al.* 2020).

Increasing sample mass without increasing constituent concentration can lead to a false "age" effect as was demonstrated in our $CaCO_3$ layer age experiment. Since we know the composition of the $CaCO_3$ powder to be uniform in concentration, we can hypothesize that the wavenumbers correlated to the false "age" effect resulted from the persistent carbonate ion signature coupled with changes to light absorption/penetration inherent to increasing sample mass and thickness. While wavenumber ranges used in the "layer age" prediction models were similar to those used in the otolith age models, the specific absorbance patterns varied substantially, and the peaks associated with "layer age" might simply correspond to the molecular bonds present in $CaCO_3$ that are most sensitive to changes in light penetration with increasing layer thickness, similar to the limitations of light penetration documented in Passerotti *et al.*(2020b).

Other physical considerations are apparent when age prediction capability is compared in ground relative to whole otoliths. Altering the sample structure and presentation of whole otoliths by grinding reduced explained variance by about 6% and increased model error by about 40% in standardized models, but did not inhibit age prediction capability completely. This suggests the ordered structure of whole otoliths and the associated layered growth pattern is more conducive to age prediction than homogenized samples, which is contrary to most reported effects of grinding (e.g., wheat kernels; Williams, 2019). One potential mechanism for this pattern is the spatial heterogeneity of protein distribution documented in otoliths resulting from the precipitation of otolith material from the saccular epithelium. Concentration gradients are present in the otolith cavity which result in higher constituent concentrations, namely proteins, in areas in close contact with epithelium (Payan *et al.* 1999; Borelli *et al.* 2001; Jolivet *et al.* 2008, 2013). The otolith sulcus is generally the site in direct contact with the cells responsible for deposition of protein matrix onto the surface of the accreting otolith (Dunkelberger *et al.* 1980) and collagen concentration is also highest along the sulcus (Murayama *et al.* 2004). Coincidentally, the sulcal face (convex side) of the otolith is placed on the NIRS sample window for scanning in all studies done to date based on the recommendation of Robins et al.(2015), which may improve age prediction relative to that derived from other sample presentations because of the closer proximity of integrated proteins to the NIR light. Otolith chemical gradients can also reflect the composition of the endolymph at specific points in time due to entrapment of endolymph in interstitial spaces during otolith mineralization (Thomas *et al.* 2019; Lueders-Dumont *et al.* 2020) and hence might reflect age-specific trends that also vary with habitat, diet, or

physiology, as these factors influence the composition of endolymph as well (Thomas *et al.* 2017). In ground otoliths, the model cannot incorporate variation due to size, shape, or layering structure in order to improve the prediction. Even with corrective preprocessing, there can still be variation due to pathlength (the distance the light travels through the sample) incorporated into the model as was evidenced by the "layer age" experiment, which might contribute to better NIRS age prediction in whole samples. Ostensibly attenuation might occur even over small ranges of otolith size due to differences in density, opacity, and layering of the structure (e.g., (Hoff and Fuiman, 1993; Hüssy *et al.* 2004b; Jolivet *et al.* 2013). Particle size and light scatter effects are generally reduced in ground relative to whole grains and seeds (Williams, 2019), and the same is likewise apparent in otoliths. Overall, the assumption that the behavior of light is uniform as it passes through inherently heterogeneous otoliths must be discarded, and acknowledgement made of the physical effects surrounding FT-NIRS analysis of otoliths.

The spectral region 4688-4544 $cm^{-1}$, which is known to be associated with protein discrimination in a range of other NIRS applications (Workman and Weyer, 2012), was used to inform the optimized age prediction model for FMG samples but was not included in whole otolith optimized age models. This might seem to discount previously published theories, e.g., Helser *et al.* (2019), that FT-NIRS age models reflect changes in protein concentration with age; however, this is not necessarily the case. Vibrational modes are harmonic so the impact of one type of bond vibration will appear at multiple points in the NIR spectrum, primarily as combination bands in the lower wavenumber regions and again as overtones at higher wavenumbers. Proteins and peptides (detected in NIR spectra using their amide content) can be detected in other regions including 10277-

9804 $cm^{-1}$, 6667-6536 $cm^{-1}$, 4878-4854 $cm^{-1}$ and 4400-4000 $cm^{-1}$ (Workman and Weyer, 2012). Hence, exclusion of a specific wavenumber from a model does not mean other corresponding molecular vibrations are not present elsewhere in the signature. The 4688-4544 $cm^{-1}$ region reflects C-H, C=O, C-N and N-H bonds, all of which are present in protein molecules. Overtones of C-H vibrations appear between 6030-5500 $cm^{-1}$ followed by N-H overtones between 6770-6030 $cm^{-1}$ (Workman and Weyer, 2012), and both of these regions are included in whole otolith optimized age models. Additionally, the age-correlated decrease in mineral fraction that ostensibly happens concurrent to the increasing organic fraction is itself measurable, as demonstrated in part by our "layer age" experiment, and might produce a more easily detectable and less variable signal than organic components due to the higher percent composition of $CaCO_3$. This type of correlation, in which a characteristic is measured via the change in an associated but more easily measured constituent, is commonly used in NIRS analyses (Williams, 2019). Hence, the effect of changing protein content on age prediction is captured at multiple points throughout the spectral signature, and at wavenumber regions associated with both protein and carbonate molecules, an argument that is supported by our analysis of age model regression coefficients using carbonate and collagen-associated wavenumbers. As such, both the magnitude and direction of correlation are important when evaluating the influence of wavenumber regions on age models.

Age related trends in amino acid concentrations relative to total protein weight suggest the composition of otolith proteins varies significantly across the lifespan of red snapper, which has manifold impacts on how spectral signatures of otoliths change with age. Amino acids contain characteristic amide groups in varying quantities and molecular

configurations and, in addition to the overall quantity of bonds, their positioning within the amino acid structure as well as protein folding patterns affect the molecular architecture and thus bond vibration characteristics (Workman and Weyer, 2012; Czarnecki *et al.* 2015; Williams, 2019). Hence specific amino acid and thus protein composition as a whole affect the corresponding spectral signature. Otolith protein composition changes with age (Morales-Nin, 1986a; Baba *et al.* 1991; Davis *et al.* 1995; Hüssy *et al.* 2004b; Thomas *et al.* 2019), and species-specific patterns in otolith amino acid composition have also been documented (Söllner *et al.* 2003; Tohse *et al.* 2008; Weigele *et al.* 2016; Lueders-Dumont *et al.* 2020). Without knowing the specific proteins contained in red snapper otoliths, it is difficult to interpret specific effects on the otolith spectral signature and overall age prediction. These findings have impacts on the future use of FT-NIRS not only for age prediction, but also to infer habitat and life history-related information from otolith signatures. Otolith chemistry is widely utilized in ecological studies to reconstruct migration, habitat use, and diet via the chronologically-ordered recording of trace element and isotopic profiles within the otolith (e.g., Elsdon *et al.*2008; Walther, 2019). Future studies examining the ability of FT-NIRS to reflect fine-scale otolith protein dynamics would be beneficial in the pursuit of a less-expensive and non-destructive method of discriminating otolith chemistry for application to broader fisheries management goals.

### 4.6 Conclusions

Near infrared spectroscopy in otoliths shows potential for application to a wide range of fisheries research areas, including age estimation. The realization of its potential, however, will only progress as fast as our understanding of otolith compositional

dynamics, which act alongside otolith morphometrics to drive NIRS spectral signatures. In-depth holistic studies of otolith compositional dynamics are rare, but recent advances in high-resolution detection and visualization of key constituents (e.g., Thomas *et al.* 2019, 2020; Hüssy *et al.* 2020a) highlight their usefulness. Otoliths are increasingly used as fine-scale chemical chronometers to reconstruct environmental and metabolic histories; NIRS could be a transformative tool in these pursuits, but the integrative nature of physical and chemical properties inherent to NIRS analysis cannot be disregarded.

**Table 4.1.** PLS age prediction model results for all red snapper otolith treatments and calcium carbonate "layer age" regressions.

| Model | n | Wavenumber Region(s) | $R^2$ | RMSECV | RPD | Bias | Rank |
|---|---|---|---|---|---|---|---|
| Whole otolith, ambient, standardized | 84 | 6104-4200 | 94.1 | 1.67 | 4.11 | 0.022 | 5 |
| Whole otolith, ambient, optimized | 84 | 6032-5492<br>4952-4767 | 94.8 | 1.57 | 4.37 | 0.002 | 4 |
| Whole otolith, dried, standardized | 84 | 6104-4200 | 93.8 | 1.71 | 4.03 | -0.014 | 5 |
| Whole otolith, dried, optimized | 84 | 7456-6768<br>6032-5496<br>4952-4768 | 94.4 | 1.62 | 4.23 | -0.016 | 4 |
| Whole ground, standardized | 84 | 6104-4200 | 88.0 | 2.38 | 2.89 | -0.013 | 4 |
| Whole ground, optimized | 84 | 7456-6768<br>6032-5496<br>4952-4768 | 89.9 | 2.19 | 3.15 | -0.011 | 5 |
| Fixed mass ground, standardized | 71 | 6104-4200 | 83.4 | 2.48 | 2.45 | 0.047 | 3 |
| Fixed mass ground, optimized | 71 | 6104-4544 | 89.0 | 2.02 | 3.02 | 0.033 | 8 |
| Powdered $CaCO_3$, standardized | 30 | 6104-4200 | 87.4 | 1.02 | 2.82 | 0.008 | 5 |

**Table 4.2.** PLS prediction model results for red snapper otolith protein concentration (% otolith weight).

| Model | n | Wavenumber Region(s) | $R^2$ | RMSECV | RPD | Bias | Rank |
|---|---|---|---|---|---|---|---|
| Whole otolith protein, standardized | 26 | 6104-4200 | 59.9 | 0.078 | 1.58 | 8.3 e-5 | 2 |
| Whole otolith protein, optimized | 26 | 7456-6768<br>6400-6024 | 67.9 | 0.070 | 1.76 | 1.3 e-4 | 2 |
| Whole otolith protein reduced, optimized | 23 | 4688-4600 | 86.3 | 0.035 | 2.7 | 5.0 e-4 | 2 |
| Fixed mass ground otolith protein, standardized | 21 | 6104-4200 | 30.9 | 0.083 | 1.2 | 8.6 e-4 | 1 |
| Fixed mass ground otolith protein, optimized | 21 | 6032-5496 | 52.9 | 0.069 | 1.46 | 4.0 e-3 | 8 |
| Fixed mass ground otolith protein reduced, optimized | 18 | 4600-4544 | 90.5 | 0.019 | 3.25 | 8.1 e-5 | 5 |

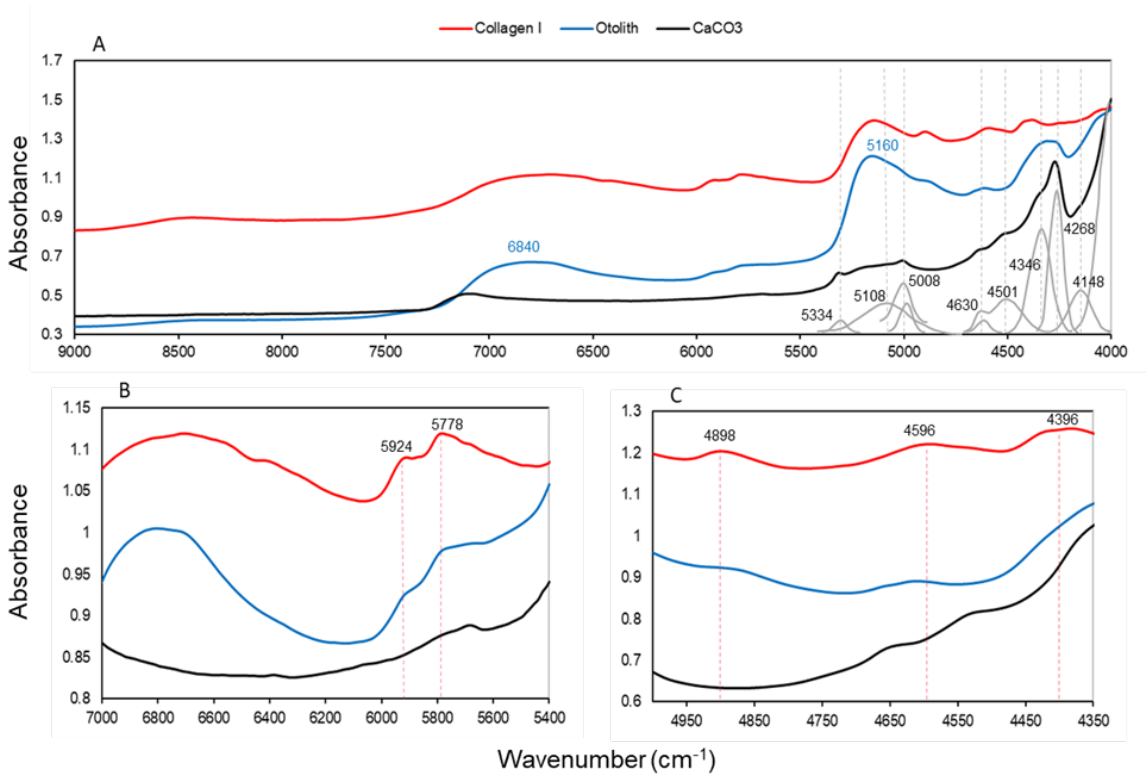


**Figure 4.1**. Comparison of NIR spectral signatures from powdered Type I collagen (Kandel et al. 2020), whole red snapper otolith (age=16 years), and powdered calcium carbonate, with resolved $CaCO_3$ band contributions from respective vibrational modes represented with gray curves (Hopkinson *et al.* 2017). Gray dashed lines are given to visualize alignment of deconvolved $CaCO_3$ peaks with other spectra. Numbered peaks in blue for the otolith spectrum denote water features as described by Gauldie *et al.* (1998). Collagen peak assignments are numbered in B and C, and red dashed lines are given to visualize alignment of collagen peaks to the otolith spectrum.

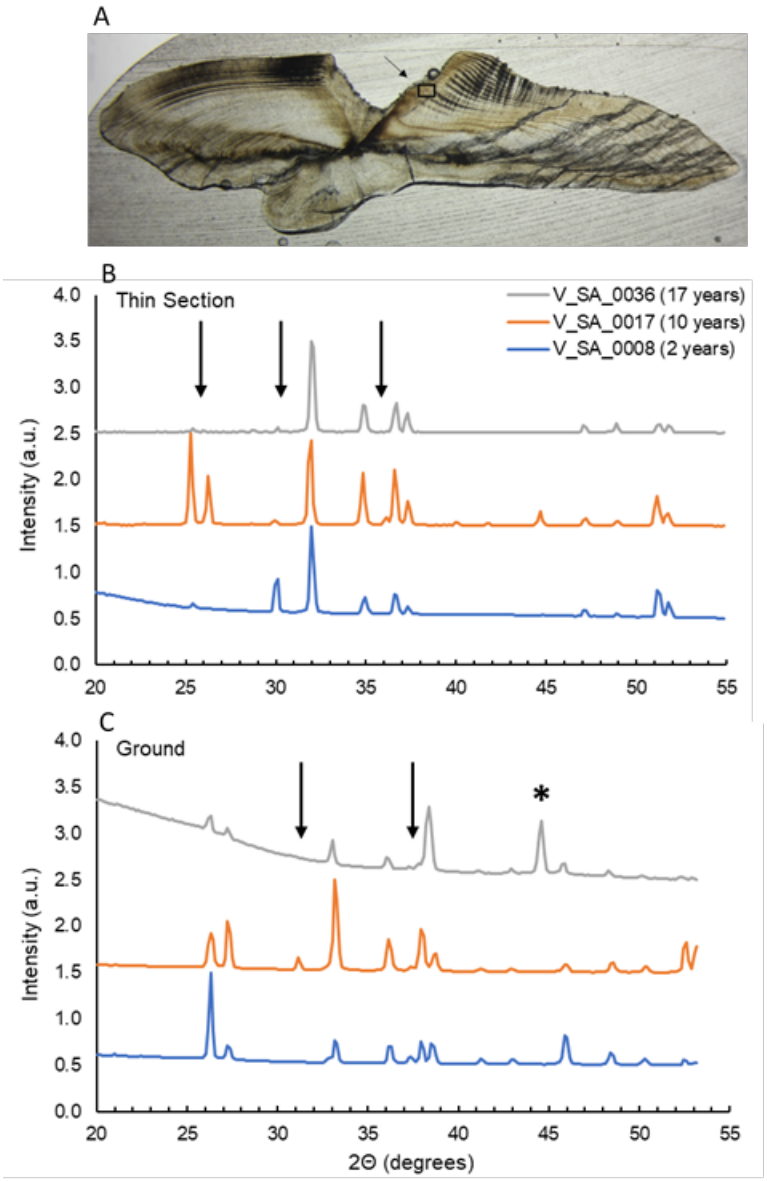


**Figure 4.2.** A) Red snapper otolith section from V_SA_0032, a 17 year old fish evaluated with X-Ray diffraction (XRD). Black box (indicated by arrow) shows the approximate location of XRD sampling, which was standardized among the three sections analyzed. B) Results of XRD measurements from thin sectioned and C) ground red snapper otoliths aged 2, 10, and 17 years. Arrows in B and C denote peaks where differences were evident between samples, and * denotes a peak that was not assignable to any tested polymorph and which is a presumed artifact or impurity in the sample.

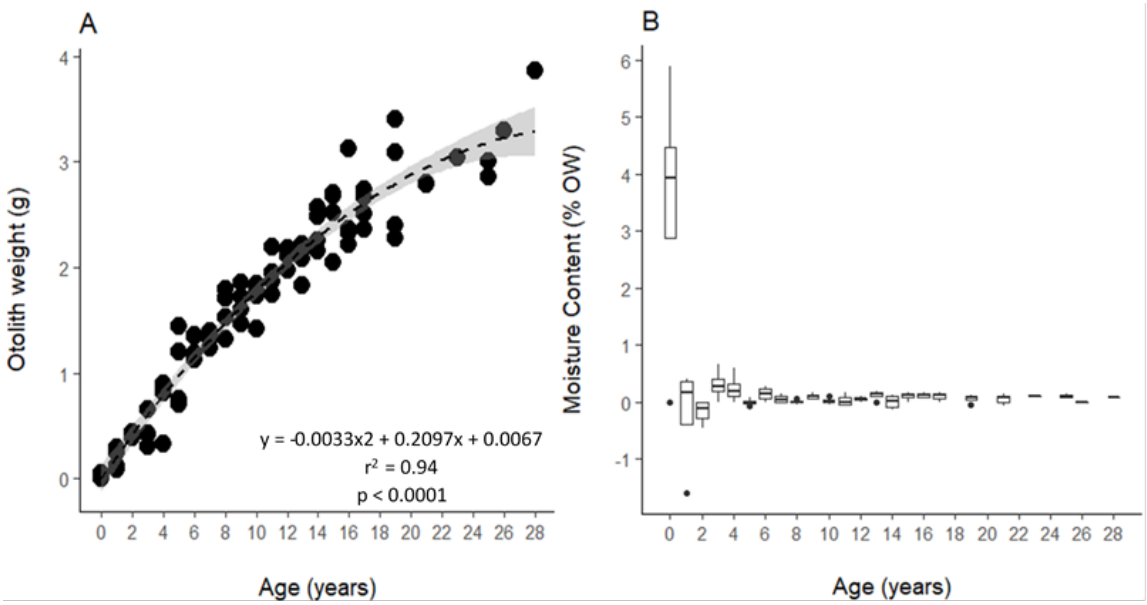


**Figure 4.3.** A) Red snapper ambient otolith weight (g) regressed with age, fitted with a quadratic linear regression (dashed line) and 95% confidence intervals (shaded region). B) Boxplot of free water content (% otolith weight) by age.

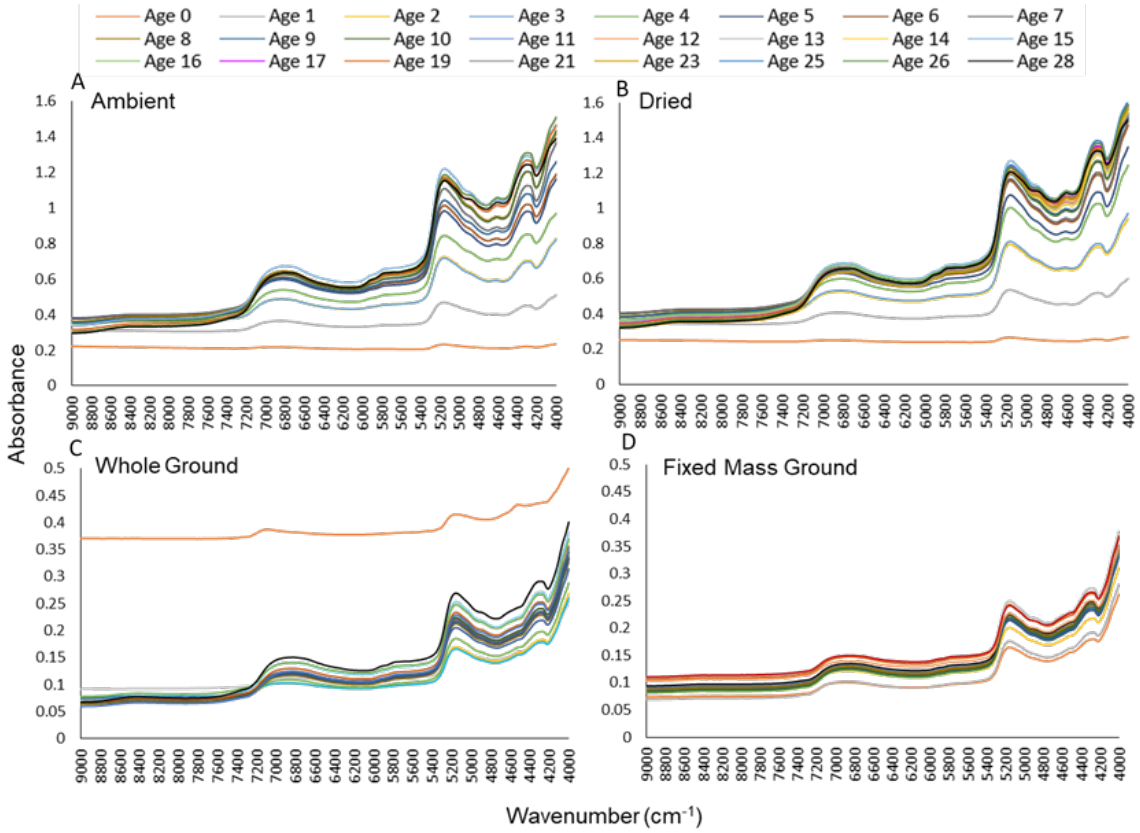


**Figure 4.4.** Averaged red snapper FT-NIRS spectral signatures for A) ambient, B) dry, C) ground, and D) fixed mass ground otoliths by age.

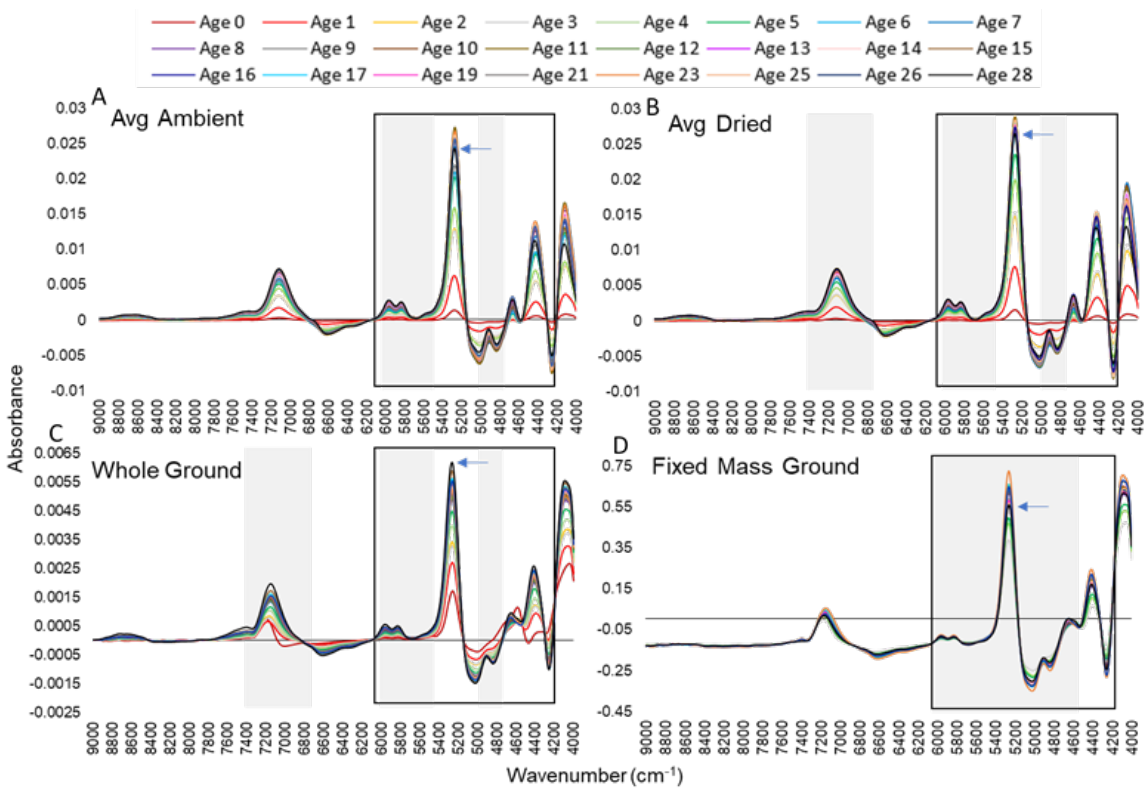


**Figure 4.5.** Red snapper otolith first-derivative (A-C) and first-derivative + SNV (D) preprocessed FT-NIRS spectra, averaged by age, for each sample treatment. Arrows denote the absorbance value of the oldest otolith (Age 28) near 5200 $cm^{-1}$, for reference. Fixed Mass Ground samples did not include ages < 3 years. Black boxes delineate the wavenumber regions included in the standardized age prediction models, while grey shading delineates wavenumber regions included in optimized age prediction models.

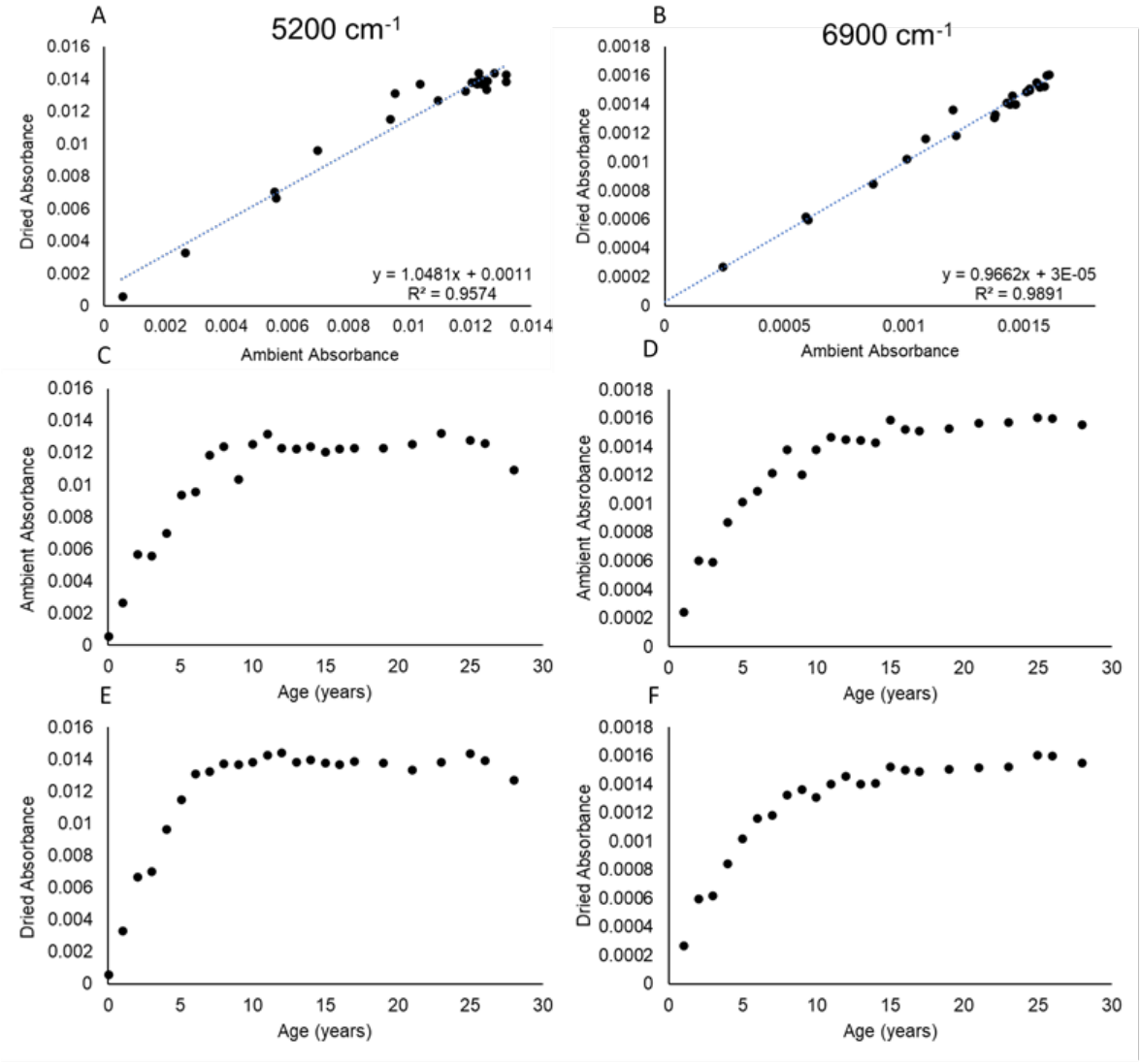


**Figure 4.6.** Comparison of drying effects on first derivative-transformed spectral absorbance measurements for water-associated peaks near 5200 $cm^{-1}$ (A, C, E) and 6900 $cm^{-1}$ (B, D, F) in red snapper otoliths.

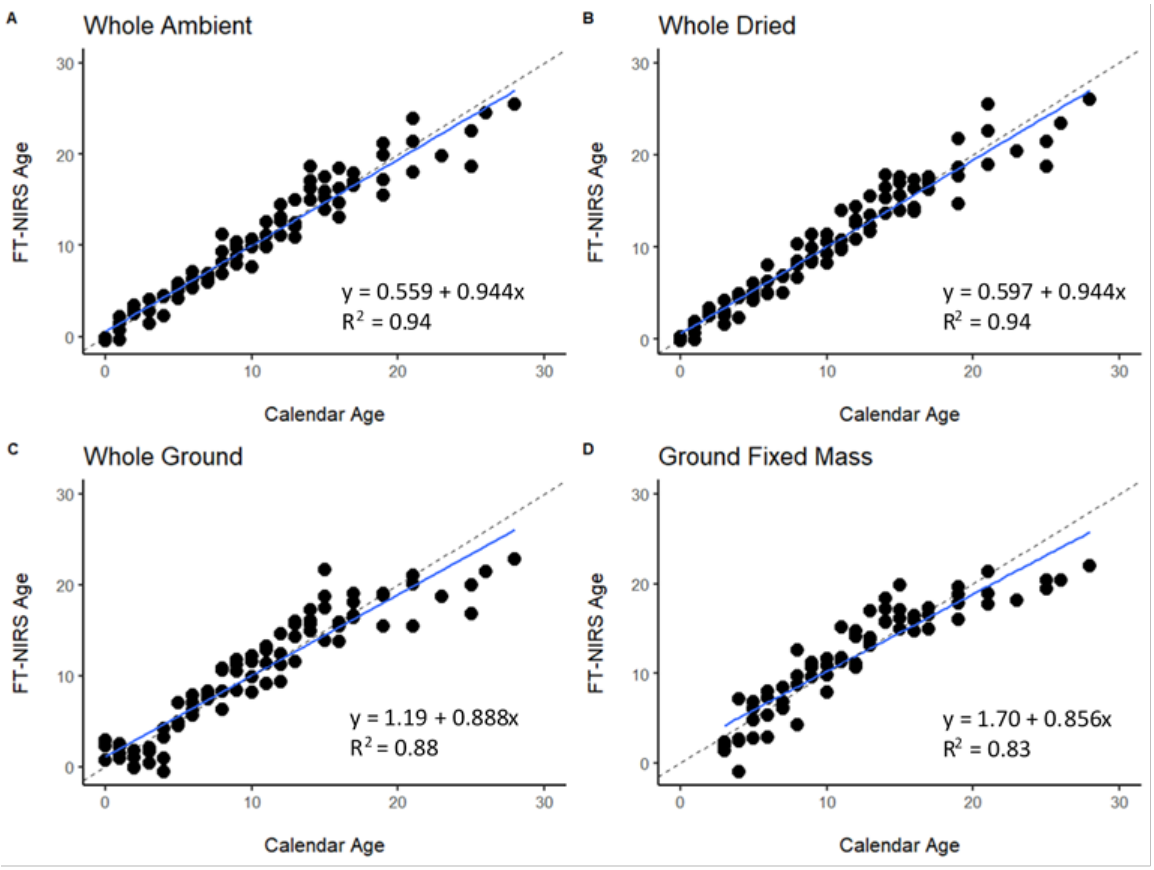


**Figure 4.7.** Red snapper otolith standardized PLS age regressions based on A) ambient spectra, B) dry spectra, C) ground spectra, and D) fixed mass ground spectra.

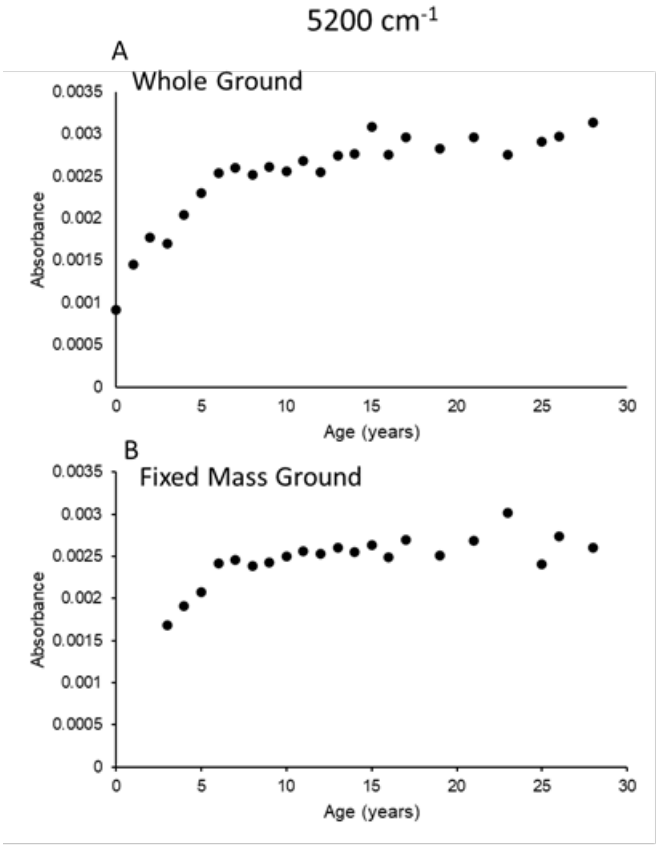


**Figure 4.8.** Comparison of (A) grinding and (B) subsampling effects on first-derivative transformed spectral absorbance measured at the water-associated peak near 5200 $cm^{-1}$ in red snapper otoliths.

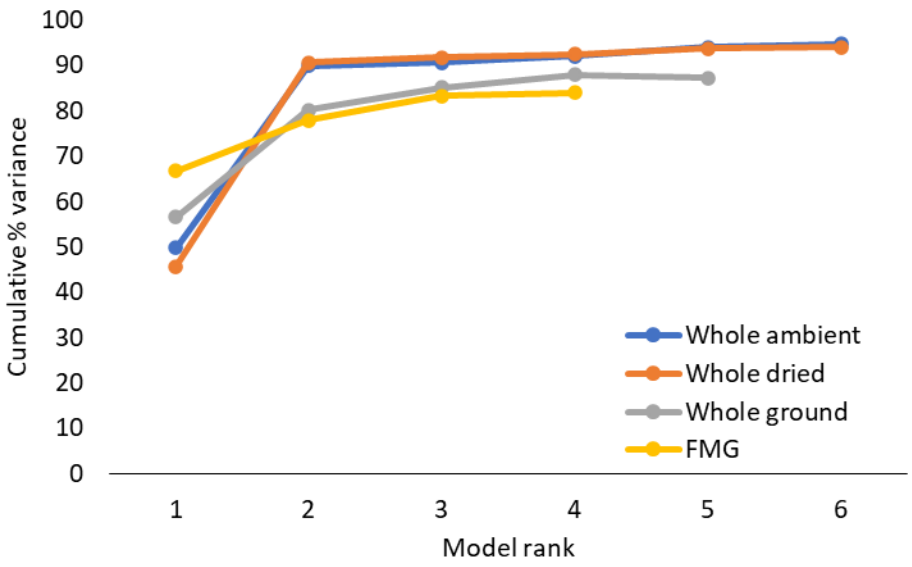


**Figure 4.9.** Scree plot of standardized age model variance explained per modelled rank (number of latent variables) for each of the red snapper otolith treatments.

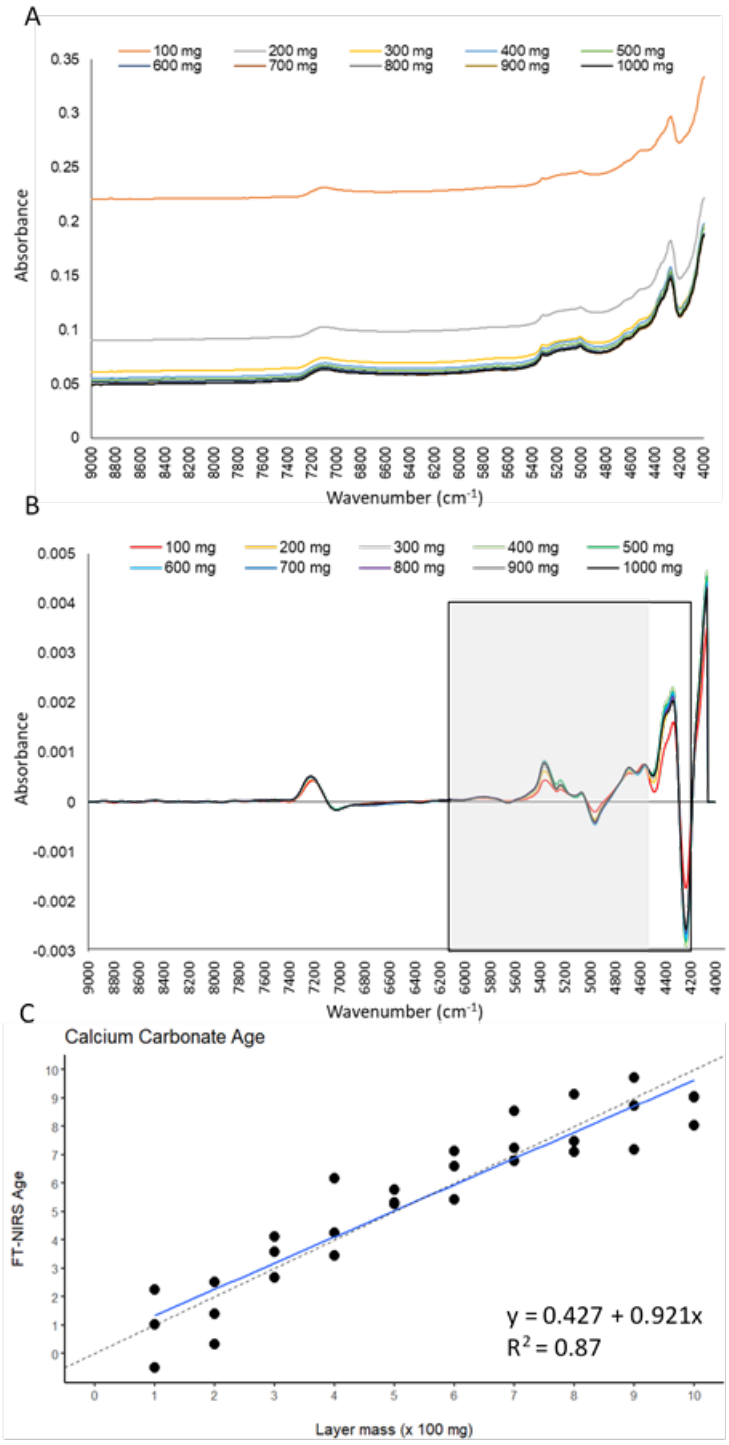


**Figure 4.10.** Results of calcium carbonate layering experiment: A) raw and B) preprocessed spectral signatures by layer thickness, and C) standardized PLS regression results of "layer age" prediction.

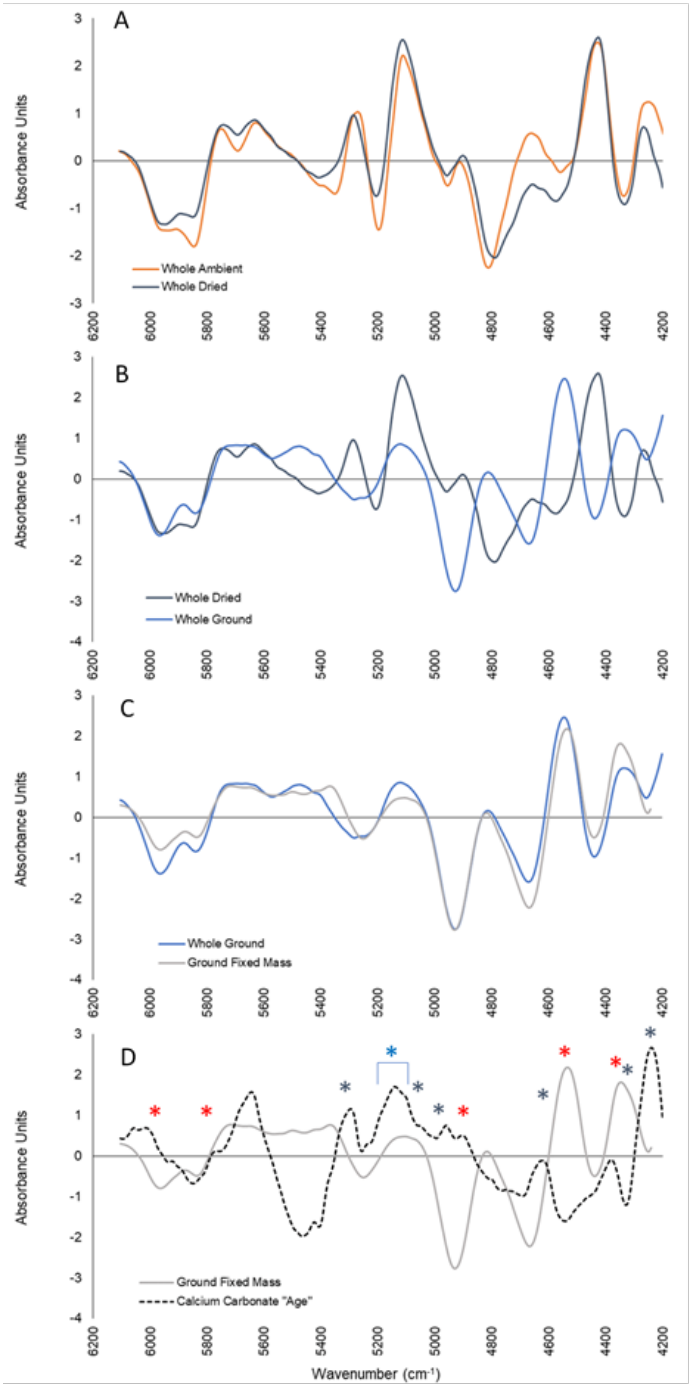


**Figure 4.11.** Red snapper age PLS regression coefficients for the standardized age model (6104-4200 $cm^{-1}$) comparing A) drying, B) grinding and C) subsampling otolith treatments and D) the calcium carbonate "layer age" treatment compared with FMG otolith age regression. All coefficients were standardized to Z scores to facilitate comparisons. In (D), colored asterisks correspond to influential wavenumbers for collagen (red), $CaCO_3$ (gray) and water (blue) signatures as documented in Figure 1.

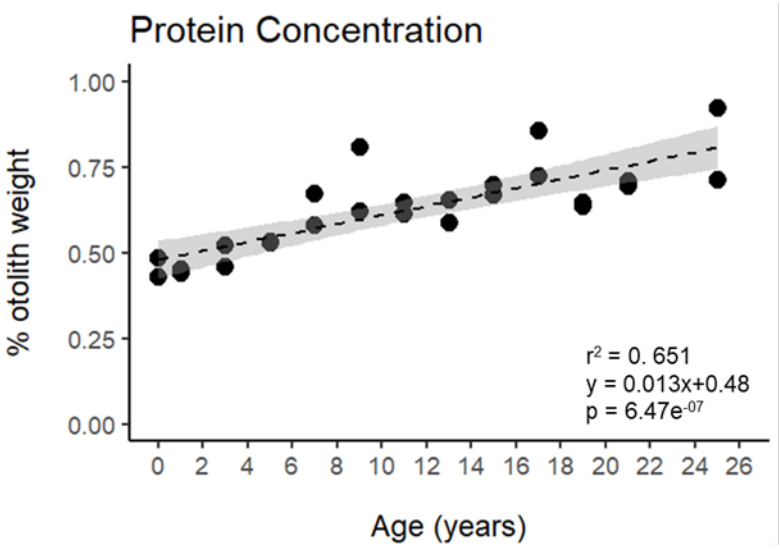


**Figure 4.12.** Red snapper otolith protein concentration as a function of age, with best-fit regression line and 95% confidence interval plotted.

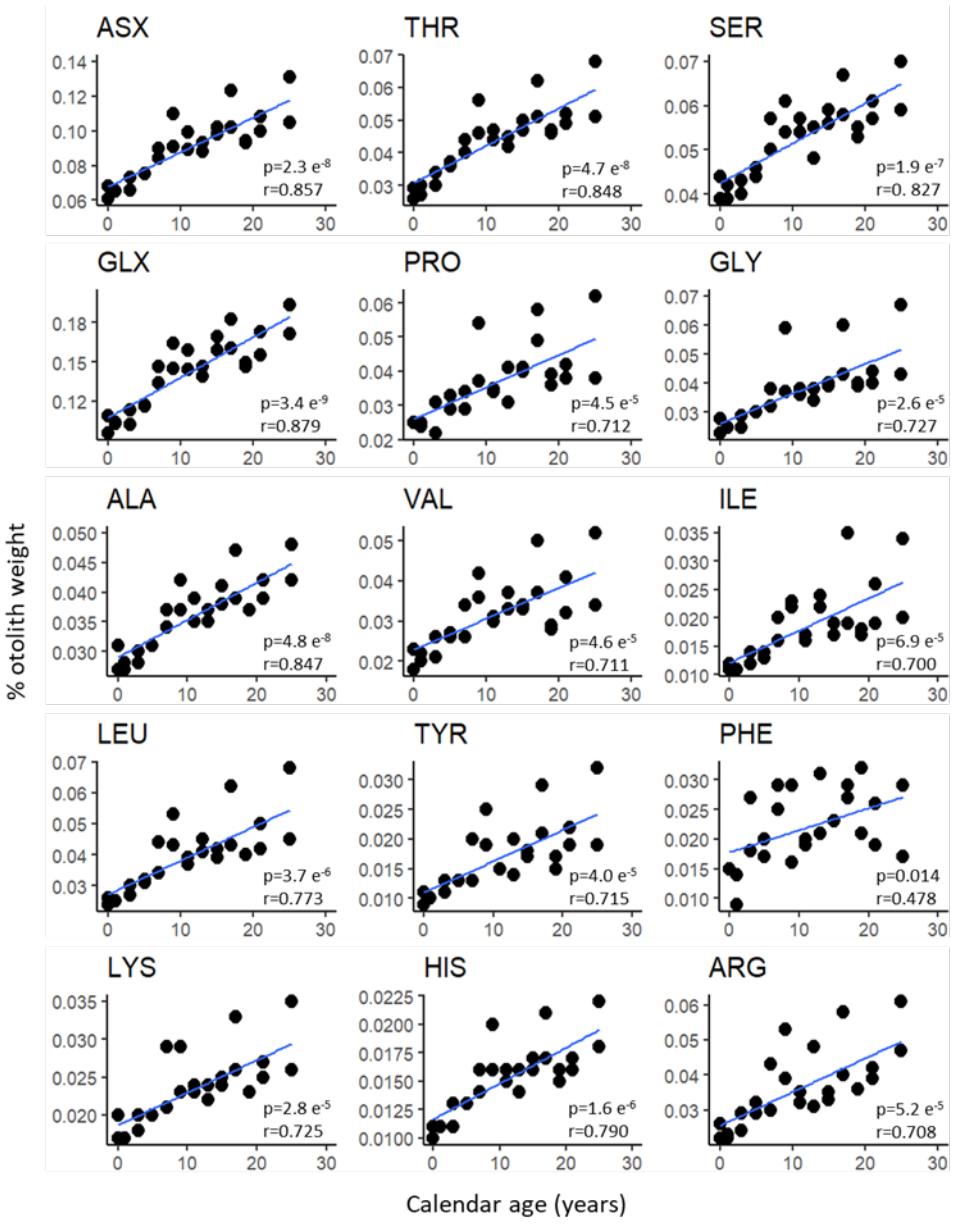


**Figure 4.13.** Red snapper otolith amino acid concentrations (% otolith weight) for aspartic acid/asparagine (ASX), threonine (THR), serine (SER), glutamic acid/glutamine (GLX), proline (PRO), glycine (GLY), alanine (ALA), valine (VAL), isoleucine (ILE), leucine (LEU), tyrosine (TYR), phenylalanine (PHE), lysine (LYS), histidine (HIS), and arginine (ARG) plotted by age. Correlation coefficients and significance are given for each regression.

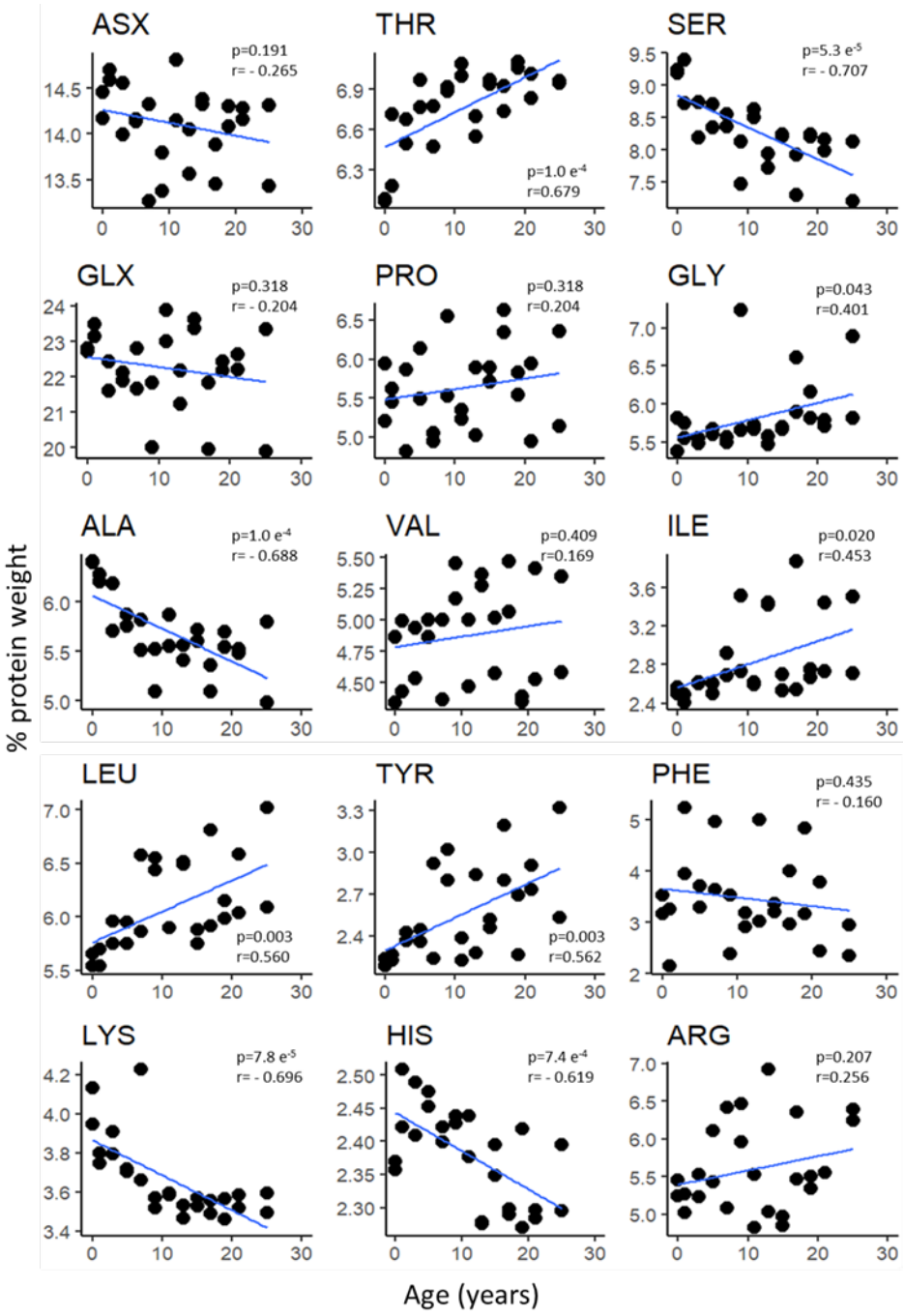


**Figure 4.14.** Red snapper otolith amino acid concentration (% total protein weight), plotted by age for aspartic acid/asparagine (ASX), threonine (THR), serine (SER), glutamic acid/glutamine (GLX), proline (PRO), glycine (GLY), alanine (ALA), valine (VAL), isoleucine (ILE), leucine (LEU), tyrosine (TYR), phenylalanine (PHE), lysine (LYS), histidine (HIS), and arginine (ARG). Correlation coefficients and significance are given for each regression.

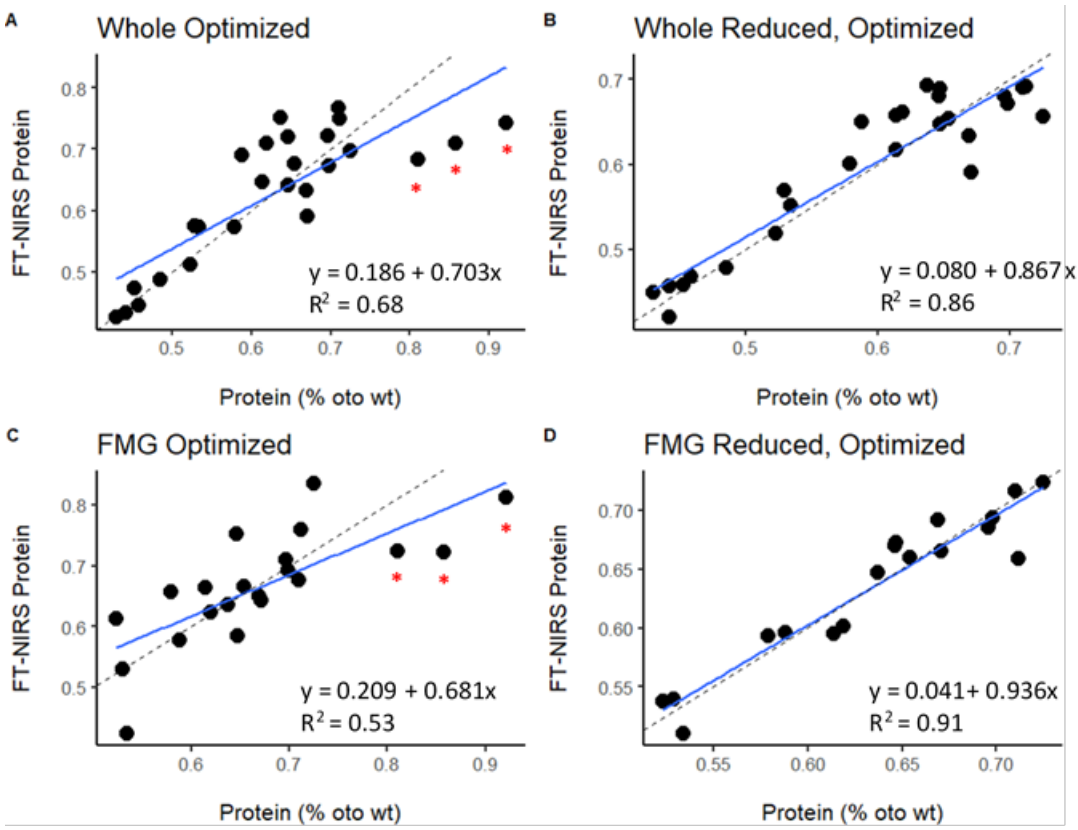


**Figure 4.15.** Red snapper otolith protein PLS regression results for predicting protein concentration. Outliers are denoted in A & C with red asterisks.

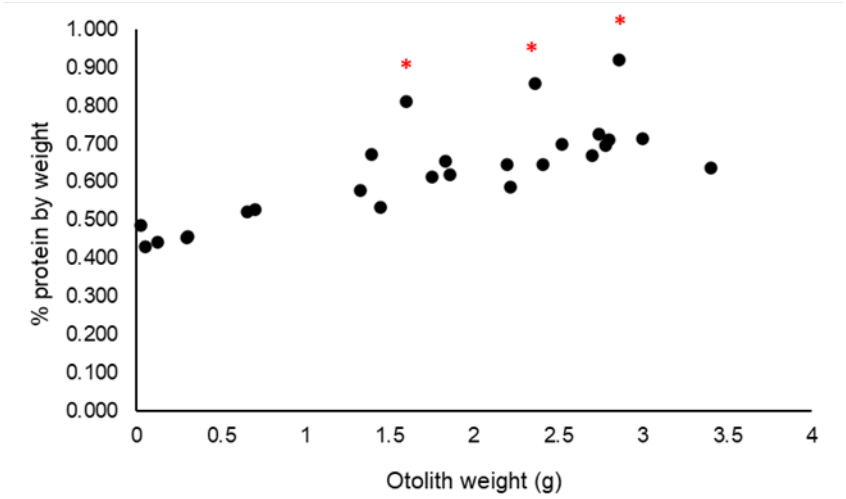


**Figure 4.16.** Red snapper otolith protein concentration (% otolith weight) plotted as a function of otolith weight. Samples indicated by red asterisks were identified as outliers in protein prediction PLS regression models and were removed to produce optimized protein prediction models.

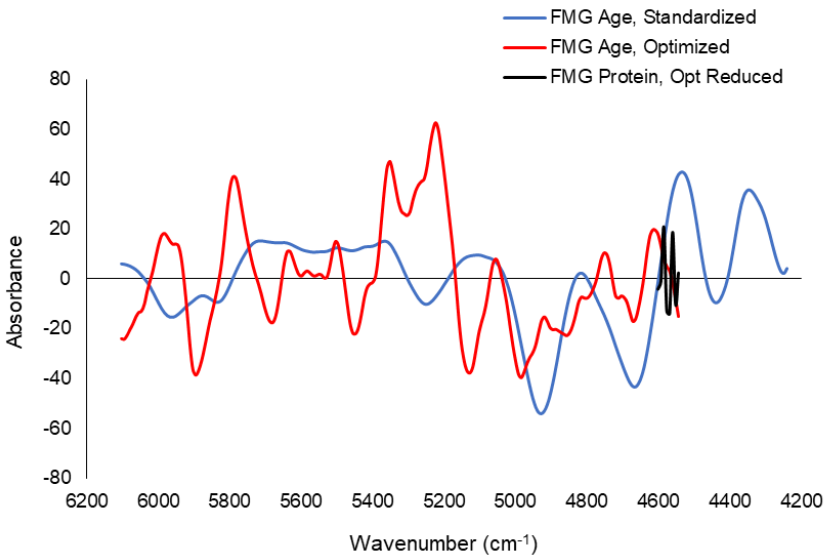


**Figure 4.17.** Red snapper otolith PLS regression coefficients for standardized and optimized Fixed Mass Ground age prediction and Optimized reduced protein prediction models.

# CHAPTER 5

# CONCLUSIONS

This work fills important knowledge gaps associated with the development of novel spectroscopic methods for generating fish age estimates for use in fisheries research and management. Accurate characterization of fish population age structure is a critical component of fisheries stock assessment and ultimately in the setting of management policy. The stock assessment process is necessarily transparent and inclusive of input from all interested stakeholders. Because of the wide range of potential impacts of management decisions on various stakeholders, decisions to adopt new stock assessment methods, including those for data generation, are rightly subject to intense scrutiny. There is great potential for NIRS age prediction to improve the timeliness and reduce costs associated with generating ages for stock assessments, and it is of vast interest to fisheries managers. However, there also exists a very real need to fully vet the NIRS method, to understand its benefits and potential shortcomings in the context of currently employed (i.e., traditional) age estimation methods, and to clearly and unequivocally communicate the science involved to stakeholders. Of paramount importance in this pursuit is understanding the fundamental mechanisms of NIRS age prediction.

In this dissertation, I have presented data and drawn conclusions to address several fundamental aspects of NIRS age prediction in otoliths: 1) Expanded the

application of NIRS age prediction to a new species, red snapper *Lutjanus campechanus*, 2) expanded understanding of the applicable time scales over which NIRS can predict age in otoliths to include daily age resolution, 3) demonstrated the utility of NIRS age prediction for production ageing in a heavily managed species, 4) demonstrated the effects of differential light interaction on NIRS age prediction and conceived a novel use of light aperture to improve prediction capability, 5) demonstrated the equivalence of data products formulated with NIRS ages to those formulated with traditional ages, and 6) demonstrated age-related physical and chemical dynamics in otoliths that provide a basis for the mechanism of NIRS age prediction in otoliths.

### 5.1 Species-specific NIRS age prediction models from otoliths of red snapper

In Chapters 2 and 3, I present novel spectroscopic data from approximately 1500 red snapper otoliths ranging in age from 39 days to 38 years. Using paired traditional age estimates from these otoliths, I generate NIRS age prediction models optimized for daily and annual ages in juvenile and adult red snapper, respectively. Age prediction using NIRS otolith models has been previously demonstrated in four other teleost species, and the models are known to be species-specific, and in some cases region-specific (e.g., (Robins *et al.* 2015). In red snapper otoliths, regional variability in NIRS predictive models was evident, but age prediction was optimal when models included all samples across all regions. Optimized models presented herein comprise both the youngest and oldest otoliths analyzed with NIRS to date, and represent the first NIRS age models produced for red snapper.

## 5.2 NIRS discriminates daily ages from whole otoliths of juveniles

In Chapter 2, I present spectroscopic data from 153 otoliths of juvenile red snapper and demonstrate the first application of NIRS to predict daily ages from whole otoliths of juvenile fish. Age estimation of juvenile fish is of vital importance to understanding recruitment dynamics and broader ecological aspects of the early life history of fishes. The capability of NIRS to rapidly and non-destructively estimate ages with high precision from scans of whole otoliths is of great consequence to larval fish research. In this chapter, I also demonstrate the capability of NIRS to predict otolith weight from spectral data, and discuss the implications of this on understanding the mechanisms underlying NIRS age prediction in otoliths. Regression coefficient patterns were different for age prediction models relative to otolith weight prediction models, suggesting that the relationships of chemical bonds with otolith age and weight differ. These insights support the findings of Robins et al.(2015) that NIRS age prediction is not solely dependent on age-related increases in otolith size to inform predictive models.

## 5.3 NIRS predicts annual ages with similar accuracy and reduced turnaround time relative to traditional methods

In Chapter 3, I present NIRS models that predict annual ages of red snapper otoliths test sets to within an average of 1 year relative to traditional estimates. Average Percent Error (APE) metrics, which are used to monitor the quality of age estimates provided to stock assessments, were similar to those generated for traditional ages, although the ages of the oldest otoliths tended to be underestimated. The time required for collection of NIRS spectral data averaged about 90 seconds per otolith, and once

predictive models have been developed, age prediction could happen instantaneously upon completion of spectral scanning. Hence, relative to traditional methods which might average about 300 otoliths aged in a given work week, NIRS age prediction could allow efficiency improvement of roughly 300% in a production ageing environment. Owing to the growing number of fish stocks being assessed and the constant demand for age estimates in assessments, there is great potential for NIRS age prediction to improve the process of production ageing at a broad scale.

### 5.4 Light interaction varies with otolith size and must be considered when evaluating NIRS age prediction

In Chapters 2 and 3, I present evidence that otolith size can negatively impact NIRS age prediction due to its varying effects on light interaction with the otolith itself. In Chapter 2, the small size of juvenile otoliths resulted in poor consistency of sample placement onto the spectrometer window as well as poor resolution of spectral signatures relative to background signal.The use of a light aperture for scanning these otoliths improved age prediction by enabling better precision of sample presentation and increasing the otolith signal relative to that of the background. In Chapter 3, I experimentally demonstrate that light is attenuated in the oldest, thickest otoliths used in the study, which potentially affected the ability of NIRS to predict ages of these otoliths. When taken together, it is evident that age-related changes to otolith morphometrics can have significant impacts on age prediction; hence, physical characteristics of ageing structures must be taken into consideration when considering the applicability of NIRS methods.

## 5.5 NIRS ages are capable of producing equivalent growth and age structure models relative to traditional ages

In Chapters 2 and 3, I present growth model and age structure comparisons using traditionally-derived and NIRS-predicted ages. In both cases, the models produced with NIRS-predicted ages were not statistically different than those produced with traditional ages. This is an important result in terms of future expansion of NIRS to production ageing roles for management. Data products based on population age estimates e.g., mortality estimates and spawning stock biomass, form the basis of decision-making in stock assessment models. The ability of NIRS models to produce equivalent ages is of paramount importance to vetting of NIRS-predicted ages for use in management. Further characterization of error structure surrounding NIRS age estimates is needed, as well as the use of sensitivity analyses to determine downstream effects of using NIRS-predicted ages in comparison to traditional estimates.

## 5.6 Compositional dynamics determine the majority of NIRS age prediction capability, but otolith morphology and physical traits also contribute to age prediction

In Chapter 4, I present the first data on otolith protein and amino acid dynamics over multi-decadal time scales, not only for red snapper but across all fish species, with corresponding implications for overall compositional changes potentially underlying NIRS age prediction. This targets a large knowledge gap in understanding not only the changes in the otolith organic matrix over the lifespan of fish, but also its role in NIRS age prediction. Previous studies have implicated the organic matrix as potentially

underlying the age-related molecular differences discernable with NIRS (Helser et al. 2018). Red snapper otolith protein concentration was low and varied considerably among some replicates; however, protein concentration was predictable using NIRS analysis, and wavenumber regions associated with protein content were useful in age prediction models. Further, regression coefficients for age prediction models overlapped with regions evident in both collagen and calcium carbonate signatures, which supports the contribution of both carbonate and protein-related chemical bonds to NIRS prediction of age in otoliths. Finally, grinding and subsampling experiments presented in Chapter 4 confirm that true compositional changes underlie NIRS age prediction capabilities, but also demonstrate that age-related morphometric changes inherent in whole otoliths explain a non-trivial amount of variance in NIRS age prediction models.

This work is the first to provide empirical evidence of the mechanisms underlying age prediction in otoliths, with broad implications for further use of this technology across fisheries science. Specifically, the physical dynamics that appear to impact age prediction must not be overlooked. The use of NIRS to predict age from other types of ageing structures, such as fin spines and vertebrae, has been superficially demonstrated (e.g., Rigby et al. 2019), but the experimental results given herein suggest morphometric characteristics could play an overarching role in the success of age prediction beyond simple proof-of-concept.

# REFERENCES


Afara, I., Prasadam, I., Crawford, R., Xiao, Y., and Oloyede, A. 2012. Non-destructive evaluation of articular cartilage defects using near-infrared (NIR) spectroscopy in osteoarthritic rat models and its direct relation to Mankin score. Osteoarthritis and Cartilage, 20: 1367–1373.

Ailavajhala, R., Querido, W., Rajapakse, C. S., and Pleshko, N. 2020. Near infrared spectroscopic assessment of loosely and tightly bound cortical bone water. The Analyst, 145: 3713–3724.

Allman, R., Barnett, B. K., Trowbridge, H., Goetz, L., and Evou, N. 2012. Red snapper otolith ageing summary 2009-2011. SEDAR31-DW05. SEDAR, North Charleston, SC.

Allman, R. J., Lombardi, L., Fitzhugh, G. R., and Fable, W. A. 2002. Age structure of red snapper (*Lutjanus campechanus*) in the Gulf of Mexico by fishing mode and region. Gulf and Caribbean Fisheries Institute, 53: 482–495.

Allman, R. J., Fitzhugh, G. R., Starzinger, K. J., and Farsky, R. A. 2005. Precision of age estimation in red snapper (*Lutjanus campechanus*). Fisheries Research, 73: 123–133.

Allman, R. J., Patterson, W. F., Fioramonti, C. L., and Pacicco, A. E. 2018. Factors affecting estimates of size at age and growth in grey triggerfish *Balistes capriscus* from the northern Gulf of Mexico. Journal of Fish Biology, 92: 386–398.

Alm, E., Bro, R., Engelsen, S. B., Karlberg, B., and Torgrip, R. J. O. 2007. Vibrational overtone combination spectroscopy (VOCSY)—a new way of using IR and NIR data. Analytical and Bioanalytical Chemistry, 388: 179–188.

Andrews, A. H., Yeman, C., Welte, C., Hattendorf, B., Wacker, L., and Christl, M. 2019. Laser ablation–accelerator mass spectrometry reveals complete bomb 14C signal in an otolith with confirmation of 60-year longevity for red snapper (*Lutjanus campechanus*). Marine and Freshwater Research, 70: 1768.

Baba, K., Shimizu, M., Mugiya, Y., and Yamada, J. 1991. Otolith Matrix Proteins of Walleye Pollock; Biochemical Properties and Immunohistochemical Localization in the Saccular Tissue. *In* Mechanisms and Phylogeny of Mineralization in Biological Systems, pp. 57–61. Ed. by S. Suga and H. Nakahara. Springer Japan, Tokyo.

Bagratashvili, V. N., Sobol, E. N., and Sviridov, A. P. 1997. Thermal and diffusion processes in laser-induced stress relaxation and reshaping of cartilage. Journal of Biomechanics, 30: 813–817.

Bajoghli, B., Ramialison, M., Aghaallaei, N., Czerny, T., and Wittbrodt, J. 2009. Identification of starmaker-like in medaka as a putative target gene of Pax2 in the otic vesicle. Developmental Dynamics, 238: 2860–2866.

Baker, S. Jr. M., and Wilson, C. A. 2001. Use of bomb radiocarbon to validate otolith section ages of red snapper *Lutjanus campechanus* from the northern Gulf of Mexico. Limnology and Oceanography, 46: 1819–1824.

Barnett, B. K., Patterson, W. F., Kellison, T., Garner, S. B., and Shiller, A. M. 2016. Potential sources of red snapper (*Lutjanus campechanus*) recruits estimated with Markov Chain Monte Carlo analysis of otolith chemical signatures. Marine and Freshwater Research, 67(7): 992-1001.

Barnett, B. K., Thornton, L., Allman, R., Chanton, J. P., and Iii, W. F. P. 2018. Linear decline in red snapper (*Lutjanus campechanus*) otolith D14C extends the utility of the bomb radiocarbon chronometer for fish age validation in the Northern Gulf of Mexico. ICES Journal of Marine Science 75(5): 1664-1671.

Barnett, B. K., Helser, T. E., Benson, I. M., and Passerotti, M. S. 2019. Age prediction of Gulf of Mexico Red Snapper (*Lutjanus campechanus*) using near-infrared spectroscopy. *In* Proceedings of the Research Workshop on the Rapid Estimation of Fish Age Using Fourier Transform Near-Infrared Spectroscopy (FT-NIRS), p. 195. Alaska Fisheries Science Center, NOAA, National Marine Fisheries Service, 7600 Sand Point Way NE, Seattle, WA.

Barnett, L. A. K. 2008. Life history, abundance, and distribution of the spotted ratfish, *Hydrolagus colliei*. Thesis, California State University, Monterey Bay.

Beamish, R. J., and Fournier, D. A. 1981. A Method for Comparing the Precision of a Set of Age Determinations. Canadian Journal of Fisheries and Aquatic Sciences, 38: 982–983.

Beamish, R. J., and McFarlane, G. A. 1985. Annulus Development on the Second Dorsal Spine of the Spiny Dogfish (*Squalus acanthias*) and Its Validity for Age Determination. Canadian Journal of Fisheries and Aquatic Sciences, 42(11): 1799-1805.

Beamish, R. J., and McFarlane, G. A. 1995. A discussion of the importance of aging errors, and an application to walleye pollock: the world's largest fishery. *Recent developments in fish otolith research*. University of South Carolina Press, Columbia: 545–565.

Beebe, K. R., Pell, R. J., and Seasholtz, M. B. 1998. Chemometrics: A Practical Guide. Wiley. 348 pp.

Bird, N. C., and Mabee, P. M. 2003. Developmental morphology of the axial skeleton of the zebrafish, Danio rerio (Ostariophysi: Cyprinidae). Developmental Dynamics, 228: 337–357.

Blanco, M., and Alcalá, M. 2006. Content uniformity and tablet hardness testing of intact pharmaceutical tablets by near infrared spectroscopy: A contribution to process analytical technologies. Analytica Chimica Acta, 557: 353–359.

Boehlert, G. W. 1985. Using objective criteria and multiple regression models for age determination in fishes. Fishery Bulletin, 83: 103–117.

Borelli, G., Mayer-Gostan, N., De Pontual, H., Boeuf, G., and Payan, P. 2001. Biochemical relationships between endolymph and otolith matrix in the trout (*Oncorhynchus mykiss*) and turbot (*Psetta maxima*). Calcified tissue international, 69: 356–364.

Brander, K. 1974. The effects of age-reading errors on the statistical reliability of marine fishery modelling. *In* International Symposium on the Ageing of Fish. Reading (UK). 19 Jul 1973.

Britton, J. R., and Blackburn, R. 2014. Application and utility of using otolith weights in the ageing of three flatfish species. Fisheries Research, 154: 147–151.

Brown, C. P., Jayadev, C., Glyn-Jones, S., Carr, A. J., Murray, D. W., Price, A. J., and Gill, H. S. 2011. Characterization of early stage cartilage degradation using diffuse reflectance near infrared spectroscopy. Physics in Medicine and Biology, 56: 2299–2307.

Brown, C. P., Oloyede, A., Crawford, R. W., Thomas, G. E. R., Price, A. J., and Gill, H. S. 2012. Acoustic, mechanical and near-infrared profiling of osteoarthritic progression in bovine joints. Physics in Medicine and Biology, 57: 547–559.

Brusher, J. H., and Schull, J. 2009. Non-lethal age determination for juvenile goliath grouper *Epinephelus itajara* from southwest Florida. Endangered Species Research, 7: 205–212.

Buckley, L., Lough, R., and Mountain, D. 2010. Seasonal trends in mortality and growth of cod and haddock larvae result in an optimal window for survival. Marine Ecology Progress Series, 405: 57–69.

Burns, D. A., and Ciurczak, E. W. 2007. Handbook of Near-Infrared Analysis. CRC Press. 836 pp.

Cailliet, G. M. 1990. Elasmobranch age determination and verification: an updated review. NOAA Technical Report NMFS, 90: 157–165.

Cailliet, G. M., and Goldman, K. J. 2004. Age determination and validation in chondrichthyan fishes. *Biology of sharks and their relatives, First edition. CRC Press, Boca Raton, Florida*, pp. 399–447.

Cailliet, G. M., and Andrews, A. H. 2008. Age-validated Longevity of Fishes: Its Importance for Sustainable Fisheries. *Fisheries for Global Welfare and Environment (Eds K. Tsukamoto, T. Kawamura, T. Takeuchi, TD Beard Jr, and MJ Kaiser.)* pp.103-20.

Calis, E., Nolan, C. P., and Jeal, F. 2005. Preliminary Age and Growth Estimates of the Rabbitfish, *Chimaera monstrosa*, with Implications for Future Resource Management. Journal of Northwest Atlantic Fisheries Science, 35: 15–26.

Campana, S. 1999. Chemistry and composition of fish otoliths: pathways, mechanisms and applications. Marine Ecology Progress Series, 188: 263–297.

Campana, S. E., and Neilson, J. D. 1985. Microstructure of Fish Otoliths. Canadian Journal of Fisheries and Aquatic Sciences, 42: 1014–1032.

Campana, S. E., and Jones, C. M. 1992. Analysis of otolith microstructure data. Otolith microstructure examination and analysis. Canadian Journal of Fisheries and Aquatic Sciences, 117: 73–100.

Campana, S. E. 2001. Accuracy, precision and quality control in age determination, including a review of the use and abuse of age validation methods. Journal of Fish Biology, 59: 197–242.

Campana, S. E., and Thorrold, S. R. 2001. Otoliths, increments, and elements: keys to a comprehensive understanding of fish populations? Canadian Journal of Fisheries and Aquatic Sciences, 58: 30–38.

Campana, S. E., Natanson, L. J., and Myklevoll, S. 2002. Bomb dating and age determination of large pelagic sharks. Canadian Journal of Fisheries & Aquatic Sciences, 59(3): 450-455.

Campana, S. E., Jones, C., McFarlane, G. A., and Myklevoll, S. 2006. Bomb dating and age validation using the spines of spiny dogfish (*Squalus acanthias*). Environmental Biology of Fishes, 77: 327–336.

Carlström, D. 1963. A crystallographic study of vertebrate otoliths. The Biological Bulletin, 125: 441–463.

Carragher, J. F., and Sumpter, J. P. 1991. The mobilization of calcium from calcified tissues of rainbow trout (*Oncorhynchus mykiss*) induced to synthesize vitellogenin. Comparative Biochemistry and Physiology Part A: Physiology, 99: 169–172.

Casselman, J. M. 1987. Determination of age and growth. *The Biology of Fish Growth (Eds A.H. Weatherly and H.S. Gill)*: pp. 209–242. Academic Press.

Chakravartula, S. S. N., Cevoli, C., Balestra, F., Fabbri, A., and Dalla Rosa, M. 2019. Evaluation of drying of edible coating on bread using NIR spectroscopy. Journal of Food Engineering, 240: 29–37.

Chang, M.-Y., and Geffen, A. J. 2013. Taxonomic and geographic influences on fish otolith microchemistry. Fish and Fisheries, 14: 458–492.

Chen, J., and Wang, X. Z. 2001. A New Approach to Near-Infrared Spectral Data Analysis Using Independent Component Analysis. Journal of Chemical Information and Computer Sciences, 41: 992–1001.

Chen, Y., Jackson, D. A., and Harvey, H. H. 1992. A comparison of von Bertalanffy and polynomial functions in modelling fish growth data. Canadian Journal of Fisheries and Aquatic Sciences, 49(6): 1228-1235.

Clark, W. G. 2011. Groundfish exploitation rates based on life history parameters. Canadian Journal of Fisheries and Aquatic Sciences, 48(5): 734-750.

Clement, J. G. 1992. Re-examination of the fine structure of endoskeletal mineralization in Chondrichthyans: Implications for growth, ageing and calcium homeostasis. Marine and Freshwater Research, 43: 157–181.

Cohen, L., Dean, M., Shipov, A., Atkins, A., Monsonego-Ornan, E., and Shahar, R. 2012. Comparison of structural, architectural and mechanical aspects of cellular and acellular bone in two teleost fish. Journal of Experimental Biology, 215: 1983–93.

Conover, D. O., and Munch, S. B. 2002. Sustaining Fisheries Yields Over Evolutionary Time Scales. Science, 297: 94–96.

Cook, P. K., Mocuta, C., Dufour, É., Languille, M.-A., and Bertrand, L. 2018. Full-section otolith microtexture imaged by local-probe X-ray diffraction. Journal of Applied Crystallography, 51: 1182–1196.

Cooper, C., Packer, N., and Williams, K. 2000. Amino Acid Analysis Protocols. Humana Press, New Jersey.

Cort, J. L. 1991. Age and growth of bluefin tuna *Thunnus thynnus* (L.) of the Northeast Atlantic. ICCAT Rep. SCRS/94/66. Madrid-Spain.

Cotton, C. F., Andrews, A. H., Cailliet, G. M., Grubbs, R. D., Irvine, S. B., and Musick, J. A. 2014. Assessment of radiometric dating for age validation of deep-water dogfish (Order: Squaliformes) finspines. Fisheries Research, 151: 107–113.

Couture, J. J., Singh, A., Rubert-Nason, K. F., Serbin, S. P., Lindroth, R. L., and Townsend, P. A. 2016. Spectroscopic determination of ecologically relevant plant secondary metabolites. Methods in Ecology and Evolution, 7: 1402–1412.

Cowan, J. H. 2011. Red snapper in the Gulf of Mexico and US South Atlantic: data, doubt, and debate. Fisheries, 36: 319–331.

Cozzolino, D., Dambergs, R. G., Janik, L., Cynkar, W. U., and Gishen, M. 2006. Analysis of grapes and wine by near infrared spectroscopy. Journal of Near Infrared Spectroscopy, 14(5): 279-289.

Czarnecki, M. A., Morisawa, Y., Futami, Y., and Ozaki, Y. 2015. Advances in Molecular Structure and Interaction Studies Using Near-Infrared Spectroscopy. Chemical Reviews, 115: 9707–9744.

Dauphin, Y., and Dufour, E. 2003. Composition and properties of the soluble organic matrix of the otolith of a marine fish: *Gadus morhua* Linne, 1758 (Teleostei, Gadidae). Comparative Biochemistry and Physiology Part A: Molecular & Integrative Physiology, 134: 551–561.

Davesne, D., Meunier, F. J., Schmitt, A. D., Friedman, M., Otero, O., and Benson, R. B. J. 2019. The phylogenetic origin and evolution of acellular bone in teleost fishes: insights into osteocyte function in bone metabolism. Biological Reviews, 94: 1338–1363.

Davis, J., Oberholtzer, J., Burns, F., and Greene, M. 1995. Molecular cloning and characterization of an inner ear-specific structural protein. Science, 267: 1031–1034.

Degens, E.T., Deuser, W.G. and Haedrich, R.L., 1969. Molecular structure and composition of fish otoliths. Marine biology, 2(2): 105-113.

Doubleday, Z. A., Harris, H. H., Izzo, C., and Gillanders, B. M. 2014. Strontium Randomly Substituting for Calcium in Fish Otolith Aragonite. Analytical Chemistry, 86: 865–869.

Dunkelberger, D. G., Dean, J. M., and Watabe, N. 1980. The ultrastructure of the otolithic membrane and otolith in the juvenile mummichog, Fundulus heteroclitus. Journal of Morphology, 163: 367–377.

Elsdon, T. S., Wells, B. K., Campana, S. E., Gillanders, B. M., Jones, C. M., Limburg, K. E., Secor, D. H. 2008. Otolith chemistry to describe movements and life-history parameters of fishes: hypotheses, assumptions, limitations and inferences. Oceanography and Marine Biology - An Annual Review, 46: 297–330.

Ferreira, L. C. G., Beamish, R. J., and Youson, J. H. 1999. Macroscopic structure of the fin-rays and their annuli in pectoral and pelvic fins of chinook salmon, *Oncorhynchus tshawytscha*. Journal of Morphology, 239: 297–320.

Findeis, E. K. 1997. Osteology and phylogenetic relationships of recent sturgeons. Environmental Biology of Fishes, 48: 73–126.

Fossen, I., Albert, O. T., and Nilssen, E. M. 2003. Improving the precision of ageing assessments for long rough dab by using digitised pictures and otolith measurements. Fisheries Research, 60: 53–64.

Francis, R. C., and Campana, S. E. 2004. Inferring age from otolith measurements: a review and a new approach. Canadian Journal of Fisheries and Aquatic Sciences, 61(7): 1269-1284.

Francis, R. I. C. C., Harley, S. J., Campana, S. E., and Doering-Arjes, P. 2005. Use of otolith weight in length-mediated estimation of proportions at age. Marine and Freshwater Research, 56: 735.

Gaffey, S. J. 1987. Spectral reflectance of carbonate minerals in the visible and near infrared (0.35–2.55 um): Anhydrous carbonate minerals. Journal of Geophysical Research: Solid Earth, 92: 1429–1440.

Gauldie, R. W. 1993. Polymorphic crystalline structure of fish otoliths. Journal of Morphology, 218: 1–28.

Gauldie, R. W., Thacker, C. E., West, I. F., and Wang, L. 1998. Movement of water in fish otoliths. Comparative Biochemistry and Physiology Part A: Molecular & Integrative Physiology, 120: 551–556.

Gauldie, R. W. 1999. Ultrastructure of lamellae, mineral and matrix components of fish otolith twinned aragonite crystals: implications for estimating age in fish. Tissue and Cell, 31: 138–153.

Gazey, W. J., Gallaway, B. J., Cole, J. G., and Fournier, D. A. 2008. Age Composition, Growth, and Density-Dependent Mortality in Juvenile Red Snapper Estimated from Observer Data from the Gulf of Mexico Penaeid Shrimp Fishery. North American Journal of Fisheries Management, 28: 1828–1842.

Gillanders, B. M. 2001. Trace metals in four structures of fish and their use for estimates of stock structure. Fishery Bulletin, 99: 410–410.

Goldman, K. J., Cailliet, G. M., Andrews, A. H., and Natanson, L. J. 2012. Assessing the Age and Growth of Chondrichthyan Fishes. *Biology of Sharks and their Relatives (eds J. Carrier, J.A. Musick, M.R. Heithaus)*: pp. 423–451. CRC Press, Boca Raton.

Goodwin, N. B., Grant, A., Perry, A. L., Dulvy, N. K., and Reynolds, J. D. 2006. Life history correlates of density-dependent recruitment in marine fishes. Canadian Journal of Fisheries and Aquatic Sciences, 63: 494–509.

Gutherz, E. J., and Pellegrin, G. J. 1988. Estimate of the catch of red snapper, *Lutjanus campechanus*, by shrimp trawlers in the US Gulf of Mexico. Marine Fisheries Review, 50: 17–25.

Haddon, M. 2001. Modelling and quantitative methods in fisheries. CRC Press.

Hale, L. F., Dudgeon, J. V., Mason, A. Z., and Lowe, C. G. 2006. Elemental signatures in the vertebral cartilage of the round stingray, *Urobatis halleri*, from Seal Beach, California. Environmental Biology of Fishes, 3(77): 317-325.

Hanson, S. D., and Stafford, C. P. 2017. Modeling Otolith Weight using Fish Age and Length: Applications to Age Determination. Transactions of the American Fisheries Society, 146: 778–790.

Harry, A. V. 2018. Evidence for systemic age underestimation in shark and ray ageing studies. Fish and Fisheries, 19: 185–200.

Heimbrand, Y., Limburg, K. E., Hüssy, K., Casini, M., Sjöberg, R., Bratt, A.-M. P., Levinsky, S.-E. 2020. Seeking the true time: Exploring otolith chemistry as an age-determination tool. Journal of Fish Biology, 97: 552–565.

Helser, T. E., Benson, I. M., and Barnett, B. K. 2019a. Proceedings of the research workshop on the rapid estimation of fish age using Fourier Transform Near Infrared Spectroscopy (FT-NIRS). AFSC Processed Rep. 2019-06, 195 p. Alaska Fish. Sci. Cent., NOAA, Natl. Mar. Fish. Serv., 7600 Sand Point Way NE, Seattle WA 98115.

Helser, T. E., Benson, I., Erickson, J., Healy, J., Kastelle, C., and Short, J. A. 2019b. A transformative approach to ageing fish otoliths using Fourier transform near infrared spectroscopy: a case study of eastern Bering Sea walleye pollock (*Gadus chalcogrammus*). Canadian Journal of Fisheries and Aquatic Sciences, 76: 780–789.

Hixon, M. A., Johnson, D. W., and Sogard, S. M. 2014. BOFFFFs: on the importance of conserving old-growth age structure in fishery populations. ICES Journal of Marine Science, 71: 2171–2185.

Hoff, G. R., and Fuiman, L. A. 1993. Morphometry and composition of red drum otoliths: Changes associated with temperature, somatic growth rate, and age. Comparative Biochemistry and Physiology Part A: Physiology, 106: 209–219.

Hoie, H., and Folkvord, A. 2006. Estimating the timing of growth rings in Atlantic cod otoliths using stable oxygen isotopes. Journal of Fish Biology, 68: 826–837.

Høie, H., Folkvord, A., Mosegaard, H., Li, L., Clausen, L. A. W., Norberg, B., and Geffen, A. J. 2008. Restricted fish feeding reduces cod otolith opacity. Journal of Applied Ichthyology, 24: 138–143.

Holden, M. J., and Meadows, P. S. 1962. The structure of the spine of the spur dogfish (*Squalus acanthias* L.) and its use for age determination. Journal of the Marine Biological Association of the United Kingdom, 42: 179–197. Cambridge University Press.

Hopkinson, L., and Rutt, K. J. 2016. Crystal chemical correlations between the mid and near-infrared in carbonate minerals. Spectrochimica Acta Part A: Molecular and Biomolecular Spectroscopy, 162: 105–108.

Hopkinson, L., Kristova, P., and Rutt, K. 2017. The near-infrared (NIR) spectra of powdered calcite in the 3–121 μm mode particle size range. Vibrational Spectroscopy, 90: 69–73.

Hüssy, D. K., Krüger-Johnsen, M. M., Thomsen, D. T. B., Heredia, D. B. D., Naeraa, D. T., Limburg, D. K. E., Heimbrand, M. Y. 2020a. It's elemental, my dear Watson: validating seasonal patterns in otolith chemical chronologies. https://doi-org.pallas2.tcl.sc.edu/10.1139/cjfas-2020-0388

Hüssy, K., Limburg, K. E., de Pontual, H., Thomas, O. R. B., Cook, P. K., Heimbrand, Y., Blass, M. 2020b. Trace Element Patterns in Otoliths: The Role of Biomineralization. Reviews in Fisheries Science & Aquaculture: 1–33.

Hüssy, K., Mosegaard, H., and Jessen, F. 2004. Effect of age and temperature on amino acid composition and the content of different protein types of juvenile Atlantic cod (*Gadus morhua*) otoliths. Canadian Journal of Fisheries and Aquatic Sciences, 61: 1012–1020.

Hüssy, K., and Mosegaard, H. 2004. Atlantic cod (*Gadus morhua*) growth and otolith accretion characteristics modelled in a bioenergetics context. Canadian Journal of Fisheries and Aquatic Sciences, 61(6): 1021-1031.

Hutchings, J. A., and Kuparinen, A. 2017. Empirical links between natural mortality and recovery in marine fishes. Proceedings of the Royal Society B: Biological Sciences, 284: 20170693.

Hutchinson, J. J., and Trueman, C. N. 2006. Stable isotope analyses of collagen in fish scales: limitations set by scale architecture. Journal of Fish Biology, 69: 1874–1880.

Ingle, J. D. J., and Crouch, S. R. 1988. The Beer Lambert Law. *Spectrochemical Analysis*. Prentice Hall: New Jersey.

Izzo, C., Doubleday, Z. A., and Gillanders, B. M. 2016a. Where do elements bind within the otoliths of fish? Marine and Freshwater Research, 67: 1072.

Izzo, C., Doubleday, Z. A., Grammer, G. L., Gilmore, K. L., Alleway, H. K., Barnes, T. C., Disspain, M. C. F. 2016b. Fish as proxies of ecological and environmental change. Reviews in Fish Biology and Fisheries, 26: 265–286.

Jaffe, F. F., Mankin, H. J., Weiss, H., and Zarins, A. 1974. Water Binding in the Articular Cartilage of Rabbits. Journal of Bone and Joint Surgery, 56: 1031–1039.

James, K. C., and Natanson, L. J. 2020. Positional and ontogenetic variation in vertebral centra morphology in five batoid species. Marine and Freshwater Research. https://doi.org/10.1071/MF20183.

Johnson, D. W., Grorud-Colvert, K., Sponaugle, S., and Semmens, B. X. 2014. Phenotypic variation and selective mortality as major drivers of recruitment variability in fishes. Ecology Letters, 17: 743–755.

Jolivet, A., Bardeau, J.-F., Fablet, R., Paulet, Y.-M., and de Pontual, H. 2008. Understanding otolith biomineralization processes: new insights into microscale spatial distribution of organic and mineral fractions from Raman microspectrometry. Analytical and Bioanalytical Chemistry, 392: 551–560.

Jolivet, A., Bardeau, J.-F., Fablet, R., Paulet, Y.-M., and de Pontual, H. 2013. How do the organic and mineral fractions drive the opacity of fish otoliths? Insights using Raman microspectrometry. Canadian Journal of Fisheries and Aquatic Sciences, 70: 711–719.

Jones, C. M. 2013. Growth and mortality of pre- and post-settlement age-0 red snapper, *Lutjanus campechanus* (Poey 1860), in the Gulf of Mexico. University of South Alabama.

Kacem, A., Baglinière, J. L., and Meunier, F. J. 2013. Resorption of scales in Atlantic salmon (*Salmo salar*) during its anadromous migration: a quantitative study. Cybium, 37(3): 199-206.

Kalish, J. M. 1989. Otolith microchemistry: validation of the effects of physiology, age and environment on otolith composition. Journal of Experimental Marine Biology and Ecology, 132: 151–178.

Kalish, K. M., Beamish, R. J., Brothers, E. B., Casselman, J. M., Francis, R., Mosegaard, H., Panfili, J. 1995. Glossary for otolith studies. *Recent Developments in Fish Otolith Research*. University of South Carolina Press.

Kandel, S., Querido, W., Falcon, J. M., Reiners, D. J., and Pleshko, N. 2020. Approaches for *In Situ* Monitoring of Matrix Development in Hydrogel-Based Engineered Cartilage. Tissue Engineering Part C: Methods, 26: 225–238.

Kang, Y.-J., Stevenson, A. K., Yau, P. M., and Kollmar, R. 2008. Sparc Protein Is Required for Normal Growth of Zebrafish Otoliths. Journal of the Association for Research in Otolaryngology, 9: 436–451.

Kerr, L. A., Andrews, A. H., Cailliet, G. M., Brown, T. A., and Coale, K. H. 2006. Investigations of Δ 14C, δ 13C, and δ 15N in vertebrae of white shark (*Carcharodon carcharias*) from the eastern North Pacific Ocean. Environmental Biology of Fishes, 77: 337–353.

Kerr, L. A., and Campana, S. E. 2014. Chemical Composition of Fish Hard Parts as a Natural Marker of Fish Stocks. *Stock Identification Methods*, pp. 205–234. Academic Press.

Kindsvater, H. K., Mangel, M., Reynolds, J. D., and Dulvy, N. K. 2016. Ten principles from evolutionary ecology essential for effective marine conservation. Ecology and Evolution, 6: 2125–2138.

Lai, H. L., and Gunderson, D. R. 1987. Effects of ageing errors on estimates of growth, mortality and yield per recruit for walleye pollock (*Theragra chalcogramma*). Fisheries Research, 5: 287–302.

Lambert, B., Sikulu-Lord, M. T., Mayagaya, V. S., Devine, G., Dowell, F., and Churcher, T. S. 2018. Monitoring the Age of Mosquito Populations Using Near-Infrared Spectroscopy. Scientific Reports, 8: 1-9.

Landis, W. J., and Géraudie, J. 1990. Organization and development of the mineral phase during early ontogenesis of the bony fin rays of the trout *Oncorhynchus mykiss*. The Anatomical Record, 228: 383–391.

Law, R. 2000. Fishing, selection, and phenotypic evolution. ICES Journal of Marine Science, 57: 659–668.

Law, R. 2007. Fisheries-induced evolution: present status and future directions. Marine Ecology Progress Series, 335: 271–277.

Libnau, F. O., Kvalheim, O. M., Christy, A. A., and Toft, J. 1994. Spectra of water in the near- and mid-infrared region. Vibrational Spectroscopy, 7: 243–254.

Limburg, K. E., and Elfman, M. 2017. Insights from two-dimensional mapping of otolith chemistry: Otolith chemical mapping. Journal of Fish Biology, 90: 480–491.

Loeppky, A. R., Chakoumakos, B. C., Pracheil, B. M., and Anderson, W. G. 2019. Otoliths of sub-adult Lake Sturgeon *Acipenser fulvescens* contain aragonite and vaterite calcium carbonate polymorphs. Journal of Fish Biology, 94: 810–814.

Lombardi, L. 2017. Summary of Red Snapper Age-Length Data by Data Providers for SEDAR52. SEDAR52-WP-14. SEDAR, North Charleston, SC.

Lou, D. C., Mapstone, B. D., Russ, G. R., Davies, C. R., and Begg, G. A. 2005. Using otolith weight–age relationships to predict age-based metrics of coral reef fish populations at different spatial scales. Fisheries Research, 71: 279–294.

Lowenstam, H. A., and Weiner, S. 1989. On Biomineralization. Oxford University Press. 335 pp.

Luck, W. A. P. 1984. Structure of water and aqueous systems. *Synthetic membrane processes: Fundamentals and water applications*, pp. 21–72. Academic Press New York.

Lueders-Dumont, J. A., Sigman, D. M., Johnson, B. J., Jensen, O. P., Oleynik, S., and Ward, B. B. 2020. Comparison of the isotopic composition of fish otolith-bound organic N with host tissue. Canadian Journal of Fisheries & Aquatic Sciences, 77: 264–275.

Mahamid, J., Sharir, A., Addadi, L., and Weiner, S. 2008. Amorphous calcium phosphate is a major component of the forming fin bones of zebrafish: Indications for an amorphous precursor phase. Proceedings of the National Academy of Sciences, 105: 12748–12753.

Maillet, G. L., and Checkley, D. M. 1990. Effects of starvation on the frequency of formation and width of growth increments in sagittae of laboratory-reared Atlantic menhaden *Brevoortia tyrannus* larvae. Fishery Bulletin, 88: 155–166.

Mangel, M., MacCall, A., Brodziak, J., Dick, E. J., Forrest, R., Pourzand, R., and Ralston, S. 2013. A perspective on steepness, reference points, and stock assessment. Canadian Journal of Fisheries and Aquatic Sciences 70(6): 930-940.

Mankin, H. J., and Thrasher, A. Z. 1975. Water content and binding in normal and osteoarthritic human cartilage. The Journal of Bone and Joint surgery. American Volume, 57: 76–80.

Manley, M., Van Zyl, L., and Osborne, B. G. 2002. Using Fourier Transform near Infrared Spectroscopy in Determining Kernel Hardness, Protein and Moisture Content of Whole Wheat Flour. Journal of Near Infrared Spectroscopy, 10: 71–76.

Manooch, C. S., and Potts, J. C. 1997. Age and growth of red snapper, *Lutjanus campechanus*, Lutjanidae, collected along the southeastern United States from North Carolina through the east coast of Florida. Journal of the Elisha Mitchell Scientific Society, 113: 111–122.

Matić-Skoko, S., Ferri, J., Škeljo, F., Bartulović, V., Glavić, K., and Glamuzina, B. 2011. Age, growth and validation of otolith morphometrics as predictors of age in the forkbeard, *Phycis phycis* (Gadidae). Fisheries Research, 112: 52–58.

Mayagaya, V. S., Michel, K., Benedict, M. Q., Killeen, G. F., Wirtz, R. A., Ferguson, H. M., and Dowell, F. E. 2009. Non-destructive Determination of Age and Species of *Anopheles gambiae* s.l. Using Near-infrared Spectroscopy. American Journal of Tropical Medicine and Hygeine, 81: 622–630.

McMahon, K. W., Berumen, M. L., Mateo, I., Elsdon, T. S., and Thorrold, S. R. 2011. Carbon isotopes in otolith amino acids identify residency of juvenile snapper (Family: Lutjanidae) in coastal nurseries. Coral Reefs, 30: 1135–1145.

Melancon, S., Fryer, B. J., Ludsin, S. A., Gagnon, J. E., and Yang, Z. 2005. Effects of crystal structure on the uptake of metals by lake trout (*Salvelinus namaycush*) otoliths. Canadian Journal of Fisheries and Aquatic Sciences 62(11): 2609-2619.

Meunier, F. J. 1984. Spatial Organization and Mineralization of the Basal Plate of Elasmoid Scales in Osteichthyans. American Zoologist, 24: 953–964.

Michelacci, Y. M., and Horton, D. S. P. Q. 1989. Proteoglycans from the cartilage of young hammerhead shark *Sphyrna lewini*. Comparative Biochemistry and Physiology Part B: Comparative Biochemistry, 92: 651–658.

Min, M., and Lee, W. S. 2005. Determination of significant wavelengths and prediction of nitrogen content for citrus. Transactions of the ASAE, 48: 455–461.

Montes, G. S., Becerra, J., Toledo, O. M. S., Gordilho, M. A., and Junqueira, L. C. U. 1982. Fine structure and histochemistry of the tail fin ray in teleosts. Histochemistry, 75: 363–376.

Morales-Nin, B. 1986a. Chemical composition of the otoliths of the sea bass (*Dicentrarchus labrax* Linnaeus, 1758)(Pisces, Serranidae). Cybium (Paris), 10: 115–120.

Morales-Nin, B. 1986b. Structure and composition of otoliths of Cape hake *Merluccius capensis*. South African Journal of Marine Science, 4: 3–10.

Morales-Nin, B. 2000. Review of the growth regulation processes of otolith daily increment formation. Fisheries Research, 46: 53–67.

Morison, A. K., Robertson, S. G., and Smith, D. C. 1998. An Integrated System for Production Fish Aging: Image Analysis and Quality Assurance. North American Journal of Fisheries Management, 18: 587–598.

Moss, M. L. 1961. Studies of the acellular bone of teleost fish. Cells Tissues Organs, 46: 343–362.

Mugiya, Y. 1972. On Aberrant Sagittas of Teleostean Fishes. Japanese Journal of Ichthyology, 19(1): 11-14.

Murayama, E., Okuno, A., Ohira, T., Takagi, Y., and Nagasawa, H. 2000. Molecular cloning and expression of an otolith matrix protein cDNA from the rainbow trout, *Oncorhynchus mykiss*. Comparative Biochemistry and Physiology Part B: Biochemistry and Molecular Biology, 126: 511–520.

Murayama, E., Takagi, Y., Ohira, T., Davis, J. G., Greene, M. I., and Nagasawa, H. 2002. Fish otolith contains a unique structural protein, otolin-1. European Journal of Biochemistry, 269: 688–696.

Murayama, E., Takagi, Y., and Nagasawa, H. 2004. Immunohistochemical localization of two otolith matrix proteins in the otolith and inner ear of the rainbow trout, *Oncorhynchus mykiss*: comparative aspects between the adult inner ear and embryonic otocysts. Histochemistry and Cell Biology, 121: 155–166.

Murray, I., and Williams, P. C. 1987. Chemical principles of near-infrared technology. *Near-infrared technology in the agricultural and food industries*, pp. 17–34. American Association of Cereal Chemists, Inc.

Natanson, L. J., Andrews, A. H., Passerotti, M. S., and Wintner, S. P. 2018a. History and Mystery of Age and Growth Studies in Elasmobranchs. *Shark Research: Emerging Technologies and Applications for the Field and Laboratory*, pp. 177–200. CRC Press, Boca Raton.

Natanson, L. J., Skomal, G. B., Hoffmann, S. L., Porter, M. E., Goldman, K. J., and Serra, D. 2018b. Age and growth of sharks: do vertebral band pairs record age? Marine and Freshwater Research, 69, 1440–1452. doi: 10.1071/mf17279

Nelson, R. S., and Manooch, C. S. 1982. Growth and Mortality of Red Snapper in the West-Central Atlantic Ocean and Northern Gulf of Mexico. Transactions of the American Fisheries Society, 111: 465–475.

NMFS, (National Marine Fisheries Service). 2018. Fisheries of the United States, 2017 Report. US Department of Commerce.

Norris, K. H., and Hart, J. R. 1965. Direct spectrophotometric determination of moisture content of grain and seeds. *Principles and Methods of Measuring Moisture in Liquids and Solids. Vol. 4*, pp. 19-25.

Norris, K. H. 1996. History of NIR. Journal of Near Infrared Spectroscopy, 4: 31–37.

Nowling, L., Gauldie, R. W., Cowan Jr, J. H., and Carlo, E. D. 2011. Successful Discrimination Using Otolith Microchemistry Among Samples of Red Snapper *Lutjanus campechanus* from Artificial Reefs and Samples of *L. campechanus* Taken from Nearby Oil and Gas Platforms. The Open Fish Science Journal, 4: 1–9.

Ofer, L., Zaslansky, P., and Shahar, R. 2020. A comparison of the structure, composition and mechanical properties of anosteocytic vertebrae of medaka (*O. latipes*) and osteocytic vertebrae of zebrafish (*D. rerio*). Journal of Fish Biology. https://doi.org/10.1111/jfb.14334

Ogle, D. H., Wheeler, P., and Dinno, A. 2018. FSA: fisheries stock analysis. R package version 0.8. 22. R package. https://github. com/droglenc/FSA (2018).

Oliveira, A. M., Farina, M., Ludka, I. P., and Kachar, B. 1996. Vaterite, calcite, and aragonite in the otoliths of three species of piranha. Naturwissenschaften, 83: 133–135.

Ong, O. T. W., Kho, E. A., Esperança, P. M., Freebairn, C., Dowell, F. E., Devine, G. J., and Churcher, T. S. 2020. Ability of near-infrared spectroscopy and chemometrics to predict the age of mosquitoes reared under different conditions. Parasites & Vectors, 13: 160.

Ortiz, M., Legault, C. M., and Ehrhardt, N. M. 2000. An alternative method for estimating bycatch from the U.S. shrimp trawl fishery in the Gulf of Mexico, 1972-1995. Fishery Bulletin, 98: 583–583.

Padalkar, M. V., Spencer, R. G., and Pleshko, N. 2013. Near Infrared Spectroscopic Evaluation of Water in Hyaline Cartilage. Annals of Biomedical Engineering, 41: 2426–2436.

Padalkar, M. V., and Pleshko, N. 2015. Wavelength-dependent penetration depth of near infrared radiation into cartilage. The Analyst, 140: 2093–2100.

Palukuru, U. P., McGoverin, C. M., and Pleshko, N. 2014. Assessment of hyaline cartilage matrix composition using near infrared spectroscopy. Matrix Biology, 38: 3–11.

Pannella, G. 1971. Fish Otoliths: Daily Growth Layers and Periodical Patterns. Science, 173: 1124–1127. American Association for the Advancement of Science.

Parmentier, E., Cloots, R., Warin, R., and Henrist, C. 2007. Otolith crystals (in Carapidae): Growth and habit. Journal of Structural Biology, 159: 462–473.

Passerotti, M. S., Andrews, A. H., Carlson, J. K., Wintner, S. P., Goldman, K. J., and Natanson, L. J. 2014. Maximum age and missing time in the vertebrae of sand tiger shark (*Carcharias taurus*): validated lifespan from bomb radiocarbon dating in the western North Atlantic and southwestern Indian Oceans. Marine and Freshwater Research, 65: 674.

Passerotti, M. S., Helser, T. E., Benson, I. M., Barnett, B. K., Ballenger, J. C., Bubley, W. J., Reichert, M. J. M. 2020a. Age estimation of red snapper (*Lutjanus campechanus*) using FT-NIR spectroscopy: feasibility of application to production ageing for management. ICES Journal of Marine Science, 77(6): 2144-2156.

Passerotti, M. S., Jones, C. M., Swanson, C. E., and Quattro, J. M. 2020b. Fourier-transform near infrared spectroscopy (FT-NIRS) rapidly and non-destructively predicts daily age and growth in otoliths of juvenile red snapper *Lutjanus campechanus* (Poey, 1860). Fisheries Research, 223: 105439.

Patterson, W. F., Wilson, C. A., Cowan Jr, J. H., Bentley, S. J., Henwood, T. A., Allen, Y. C., and Dufrene, T. A. 2005. Delineating essential juvenile red snapper habitat in the north central Gulf of Mexico. *Effects of fishing on benthic habitats.* American Fisheries Society Symposium: 277–288.

Patterson, W. F., Cowan, J. H., Wilson, C. A., and Chen, Z. 2008. Temporal and Spatial Variability in Juvenile Red Snapper Otolith Elemental Signatures in the Northern Gulf of Mexico. Transactions of the American Fisheries Society, 137: 521–532.

Pawson, M. G. 1990. Using otolith weight to age fish. Journal of Fish Biology, 36: 521–531.

Payan, P., Edeyer, A., de Pontual, H., Borelli, G., Boeuf, G., and Mayer-Gostan, N. 1999. Chemical composition of saccular endolymph and otolith in fish inner ear: lack of spatial uniformity. American Journal of Physiology-Regulatory, Integrative and Comparative Physiology, 277: R123–R131.

Petko, J. A., Millimaki, B. B., Canfield, V. A., Riley, B. B., and Levenson, R. 2008. Otoc1: A novel otoconin-90 ortholog required for otolith mineralization in zebrafish. Developmental Neurobiology, 68: 209–222.

Porter, M. E. 2006. Material properties and biochemical composition of mineralized vertebral cartilage in seven elasmobranch species (Chondrichthyes). Journal of Experimental Biology, 209: 2920–2928.

Potts, J. C. 2009. Age Workshop for Red Snapper, SEDAR 24. SEDAR24_DW10. SEDAR, North Charleston, SC.

Powers, S. P., Drymon, J. M., Hightower, C. L., Spearman, T., Bosarge, G. S., and Jefferson, A. 2018. Distribution and Age Composition of Red Snapper across the Inner Continental Shelf of the North-Central Gulf of Mexico. Transactions of the American Fisheries Society, 147: 791–805.

Pracheil, B. M., George, R., and Chakoumakos, B. C. 2019. Significance of otolith calcium carbonate crystal structure diversity to microchemistry studies. Reviews in Fish Biology and Fisheries, 29: 569–588.

Prince, E., Lee, D., Cort, J., McFarlane, G., and Wild, A. 1995. Age Validation Evidence for Two Tag-Recaptured Atlantic Albacore, *Thunnus alalunga*, Based on Dorsal, Anal, and Pectoral Finrays, Vertebrae, and Otoliths. *Recent Developments in Fish Otolith Research.* University of South Carolina Press.

Radtke, R. L. 1984. Cod fish otoliths: information storage structures. In: The propagation of cod *Gadus morhua* L.: an international symposium, Arendal, 14 - 17 June 1983. 273-300. Havforskningsinstituttet.

Rama, S., and Chandrakasan, G. 1984. Distribution of Different Molecular Species of Collagen in the Vertebral Cartilage of Shark (*Carcharius acutus*). Connective Tissue Research, 12: 111–118.

Reich, G. 2005. Near-infrared spectroscopy and imaging: Basic principles and pharmaceutical applications. Advanced Drug Delivery Reviews, 57: 1109–1143.

Reimer, T., Dempster, T., Wargelius, A., Fjelldal, P. G., Hansen, T., Glover, K. A., Solberg, M. F. 2017. Rapid growth causes abnormal vaterite formation in farmed fish otoliths. Journal of Experimental Biology, 220: 2965–2969.

Ressler, N., Ziauddin, Vygantas, C., Janzen, W., and Karachorlu, K. 1976. Improved Technics for the Near Infrared Study of Water Binding by Globular Proteins and Intact Tissues. Applied Spectroscopy, 30: 295–302.

Rigby, C. L., Wedding, B. B., Grauf, S., and Simpfendorfer, C. A. 2014. The utility of near infrared spectroscopy for age estimation of deepwater sharks. Deep Sea Research Part I: Oceanographic Research Papers, 94: 184–194.

Rigby, C. L., Wedding, B. B., Grauf, S., and Simpfendorfer, C. A. 2016a. Novel method for shark age estimation using near infrared spectroscopy. Marine and Freshwater Research, 67: 537.

Rigby, C. L., Daley, R. K., and Simpfendorfer, C. A. 2016b. Comparison of life histories of two deep-water sharks from eastern Australia: the piked spurdog and the Philippine spurdog. Marine and Freshwater Research, 67: 1546–1561.

Rigby, C. L., Foley, W. J., and Simpfendorfer, C. A. 2019. Near-Infrared Spectroscopy for Shark Ageing and Biology. *Shark Research: Emerging Technologies and Applications for the Field and Laboratory*, pp. 201-217. CRC Press, Boca Raton.

Rinnan, Å., Berg, F. van den, and Engelsen, S. B. 2009. Review of the most common pre-processing techniques for near-infrared spectra. Trends in Analytical Chemistry, 28: 1201–1222.

Roberts, J. J., Motin, J. Ch., Swain, D., and Cozzolino, D. 2017. A Feasibility Study on the Potential Use of Near Infrared Reflectance Spectroscopy to Analyze Meat in Live Animals: Discrimination of Muscles. Journal of Spectroscopy, 2017: 1–7.

Robins, J., Wedding, B. B., Wright, C., Grauf, S., Sellin, M., Fowler, A., Saunders, T. 2015. Revolutionising fish ageing: using near infrared spectroscopy to age fish. Department of Agriculture, Fisheries and Forestry, Brisbane, Australia. CC BY 3.0. http://frdc.com.au/research/Final_reports/2012-011-DLD.pdf .

Roff, D. A. 2002. Life history evolution. Sinauer.

Rooker, J. R., Landry, A. M., Geary, B. W., and Harper, J. A. 2004. Assessment of a shell bank and associated substrates as nursery habitat of postsettlement red snapper. Estuarine, Coastal and Shelf Science, 59: 653–661.

Santamaria, N., Bello, G., Corriero, A., Deflorio, M., Vassallo-Agius, R., Bök, T., and Metrio, G. D. 2009. Age and growth of Atlantic bluefin tuna, *Thunnus thynnus* (Osteichthyes: Thunnidae), in the Mediterranean Sea. Journal of Applied Ichthyology, 25: 38–45.

Santamaria, N., Bello, G., Pousis, C., Vassallo-Agius, R., Gándara, F. de la, and Corriero, A. 2015. Fin Spine Bone Resorption in Atlantic Bluefin Tuna, *Thunnus thynnus*, and Comparison between Wild and Captive-Reared Specimens. PLOS ONE, 10: e0121924.

Sasagawa, T., and Mugiya, Y. 1996. Biochemical Properties of Water-Soluble Otolith Proteins and the Immunobiochemical Detection of the Proteins in Serum and Various Tissues in the Tilapia *Oreochromis niloticus*. Fisheries Science, 62: 970–976.

Schnetz, L., Pfaff, C., Libowitzky, E., Johanson, Z., Stepanek, R., and Kriwet, J. 2019. Morphology and evolutionary significance of phosphatic otoliths within the inner ears of cartilaginous fishes (Chondrichthyes). BMC Evolutionary Biology, 19(1): 1-13.

Secor, D. H., Dean, J. M., and Laban, E. H. 1992. Otolith removal and preparation for microstructural examination. Otolith microstructure examination and analysis. Canadian Journal of Fisheries and Aquatic Sciences, 117: 19–57.

Secor, D. H., Dean, J. M., and Campana, S. E. 1995. Recent developments in fish otolith research. University of South Carolina Press.

SEDAR. 2008. SEDAR 15 - Red Snapper Stock Assessment Report. SEDAR, North Charleston, SC. https://sedarweb.org/docs/sar/S15%20SAR1RedSnap%20FINAL%20Revised%200309.pdf (Accessed 10 January 2020).

SEDAR. 2015. SEDAR Procedural Workshop 7: Data Best Practices. SEDAR, North Charleston, SC. http://sedarweb.org/docs/sar/SEDARPW7_DataBestPracticesReport_FINAL_9.11.2015.pdf (Accessed 15 March 2021).

SEDAR. 2017. SEDAR 41 - South Atlantic Red snapper Assessment Report. SEDAR, North Charleston, SC. http://sedarweb.org/sedar-41 (Accessed 10 January 2020).

SEDAR. 2018. SEDAR 52-Gulf of Mexico Red snapper Assessment Report. SEDAR, North Charleston, SC. http://sedarweb. org/docs/sar/S52_Final_SAR_v2.pdf.

SEDAR. 2020. SEDAR 69—Atlantic Menhaden Stock Assessment Report. SEDAR, North Charleston, SC. http://sedarweb.org/docs/sar/SEDAR%2069%20SAR%20final%20combined%20benchmark.pdf (Accessed 15 March 2021).

SFB-NMFS, (Sustainable Fisheries Branch-National Marine Fisheries Service). 2015. Development of an Ageing Error Matrix for U.S. Red Snapper (Lutjanus campechanus). SEDAR41-DW48. SEDAR, North Charleston, SC.

Shearer, W. M. 1992. Atlantic salmon scale reading guidelines. International Council for the Exploration of the Sea.

Shervette, V., Hernández, J. R., and Nunoo, F. K. E. 2021. Age and growth of Gray Triggerfish *Balistes capriscus* from trans-Atlantic populations. Journal of Fish Biology, https://doi.org/10.1111/jfb.14644.

Siesler, H. W., Ozaki, Y., Kawata, S., and Heise, H. M. 2002. Near-Infrared Spectroscopy: Principles, Instruments, Applications. John Wiley & Sons. 365 pp.

Sikulu, M. T., Monkman, J., Dave, K. A., Hastie, M. L., Dale, P. E., Kitching, R. L., Killeen, G. F. 2015. Proteomic changes occurring in the malaria mosquitoes *Anopheles gambiae* and *Anopheles stephensi* during aging. Journal of Proteomics, 126: 234–244.

Sikulu-Lord, M. T., Maia, M. F., Milali, M. P., Henry, M., Mkandawile, G., Kho, E. A., Wirtz, R. A. 2016. Rapid and Non-destructive Detection and Identification of Two Strains of Wolbachia in *Aedes aegypti* by Near-Infrared Spectroscopy. PLOS Neglected Tropical Diseases, 10: e0004759.

Sluis, M. Z., Barnett, B. K., III, W. F. P., Jr, J. H. C., and Shiller, A. M. 2012. Discrimination of Juvenile Red Snapper Otolith Chemical Signatures from Gulf of Mexico Nursery Regions. Marine and Coastal Fisheries, 4: 587–598.

Sluis, M. Z., Boswell, K. M., Chumchal, M. M., Wells, R. J. D., Soulen, B., and Cowan, J. H. 2013. Regional variation in mercury and stable isotopes of red snapper (*Lutjanus campechanus*) in the northern Gulf of Mexico, USA. Environmental Toxicology and Chemistry, 32: 434–441.

Sluis, M. Z., Barnett, B. K., Patterson, W. F., Cowan, J. H., and Shiller, A. M. 2015. Application of Otolith Chemical Signatures to Estimate Population Connectivity of Red Snapper in the Western Gulf of Mexico. Marine and Coastal Fisheries, 7: 483–496.

Söllner, C., Burghammer, M., Busch-Nentwich, E., Berger, J., Schwarz, H., Riekel, C., and Nicolson, T. 2003. Control of Crystal Size and Lattice Formation by Starmaker in Otolith Biomineralization. Science, 302: 282–286.

Sponaugle, S. 2010. Otolith microstructure reveals ecological and oceanographic processes important to ecosystem-based management. Environmental Biology of Fishes, 89: 221–238.

Stearns, S. 2000. Life history evolution: Successes, limitations, and prospects. Die Naturwissenschaften, 87: 476–86.

Stearns, S. C., and Koella, J. C. 1986. The Evolution of Phenotypic Plasticity in Life-History Traits: Predictions of Reaction Norms for Age and Size at Maturity. Evolution, 40: 893–913.

Stevenson, J. T., and Secor, D. H. 2000. Age determination and growth of Hudson River Atlantic sturgeon, *Acipenser oxyrinchus*. Fishery Bulletin, 98: 153–166.

Steward, C. A., DeMaria, K. D., and Shenker, J. M. 2009. Using otolith morphometrics to quickly and inexpensively predict age in the gray angelfish (*Pomacanthus arcuatus*). Fisheries Research, 99: 123–129.

Strong, M. B., Neilson, J. D., and Hunt, J. J. 1986. Aberrant Crystallization of Pollock (Pollachius virens) Otoliths. Canadian Journal of Fisheries and Aquatic Sciences, 43(7): 1457-1463.

Sturrock, A. M., Trueman, C. N., Darnaude, A. M., and Hunter, E. 2012. Can otolith elemental chemistry retrospectively track migrations in fully marine fishes? Journal of Fish Biology, 81: 766–795.

Sturrock, A. M., Hunter, E., Milton, J. A., EIMF, Johnson, R. C., Waring, C. P., and Trueman, C. N. 2015. Quantifying physiological influences on otolith microchemistry. Methods in Ecology and Evolution, 6: 806–816.

Szedlmayer, S. T. 1998. Comparison of growth rate and formation of otolith increments in age-0 red snapper. Journal of Fish Biology, 53: 58–65.

Thomas, O. R. B., Ganio, K., Roberts, B. R., and Swearer, S. E. 2017. Trace element–protein interactions in endolymph from the inner ear of fish: implications for environmental reconstructions using fish otolith chemistry. Metallomics, 9: 239–249.

Thomas, O. R. B., Swearer, S. E., Kapp, E. A., Peng, P., Tonkin-Hill, G. Q., Papenfuss, A., Roberts, A. 2019. The inner ear proteome of fish. The FEBS Journal, 286: 66–81.

Thomas, O. R. B., and Swearer, S. E. 2019. Otolith Biochemistry—A Review. Reviews in Fisheries Science & Aquaculture, 27: 458–489.

Thomas, O. R. B., Richards, K. L., Petrou, S., Roberts, B. R., and Swearer, S. E. 2020. In situ 3D visualization of biomineralization matrix proteins. Journal of Structural Biology, 209: 107448.

Thorson, J. T., Cope, J., Branch, T., and Jensen, O. P. 2012. Spawning biomass reference points for exploited marine fishes, incorporating taxonomic and body size information. Canadian Journal of Fisheries and Aquatic Sciences, 69(9): 1556-1568.

Tillett, B. J., Meekan, M. G., Parry, D., Munksgaard, N., Field, I. C., Thorburn, D., and Bradshaw, C. J. A. 2011. Decoding fingerprints: elemental composition of vertebrae correlates to age-related habitat use in two morphologically similar sharks. Marine Ecology Progress Series, 434: 133–142.

Tohse, H., Takagi, Y., and Nagasawa, H. 2008. Identification of a novel matrix protein contained in a protein aggregate associated with collagen in fish otoliths. The FEBS journal, 275: 2512–2523.

Tolleson, D. R., Randel, R. D., Stuth, J. W., and Neuendorff, D. A. 2005. Determination of sex and species in red and fallow deer by near infrared reflectance spectroscopy of the faeces. Small Ruminant Research, 57: 141–150.

Tzeng, W.-N., Chang, C.-W., Wang, C.-H., Shiao, J.-C., Iizuka, Y., Yang, Y.-J., You, C.-F. 2007. Misidentification of the migratory history of anguillid eels by Sr/Ca ratios of vaterite otoliths. Marine Ecology Progress Series, 348: 285–295.

Vance, C. K., Kouba, A. J., and Willard, S. T. 2014. Near Infrared Spectroscopy Applications in Amphibian Ecology and Conservation: Gender and Species Identification. NIR news, 25: 10–15.

Vance, C. K., Tolleson, D. R., Kinoshita, K., Rodriguez, J., and Foley, W. J. 2016. Near Infrared Spectroscopy in Wildlife and Biodiversity. Journal of Near Infrared Spectroscopy, 24: 1–25.

VanderKooy, S. 2009. A Practical Handbook for Determining the Ages of Gulf of Mexico Fishes-Second Edition. Gulf States Marine Fisheries Commission, Ocean Springs, Mississippi.

Vasconcelos-Filho, J. E., Thomsen, F. S. L., Stosic, B., Antonino, A. C. D., Duarte, D. A., Heck, R. J., Lessa, R. P. T. 2019. Peeling the Otolith of Fish: Optimal Parameterization for Micro-CT Scanning. Frontiers in Marine Science, 6: 728. DOI: 10.3389/fmars.2019.00728

Vilizzi, L. 2018. Age determination in common carp *Cyprinus carpio*: history, relative utility of ageing structures, precision and accuracy. Reviews in Fish Biology and Fisheries, 28: 461–484.

Villringer, A., Planck, J., Hock, C., Schleinkofer, L., and Dirnagl, U. 1993. Near infrared spectroscopy (NIRS): A new tool to study hemodynamic changes during activation of brain function in human adults. Neuroscience Letters, 154: 101–104.

Vitale, F., Clausen, L., and Chonchúir, G. 2019. Handbook of fish age estimation protocols and validation methods. ICES No. 346.

Walling, P. L., and Danbey, J. M. 1989. Moisture in skin by near-infrared reflectance spectroscopy. Journal of the Society for Cosmetic Chemistry, 40: 151–171.

Walters, C. J., and Martell, S. J. D. 2004. Fisheries Ecology and Management. Princeton University Press. 428 pp.

Walther, B. D. 2019. The art of otolith chemistry: interpreting patterns by integrating perspectives. Marine and Freshwater Research, 70(12): 1643-1658.

Wang, J., and Becker, U. 2009. Structure and carbonate orientation of vaterite (CaCO3). American Mineralogist, 94: 380–386.

Wedding, B. B., Forrest, A. J., Wright, C., Grauf, S., Exley, P., and Poole, S. E. 2014. A novel method for the age estimation of Saddletail snapper (*Lutjanus malabaricus*) using Fourier Transform-near infrared (FT-NIR) spectroscopy. Marine and Freshwater Research, 65(10): 894-900.

Weigele, J., Franz-Odendaal, T. A., and Hilbig, R. 2016. Not All Inner Ears are the Same: Otolith Matrix Proteins in the Inner Ear of Sub-Adult Cichlid Fish, *Oreochromis Mossambicus*, Reveal Insights Into the Biomineralization Process: Otolith matrix proteins in cichlid fish. The Anatomical Record, 299: 234–245.

Weiss, R. E., and Watabe, N. 1979. Studies on the biology of fish bone. III. Ultrastructure of osteogenesis and resorption in osteocytic (cellular) and anosteocytic (acellular) bones. Calcified Tissue International, 28: 43–56.

White, D. B., and Palmer, S. M. 2004. Age, growth, and reproduction of the red snapper, *Lutjanus campechanus*, from the Atlantic waters of the southeastern U.S. Bulletin of Marine Science, 75(3): 335-360.

Wiedower, E. E., Kouba, A. J., Vance, C. K., Hansen, R. L., Stuth, J. W., and Tolleson, D. R. 2012. Fecal Near Infrared Spectroscopy to Discriminate Physiological Status in Giant Pandas. PLOS ONE, 7: e38908.

Williams, A. J., Leroy, B. M., Nicol, S. J., Farley, J. H., Clear, N. P., Krusic-Golub, K., and Davies, C. R. 2013. Comparison of daily- and annual- increment counts in otoliths of bigeye (*Thunnus obesus*), yellowfin (*T. albacares*), southern bluefin (*T. maccoyii*) and albacore (*T. alalunga*) tuna. ICES Journal of Marine Science, 70: 1439–1450.

Williams, A. J., Newman, S. J., Wakefield, C. B., Bunel, M., Halafihi, T., Kaltavara, J., and Nicol, S. J. 2015. Evaluating the performance of otolith morphometrics in deriving age compositions and mortality rates for assessment of data-poor tropical fisheries. ICES Journal of Marine Science, 72: 2098–2109.

Williams, P. 2008. Near-infrared technology: getting the best out of light: a short course in the practical implementation of near-infrared spectroscopy for the user. PDK Projects Inc., Nanaimo, Canada.

Williams, P. 2013. Calibration Development and Evaluation Methods B. Set-up and Evaluation. NIR news, 24: 20–24.

Williams, P. 2019. Near Infrared Technology: Getting the best out of light. African Sun Media. 312 pp.

Williams, P. C., Norris, K. H., and Sobering, D. C. 1985. Determination of protein and moisture in wheat and barley by near-infrared transmission. Journal of Agricultural and Food Chemistry, 33: 239–244. American Chemical Society.

Wilson, C. A., and Nieland, D. L. 2001. Age and growth of red snapper, *Lutjanus campechanus*, from the northern Gulf of Mexico off Louisiana. Fishery Bulletin, 99: 653–664.

Workman, I., Shah, A., Foster, D., and Hataway, B. 2002. Habitat preferences and site fidelity of juvenile red snapper (*Lutjanus campechanus*). ICES Journal of Marine Science, 59: S43–S50.

Workman, J., and Weyer, L. 2012. Practical Guide and Spectral Atlas for Interpretive Near-Infrared Spectroscopy, Second Edition. CRC Press. 331 pp.

Worthington, D. G., Fowler, A. J., and Doherty, P. J. 1995. Determining the most efficient method of age determination for estimating the age structure of a fish population. Canadian Journal of Fisheries and Aquatic Sciences, 52: 2320–2326.

Wright, P. J., Panfili, J., Morales-Nin, B., and Geffen, A. J. 2002. Types of calcified structures. *Manual of Fish Sclerochronology*, pp. 31–56.

Wright, P. J., and Trippel, E. A. 2009. Fishery-induced demographic changes in the timing of spawning: consequences for reproductive success. Fish and Fisheries, 10: 283–304.

Wyanski, D., White, D. B., Smart, T., Kolmos, K., and Reichert, M. J. 2015. Marine Resources Monitoring, Assessment and Prediction Program: Report on Atlantic Red Snapper, *Lutjanus campechanus*, Life History for the SEDAR 41 Data Workshop. SEDAR41-DW35. SEDAR, North Charleston, SC.

Zar, J. H. 1999. Biostatistical analysis. Pearson Education India.

Zhou, S., Yin, S., Thorson, J. T., Smith, A. D. M., and Fuller, M. 2012. Linking fishing mortality reference points to life history traits: an empirical study. Canadian Journal of Fisheries and Aquatic Sciences, 69: 1292–1301.

Zylberberg, L., Bonaventure, J., Cohen-Solal, L., Hartmann, D. J., and Bereiterhahn, J. 1992. Organization and characterization of fibrillar collagens in fish scales in situ and in vitro. Journal of Cell Science, 103: 273–285.

# APPENDIX A

# COPYRIGHT PERMISSIONS FOR CHAPTERS 2 AND 3

## CHAPTER 2:

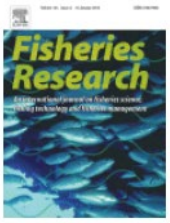


**Fourier-transform near infrared spectroscopy (FT-NIRS) rapidly and non-destructively predicts daily age and growth in otoliths of juvenile red snapper Lutjanus campechanus (Poey, 1860)**

**Author:** Michelle S. Passerotti,Christian M. Jones,Christopher E. Swanson,Joseph M. Quattro

**Publication:** Fisheries Research

**Publisher:** Elsevier

**Date:** March 2020



**Journal Author Rights**

Please note that, as the author of this Elsevier article, you retain the right to include it in a thesis or dissertation, provided it is not published commercially. Permission is not required, but please ensure that you reference the journal as the original source. For more information on this and on your other retained rights, please visit: https://www.elsevier.com/about/our-business/policies/copyright#Author-rights

CHAPTER 3:

OXFORD UNIVERSITY PRESS LICENSE
TERMS AND CONDITIONS

Feb 26, 2021

This Agreement between MICHELLE PASSEROTTI ("You") and Oxford University Press ("Oxford University Press") consists of your license details and the terms and conditions provided by Oxford University Press and Copyright Clearance Center.

| | |
|---|---|
| License Number | 5016611254167 |
| License date | Feb 26, 2021 |
| Licensed content publisher | Oxford University Press |
| Licensed content publication | ICES Journal of Marine Science |
| Licensed content title | Age estimation of red snapper (*Lutjanus campechanus*) using FT-NIR spectroscopy: feasibility of application to production ageing for management |
| Licensed content author | Passerotti, Michelle S |
| Licensed content date | Aug 8, 2020 |
| Type of Use | Thesis/Dissertation |
| Institution name | |
| Title of your work | Application of Fourier-transform near infrared spectroscopy to age estimation in red snapper Lutjanus campechanus |

**STANDARD TERMS AND CONDITIONS FOR REPRODUCTION OF MATERIAL FROM AN OXFORD UNIVERSITY PRESS JOURNAL**

1. Use of the material is restricted to the type of use specified in your order details.

2. This permission covers the use of the material in the English language in the following territory: world. If you have requested additional permission to translate this material, the terms and conditions of this reuse will be set out in clause 12.

3. This permission is limited to the particular use authorized in (1) above and does not allow you to sanction its use elsewhere in any other format other than specified above, nor does it apply to quotations, images, artistic works etc that have been reproduced from other sources which may be part of the material to be used.

4. No alteration, omission or addition is made to the material without our written consent. Permission must be re-cleared with Oxford University Press if/when you decide to reprint.

5. The following credit line appears wherever the material is used: author, title, journal, year, volume, issue number, pagination, by permission of Oxford University Press or the sponsoring society if the journal is a society journal. Where a journal is being published on behalf of a learned society, the details of that society must be included in the credit line.

6. For the reproduction of a full article from an Oxford University Press journal for whatever purpose, the corresponding author of the material concerned should be informed of the proposed use. Contact details for the corresponding authors of all Oxford University Press journal contact can be found alongside either the abstract or full text of the article concerned, accessible from www.oxfordjournals.org Should there be a problem clearing these rights, please contact journals.permissions@oup.com

7. If the credit line or acknowledgement in our publication indicates that any of the figures, images or photos was reproduced, drawn or modified from an earlier source it will be necessary for you to clear this permission with the original publisher as well. If this permission has not been obtained, please note that this material cannot be included in your publication/photocopies.

8. While you may exercise the rights licensed immediately upon issuance of the license at the end of the licensing process for the transaction, provided that you have disclosed complete and accurate details of your proposed use, no license is finally effective unless and until full payment is received from you (either by Oxford University Press or by Copyright Clearance Center (CCC)) as provided in CCC's Billing and Payment terms and conditions. If full payment is not received on a timely basis, then any license preliminarily granted shall be deemed automatically revoked and shall be void as if never granted. Further, in the event that you breach any of these terms and conditions or any of CCC's Billing and Payment terms and conditions, the license is automatically revoked and shall be void as if never granted. Use of materials as described in a revoked license, as well as any use of the materials beyond the scope of an unrevoked license, may constitute copyright infringement and Oxford University Press reserves the right to take any and all action to protect its